

EPA-600/4-76-002

February 1976

Environmental Monitoring Series

MODELING OF THE EFFECTS OF POLLUTANTS AND DISPERSION IN URBAN ATMOSPHERES



**Environmental Sciences Research Laboratory
Office of Research and Development
U.S. Environmental Protection Agency
Research Triangle Park, North Carolina 27711**

RESEARCH REPORTING SERIES

Research reports of the Office of Research and Development, U.S. Environmental Protection Agency, have been grouped into five series. These five broad categories were established to facilitate further development and application of environmental technology. Elimination of traditional grouping was consciously planned to foster technology transfer and a maximum interface in related fields. The five series are:

1. Environmental Health Effects Research
2. Environmental Protection Technology
3. Ecological Research
4. Environmental Monitoring
5. Socioeconomic Environmental Studies

This report has been assigned to the ENVIRONMENTAL MONITORING series. This series describes research conducted to develop new or improved methods and instrumentation for the identification and quantification of environmental pollutants at the lowest conceivably significant concentrations. It also includes studies to determine the ambient concentrations of pollutants in the environment and/or the variance of pollutants as a function of time or meteorological factors.

EPA-600/4-76-002
February 1976

MODELING OF THE EFFECTS OF POLLUTANTS AND DISPERSION
IN URBAN ATMOSPHERES

by

R. Viskanta, R. W. Bergstrom, Jr., and R. O. Johnson

School of Mechanical Engineering
Purdue University
West Lafayette, Indiana 47907

Grant No. R801102

Project Officer

James T. Peterson
Meteorology and Assessment Division
Environmental Sciences Research Laboratory
Research Triangle Park, North Carolina 27711

U.S. ENVIRONMENTAL PROTECTION AGENCY
OFFICE OF RESEARCH AND DEVELOPMENT
ENVIRONMENTAL SCIENCES RESEARCH LABORATORY
RESEARCH TRIANGLE PARK, NORTH CAROLINA 27711

DISCLAIMER

This report has been reviewed by the Environmental Sciences Research Laboratory, U.S. Environmental Protection Agency, and approved for publication. Approval does not signify that the contents necessarily reflect the views and policies of the U.S. Environmental Protection Agency, nor does mention of trade names or commercial products constitute endorsement or recommendation for use.

ABSTRACT

This report summarizes an effort to gain improved understanding of the short-term effects of radiatively participating pollutants upon the thermal structure and dispersion in an urban atmosphere. This goal was accomplished by constructing one- and two-dimensional numerical models of the planetary boundary layer. In the research, special attention was focused on the interaction of solar and thermal radiation with gaseous and particulate pollutants as well as natural atmospheric constituents. A number of numerical experiments have been performed with both models, and the differences between the results for simulations with and without radiatively participating pollutants in an urban atmosphere were examined.

The results of the numerical simulations performed with the one-dimensional (vertical transport only) model showed that the aerosol and gaseous pollutants could affect the temperature and pollutant concentration distributions. Under the conditions investigated, the largest surface temperature reduction due to the aerosols was 2C at noon, and the maximum rise of the atmospheric temperature due to the additional solar heating was about 1C after a two-day simulation period. The maximum predicted surface temperature increase at night due to the presence of gaseous pollutants was about 3C after a two-day simulation. Numerical experiments for different meteorological conditions have been performed and sensitivity studies have been conducted. The results obtained are summarized in the body of the report.

An unsteady, two-dimensional transport model which accounts for horizontal and vertical advection as well as turbulent diffusion and radiative transfer in an urban atmosphere has also been developed. As a specific example, the city of St. Louis, Missouri was selected for the numerical simulation of summer conditions. According to the preliminary results obtained with the model, the urban heat island intensity was found to reach a magnitude of about 4C before sunrise and about 1.3C at noon under the particular meteorological conditions considered. At night the radiative participation by the gaseous pollutants increased the surface temperature by about 1.3C above that for a simulation with nonparticipating pollutants. At noon, after a 24-hour simulation period, the surface temperature was only about 0.3C higher for the case with radiatively interacting pollutants. Air pollution was shown to decrease the atmospheric stability at night. In all of the cases considered, the pollutant concentrations in the atmosphere were always found to be lower in the simulations with radiatively participating than with nonparticipating pollutants.

This report was submitted in fulfillment of Grant Number R801102 by the School of Mechanical Engineering, Purdue University, West Lafayette, Indiana, under the partial sponsorship of the U.S. Environmental Protection Agency. This phase of the work was completed as of August 1975.

CONTENTS

ABSTRACT	iii
LIST OF FIGURES	vi
LIST OF TABLES	xi
LIST OF SYMBOLS	xiii
ACKNOWLEDGMENTS	xvi

SECTIONS

I SUMMARY AND CONCLUSIONS	I
II RECOMMENDATIONS	4
III INTRODUCTION	6
Background	6
Mathematical Modeling of Air Pollution	9
Objectives of the Study	10
Scope	11
IV ONE-DIMENSIONAL MODELING OF THERMAL STRUCTURE AND POLLUTANT DISPERSION IN AN URBAN ATMOSPHERE	12
Analysis	12
Physical Model	12
Basic Equations	14
Radiative Transfer Model	16
Turbulent Diffusivities	19
Method of Solution	20
Results and Discussion	21
Radiative Transfer in a Polluted Atmosphere	21
Test Simulation--O'Neill Observations	25
Urban Summer	25
Urban Summer Elevated Inversion	32
Urban Winter	34
Urban Winter Elevated Inversion	36
Effects of the Pollution Parameters	39
Summary of Surface Temperature Differences and Surface Concentration	40

CONTENTS

V	TWO-DIMENSIONAL MODELING OF THERMAL STRUCTURE AND POLLUTANT DISPERSION IN THE URBAN ATMOSPHERE	46
	Analysis	46
	Physical Model	46
	Governing Equations	48
	Radiative Transfer Model	51
	Turbulent Diffusivities	51
	Method of Solution	52
	Results and Discussion	53
	Parameters and Initial Conditions Used in the Simulations	55
	Some Difficulties Encountered	58
	Components of the Energy Budget at the Surface	59
	Surface Temperature	62
	Simulations with Radiative Nonparticipating Pollutants	62
	Simulations with Radiatively Participating Pollutants	65
	Surface Concentrations	67
	Velocity Distribution	70
	Temperature Distribution	73
	Radiatively Nonparticipating Pollutants	73
	Radiatively Participating Pollutants	75
	Concentration Distribution	85
	Radiatively Nonparticipating Pollutants	85
	Radiatively Participating Pollutants	88
	Urban Heat Island	94
VI	REFERENCES	97
	APPENDIX	105
	Publications	105

FIGURES

<u>No.</u>		<u>Page</u>
1	Physical Model for Solar and Atmospheric Thermal Radiation Transfer in a Polluted Urban Atmosphere	13
2	Effect of Turbidity Factor T on the Normalized Downward Directed Scattered and Total Surface Fluxes (a) and the Normalized Upward Directed Flux at the Atmosphere (Earth-Atmosphere Albedo) (b) for $\lambda = 0.55 \mu\text{m}$ and $\rho = 0.25$	24
3	Temperature Profiles for the Test (The O'Neill) Simulation	26
4	Comparison of Predicted and Observed (Lettau and Davidson, 1957) Surface Temperatures for Test Simulation	26
5	Isopleths for Simulations 1 and 5; Top Row are Temperatures (in C) and Bottom Row are Concentrations (in $\mu\text{g}/\text{m}^3$); Column 1 is Simulation 1, Column 2 is Simulation 5, and Column 3 is the Difference Between Simulations 1 and 5	29
6	Pollutant Concentration Distributions for Summer Conditions with Radiatively Nonparticipating Pollutants (Simulation 1)	31
7	Temperature Distributions for Urban Summer Inversion Conditions: (a) Simulation 2 with Radiatively Nonparticipating Pollutants, and (b) Simulation 6 with Radiatively Participating Pollutants Consisting of 20% by Weight Carbon Aerosol and Ethylene as Pollutant Gas	33
8	Concentration Profiles for Summer Inversion Conditions: (a) Simulation 2 with Radiatively Nonparticipating Pollutants, and (b) Simulation 6 with Radiatively Participating Pollutants Consisting of 20% by Weight Carbon Aerosol and Ethylene as Pollutant Gas	34
9	Isopleths for Simulations 3 and 7; Top Row are Temperatures (in C) and Bottom Row are Concentrations (in $\mu\text{g}/\text{m}^3$); Column 1 is Simulation 3, Column 2 is Simulation 7, and Column 3 is the Difference Between Simulations 3 and 7	35
10	Temperature Distributions for Urban Winter Inversion Conditions: (a) Simulation 4 with Radiatively Nonparticipating Pollutants, and (b) Simulation 8 with Radiatively Participating Pollutants Consisting of 20% by Weight Carbon Aerosol and Ethylene as Pollutant Gas	38

FIGURES
(Continued)

<u>No.</u>		<u>Page</u>
11	Concentration Profiles for Winter Elevated Inversion Conditions: (a) Simulation 4 with Radiatively Nonparticipating Pollutants, and (b) Simulation 8 with Radiatively Participating Pollutants Consisting of 20% by Weight Carbon Aerosol and Ethylene as Pollutant Gas	38

- 12 Surface Temperature Difference (Simulation with Radiatively Participating Pollutants Minus Simulation with Radiatively Nonparticipating Pollutants) for Summer Conditions

Curve	Pollutant Gas	Aerosol	$\frac{m_p}{(\mu g/m^2-s)}$	
1	C ₂ H ₄	Nonparticipating	1	
2	C ₂ H ₄	Nonabsorbing	1	
3	C ₂ H ₄	20% Carbon	1	
4	C ₂ H ₄	30% Carbon	1	
5	C ₂ H ₄	20% Carbon	1/3	
6	SO ₂	20% Carbon	1	
7	Nonparticipating	30% Carbon	1	41

- 13 Surface Pollutant Concentration Variation with Time for Summer Conditions:

Curve	Pollutant Gas	Aerosol	$\frac{m_p}{(\mu g/m^2-s)}$	
1	Nonparticipating	20% Carbon	1	
2	Nonparticipating	Nonparticipating	1	
3	SO ₂	20% Carbon	1	
4	C ₂ H ₄	30% Carbon	1	
5	C ₂ H ₄	Nonabsorbing	1	
6	C ₂ H ₄	Nonparticipating	1	42

- 14 Surface Pollutant Concentration Variation with Time for Winter Conditions:

Curve	Pollutant Gas	Aerosol	$\frac{m_p}{(\mu g/m^2-s)}$	
1	Nonparticipating	Nonparticipating	1	
1	Nonparticipating	20% Carbon	1	
2	SO ₂	20% Carbon	1	
3	C ₂ H ₄	30% Carbon	1	
4	C ₂ H ₄	Nonabsorbing	1	43

FIGURES
(Continued)

<u>No.</u>		<u>Page</u>
15	Physical Model and Coordinates	47
16	Comparison of Rectangular and Gaussian Anthropogenic Heat Source Distributions along the City	57
17	Variation of the Surface Energy Flux Components (q_t --Turbulent, q_l --Latent, q_e --Emitted, q_{at} --Absorbed Thermal, q_g --Ground Conduction, Q --Anthropogenic Heat Source) for Simulation 3 at 24:00 of the First Day	60
18	Variation of the Surface Energy Flux Components (q_t --Turbulent, q_l --Latent, q_e --Emitted, q_{as} --Absorbed Solar, q_{at} --Absorbed Thermal, q_g --Ground Conduction, Q --Anthropogenic Surface Heat Source) for Simulation 3 at 12:00 of the Second Day	60
19	Effect of Wind Speed on the Diurnal Variation of the Turbulent Heat Flux at the Surface for Simulations 1 and 3	61
20	Effect of Wind Speed on the Diurnal Variation of the Latent Heat Flux at the Surface for Simulations 1 and 3	61
21	Comparison of Surface Temperatures for Gaussian (Simulation 3) and Rectangular (Simulation 7) Distributions of Anthropogenic Heat and Pollutant Sources Along the City	62
22	Variation of Surface Temperature with Time for Simulation 1; $u_g = 12 \text{ m/s}$, $v_g = 8 \text{ m/s}$	63
23	Variation of Surface Temperature with Time for Simulation 3; $u_g = 6 \text{ m/s}$, $v_g = 4 \text{ m/s}$	64
24	Surface Temperature Difference (Simulation 2 Minus Simulation 1) Along City; $u_g = 12 \text{ m/s}$, $v_g = 8 \text{ m/s}$	66
25	Surface Temperature Difference (Simulation 5 Minus Simulation 3) Along City; $u_g = 6 \text{ m/s}$, $v_g = 4 \text{ m/s}$	66
26	Variation of Surface Pollutant Concentration Along the City for Simulation 3; $u_g = 6 \text{ m/s}$, $v_g = 4 \text{ m/s}$	67
27	Surface Pollutant Concentration Differences (Simulation 5 Minus Simulation 3) Along the City	69
28	Perturbation Velocities (Velocity at the Urban Center Minus Velocity at the Upwind Rural Location) for Simulation 3	70

FIGURES
(Continued)

<u>No.</u>		<u>Page</u>
29	Comparison of Vertical Velocity Isopleths (in cm/s) for Simulations with Radiatively Nonparticipating (Simulation 3) and Radiatively Participating (Simulation 5) Pollutants	72
30	Potential Temperature Isopleths (in K) for Simulation 3; Note that the Last Digit Denoting the Temperature of the Isotherms at 18:00, 24:00, and 06:00 Hours Has Been Truncated	74
31	Potential Temperature Distribution for Simulation 3	75
32	Potential Temperature Isopleths (in K) for Simulation 7	76
33	Comparison of Potential Temperature Isopleths (in K) Between Simulations 3 (Part a), Simulation 4 (Part b), Simulation 5 (Part c), and Simulation 6 (Part d) at 24:00 of the First Day	77
34	Comparison of Potential Temperature Isopleths (in K) Between Simulations 3 (Part a), Simulation 4 (Part b), Simulation 5 (Part c), and Simulation 6 (Part d) at 06:00 of the Second Day	78
35	Comparison of Potential Temperature Isopleths (in K) Between Simulation 3 (Part a), Simulation 4 (Part b), Simulation 5 (Part c), and Simulation 6 (Part d) at 12:00 of the Second Day	79
36	Perturbation of Potential Temperature (Temperature in the City Minus Temperature at the Upwind Rural Location) for Simulation 3	80
37	Comparison of Surface Temperatures at the Upwind Rural Location	84
38	Comparison of Surface Temperatures at the Center of the City	85
39	Gaseous Pollutant Concentration Isopleths for Simulation 3; (Multiply Numbers in Parts a, c, and d by a Factor of 10 and in Part b by a Factor of 10^2 to Obtain Concentrations in $\mu\text{g}/\text{m}^3$)	86
40	Gaseous Pollutant Concentrations Isopleths for Simulation 7 (Multiply Numbers in the Figure by a Factor of 10 to Obtain Concentrations in $\mu\text{g}/\text{m}^3$)	87
41	Comparison of Gaseous Pollutant Concentration Isopleths for Simulation 3 (Part a), Simulation 4 (Part b), Simulation 5 (Part c) and Simulation 6 (Part d) at 05:00 of the Second Day (Multiply the Numbers in Parts a, b, and d by a Factor of 10^2 and the Numbers in Part c by 10 to Obtain Concentrations in $\mu\text{g}/\text{m}^3$)	89

FIGURES
(Continued)

<u>No.</u>		<u>Page</u>
42	Comparison of Gaseous Pollutant Concentration Isopleths for Simulation 3 (Part a), Simulation 4 (Part b), Simulation 5 (Part c), and Simulation 6 (Part d) at 06:00 of the Second Day (Multiply the Numbers on the Figure by 10 to Obtain Concentrations in $\mu\text{g}/\text{m}^3$)	90
43	Comparison of Gaseous Pollutant Concentration Isopleths for Simulation 3 (Part a), Simulation 4 (Part b), Simulation 5 (Part c), and Simulation 6 (Part d) at 12:00 of the Second Day (Multiply the Numbers in the Figure by 10 to Obtain Concentrations in $\mu\text{g}/\text{m}^3$)	91
44	Comparison of Gaseous Pollutant Concentrations for Simulation 3 (Part a) and for Simulation 5 (Part b) at the Center of the City	92
45	Comparison of the Turbulent Diffusivities of Heat for Simulations 3 and 5 at $z = 5 \text{ m}$	93
46	Comparison of the Turbulent Diffusivities of Heat for Simulations 3 and 5 at $z = 200 \text{ m}$	93
47	Comparison of Maximum Urban Minus Upwind Rural Surface Temperature Differences for Simulations 3, 5, and 7	94
48	Variation of the Heating/Cooling Rates for Simulation 3 (Part a) and for Simulation 5 (Part b) During the Diurnal Cycle	95

TABLES

<u>No.</u>		<u>Page</u>
1	Eddy Diffusivity Correlation Due to Pandolfo, et al., (1971)	20
2	List of Numerical Simulations	22
3	Urban and Pollution Parameters Used in the Simulations	28
4	Comparison of the Solar and the Downward Thermal Radiant Fluxes at the Surface for the Urban Summer Simulation 1 without Radiatively Participating Pollutants and for Simulation 5 with Radiatively Participating Pollutants	30
5	Comparison of the Solar and the Downward Thermal Radiant Fluxes at the Surface for the Urban Winter Simulation 3 without Radiatively Participating Pollutants and for Simulation 7 with Radiatively Participating Pollutants	37
6	Maximum Surface Daytime (D) and Nighttime (N) Temperature and Pollution Concentration Differences (Simulation 1 Minus Simulation 5, etc.)	44
7	Effect of Time Step on Selected Meteorological Variables at the Center of the City ($z_0 = 1 \text{ m}$), $z = 1 \text{ m}$, and $t = 13:00 \text{ hr}$; Simulation Started at 12:00, Computer-CDC 6600 (C_1 Denotes the Aerosol and C_2 the Pollutant Gas Concentrations)	54
8	Summary of Simulations Performed to Study the Effects of Radiative Participation on Pollutant Dispersion and Thermal Structure in St. Louis, Missouri, During the Summer; Computer-CDC 7600	56
9	Variations of the Urban Surface Parameters Along the Horizontal Direction Assumed for the Simulations	56
10	Diurnal Variation of the Absorbed Thermal Flux at the Surface (q_{at} in W/m^2) for Simulations 3 and 5 at the Upwind Rural and the Center of the City Locations	68
11	Comparison of Aerosol Mass Loadings for Various Simulations	71
12	Surface Temperatures (in K) at the Center of the City ($x = 10.5 \text{ km}$) for Simulations 3, 4, 5, and 6 at Selected Times	71

TABLES
(Continued)

<u>No.</u>		<u>Page</u>
13	Comparison of Downwind Thermal Fluxes (W/m^2) at the Surface as a Function of the Horizontal Location Before Sunrise (05:00)	82
14	Ratio of the Radiative Flux Divergence ($-\partial F/\partial z$) to the Turbulent Diffusion [$\partial/\partial z(K^0 \partial \theta/\partial z)$] in the Vertical Direction for Simulation 3 with Radiatively Nonparticipating Pollutants (NP) and Simulation 5 with Radiatively Participating Pollutants (P)	83

LIST OF SYMBOLS

C_n	Concentration of species n
\dot{C}_n	Volumetric rate of production of species n
$C_{w,sat}$	Concentration of water vapor at saturated conditions
c_p	Specific heat at constant pressure
D_n	Diffusion coefficient of species n
e_t	Emittance (emissivity) of the earth's surface in the thermal part of the spectrum
F	Net radiative flux defined by Eq. (15)
F^+	Radiative flux in the positive z-direction
F^-	Radiative flux in the negative z-direction
f	Coriolis parameter
G	Incident radiation defined by Eq. (14)
g	Gravitational constant
I	Intensity of radiation
I_{bv}	Planck's function
K	Turbulent eddy diffusivity
k	Molecular conductivity of air
L	Latent heat of vaporization of water
ℓ	Mixing length, see Eq. (20)
M	Halstead's moisture parameter, see Eq. (11)
M_n	Mass loading of species n in the atmosphere defined as $\int_0^{z_\delta} C_n(z) dz$
m_p	Surface source of pollutant emissions, see Eq. (12)
p	Pressure
p_v	Scattering distribution function, see Eq. (16)

Q	Anthropogenic heat emission source at the surface, see Eq. (10)
\dot{q}	Volumetric rate of heat generation
r_s	Reflectance (albedo) of the earth's surface in the solar part of the spectrum
Ri	Richardson number
T	Thermodynamic temperature
T_s	Temperature of the soil
t	Time
u	Horizontal north velocity component
v	Horizontal west velocity component
w	Vertical velocity component
x	Horizontal coordinate, see Figure 15
y	Horizontal coordinate
z	Vertical coordinate, see Figures 1 and 15
z_o	Surface roughness
α_s	Thermal diffusivity of soil
θ	Potential temperature defined as $\theta = T(p_o/p)^{(\kappa-1)/\kappa}$
κ	Absorption coefficient or the ratio of specific heat at constant pressure to specific heat at constant volume
λ	Wavelength
μ	Direction cosine or dynamic viscosity
ν	Frequency
ρ	Density
σ	Scattering coefficient or Stefan-Boltzmann constant
ϕ	Azimuthal angle

Subscripts

n	Refers to species n
-----	-----------------------

p	Refers to pollutants both aerosols and gases
w	Refers to water vapor
Δ	Refers to the bottom of the soil layer
δ	Refers to the edge of the planetary boundary layer
ν	Refers to frequency or per unit frequency
1	Refers to aerosol
2	Refers to pollutant gas
∞	Refers to top of the free atmosphere

Superscripts

M	Refers to turbulent eddy diffusivity of momentum
θ	Refers to turbulent eddy diffusivity of heat
C_n	Refers to turbulent eddy diffusivity of mass of species n

ACKNOWLEDGMENTS

This research was supported by the Meteorology and Assessment Division, Environmental Protection Agency, under Public Health Service Grant No. APO 1278, and Environmental Protection Agency Grant No. R801102. National Science Foundation provided financial support to one of the authors (R.W.B.) in the form of a traineeship. Computer facilities were made available by Purdue University Computing Center and the National Center for Atmospheric Research which is supported by the National Science Foundation.

The authors wish to acknowledge Mr. A. Venkatram for his contributions to this effort. They also wish to express their appreciation to Professor Gerald M. Jurica, Department of Geosciences, Purdue University for his valuable comments.

The support of the project by the Environmental Protection Agency and the help provided by Drs. George W. Griffing and James T. Peterson, the Grant Project Officer, is acknowledged with sincere thanks.

SECTION I

SUMMARY AND CONCLUSIONS

Progress has been made toward the goal of improved understanding of the effects of gaseous and particulate pollutants on the transport processes in the urban atmosphere. One- and two-dimensional models have been developed for numerically simulating the atmospheric boundary layer and sensitivity studies have been conducted. A large number of numerical experiments have been performed using a one-dimensional model and some preliminary numerical simulations with the two-dimensional model have also been carried out. The results presented in the report demonstrate that the models are currently capable of providing results of interest to EPA.

Specifically, some interesting conclusions based on the results obtained from the unsteady one-dimensional (vertical transport only) model are that:

1. The pollutant aerosols reduced the solar radiative flux by about 10 percent on the first day and 20 percent on the second day for a summer simulation with relatively calm winds ($u_g = 3$ m/s, $v_g = 2$ m/s). As a result of this flux reduction, the surface temperature was decreased by a maximum of 2C in a two-day simulation period. However, the additional solar heating due to the aerosols increased the atmospheric temperature during the day by a maximum of about 1C after a two-day period.
2. Absorption and emission of thermal (long-wave) radiation increased the downward thermal radiative flux and thus raised the nighttime surface temperature. The maximum predicted surface temperature increase was about 3C after a two-day simulation.
3. In the simulations the net influence of particulates was to decrease the temperature of the atmosphere-earth system, whereas the influence of absorption and emission of thermal radiation by gases was to increase the system temperature. The gaseous and particulate pollutants thus had opposite and partially compensating effects.
4. The warmer surface temperature during the night decreased the stability of the atmosphere causing lower ground level maximum pollutant concentrations from ground level sources. This decrease was quite significant. In some summer simulations, for example, the surface concentration for a simulation with radiatively participating pollutants decreased to about 1.6 ppm (volume) from a value of about 3.2 with radiatively nonparticipating pollutants at 06:00 in the morning.

5. During the day the aerosols affected the pollutant concentration in the urban planetary boundary layer only slightly by reducing the instability of the atmosphere. This hindered the breakup of an elevated stable layer and in this instance increased the pollutant concentrations.
6. The infrared cooling due to gaseous pollutants moved an elevated stable layer upward. As a result of this modification, the pollutant concentration in the boundary layer was significantly decreased. For example, during the winter simulations with an elevated inversion, the stable layer was moved from 600 m to 1000 m, and the ground level pollutant concentration decreased from about 2.8 ppm (volume) for the simulation with radiatively nonparticipating pollutants to about 2 ppm for the radiatively participating one at 12:00 noon. Since advection and a removal mechanism were not considered in the model the ground level pollutant concentrations built up to high values (~ 30 ppm at 06:00 in the morning) for a summer simulation with an elevated inversion. Also, use of ethylene as a representative gaseous pollutant was considered to be a "worst possible case."

A few specific conclusions based on a limited number of preliminary simulations performed with the unsteady two-dimensional transport model for the city of St. Louis, Missouri under the selected meteorological conditions are that:

1. The urban heat island developed and reached a magnitude of about 4°C near sunrise and about 1.3°C at noon. The urban heat island intensity is quite sensitive to wind speed and to the value of Halstead's moisture parameter (latent energy transport).
2. For the meteorological conditions considered ($u_g = 6$ m/s, $v_g = 4$ m/s), the radiatively participating air pollutants increased the surface temperature at the urban center by about 1.3°C just before sunrise and about 0.3°C at noon after a one-day simulation. However, under more restrictive dispersion conditions which may arise during stagnating air masses such as lower wind speeds, stable upper layer temperatures, and higher pollutant concentrations, air pollutants have the potential to more significantly modify the surface temperature of the city.
3. The largest effect of radiatively participating air pollutants was to decrease the stability of the atmosphere at night and hence to increase turbulent diffusion near the surface. This was particularly noticeable at heights below 500 m.
4. The feedback mechanism between pollutants, thermal structure, stability, and dispersion has the potential of being important in modifying pollutant concentrations under more stable atmospheric conditions and higher pollutant loadings. However, the magnitudes of the concentration differences predicted for simulations with

radiatively participating and nonparticipating pollutants are dependent on a coupling between the radiative properties of air pollution and buoyancy enhanced turbulence, neither of which is very well known. Thus, the magnitude of the temperature and pollutant concentration differences between simulations with radiatively interacting and noninteracting pollutants is uncertain.

5. The unsteady two-dimensional model is capable of simulating the thermal structure and pollutant dispersion in the urban atmosphere. There are, however, a very large number of parameters which affect the temperature and pollutant concentrations in the urban planetary boundary layer and need to be examined. Only a few numerical simulations for unstable meteorological conditions during the day and relatively high wind speeds have been performed. Before more extensive simulations under more stable meteorological conditions and other urban parameters are undertaken, improved methods of modeling turbulence, latent energy transport, and the diurnal and longitudinal (along the city) variation of surface pollutant and urban heat sources must be found.
6. The research is continuing under a new EPA Grant No. R803514. The major thrust of the research program will be to perform numerical simulations for different atmospheric conditions, pollutants, and surface parameters, and to examine the differences between the results obtained for simulations with and without radiatively participating pollutants. Sensitivity studies will be continued and special consideration in the numerical experiments will be given to simulating radiative effects of pollutant layers above the city.

SECTION II

RECOMMENDATIONS

From the results of this project, there are two types of recommendations which can be made. The first are general problems areas which need attention for improved modeling of the urban area, while the second are more specific topics which should be investigated with the model.

Some of the problem areas which remain and require further work are the following:

1. An improved turbulent transport model is needed. The sensitivity of the empirical eddy diffusivity correlations to the local temperature and velocity gradients give rise to physically unrealistic "jagged" diffusivity profiles. This is particularly true when the atmosphere is composed of regions of widely differing stabilities. An example of such a situation is the common one of an unstable mixed layer capped by a stable layer. An improved procedure for incorporating the change in the roughness along the urban area into the turbulence model is also required.
2. Improved procedures for modeling the spatial and temporal variation of air pollution and heat and water vapor source emissions in the city must be developed. For example, how can the variation of the anthropogenic sources along the urban area and with the time of the day as well as season be best approximated?
3. A more physically realistic procedure must be found for modeling evapotranspiration at the air-soil interface and transport of water in the soil since latent transport (evaporation or condensation) is often a significant fraction of the net energy transport at the earth's surface.
4. Radiative transfer in the polluted urban atmosphere is at least two-dimensional and very complicated. Some simple approximate (i.e., semiempirical) yet mathematically and numerically tractable analyses must be developed to account for two-dimensional effects.
5. More efficient and computationally less time consuming numerical procedures for solving a system of coupled conservation equations need to be developed. There is also a great incentive to streamline the computer output because of the large amount of data to be analyzed.

While these problem areas remain, the model developed predicts the time-dependent temperature, velocity, and pollution concentration distributions over an urban area. The model can be used to investigate the various

feedback mechanisms which could amplify the influence of variation in factors such as atmospheric stability, surface temperature, planetary albedo, and dynamics of the inversion layer which are important for understanding local weather modification and pollutant dispersion. The conditions which are of particular interest are periods of stagnating high pressure centers with light winds since air pollution episodes often occur during these types of meteorological conditions. Specifically, it is recommended that the following topics be investigated by the model:

1. The effects of urban and pollution parameters under different meteorological and seasonal conditions should be simulated. Using the unsteady two-dimensional model, sensitivity studies should be conducted to determine which of the parameters are significant in altering temperature and concentration profiles in a polluted urban atmosphere. For example, under what meteorological conditions is radiative transfer important to compete with turbulent transport and what would the pollutant concentration have to be in order to significantly affect the thermal structure and pollutant dispersion? Understanding the effects of pollutants is needed for developing predictive models for the management of air resources in urban areas.
2. The thermal structure and pollutant dispersion under meteorological conditions of interest should be simulated. The effect of the radiatively participating pollutants on the height of the mixing layer during the day, on the formation of a surface inversion at night and on the dynamics (formation and breakup) of an elevated inversion should be studied using the two-dimensional model.
3. The numerical model should be verified by comparing the predictions of the model with available experimental data for the purpose of confirming and improving the model. The rural and urban data on solar (short-wave) and atmospheric (long-wave) radiative fluxes, temperature, humidity, wind speed, etc. that will become available from the RAPS program for the St. Louis, Missouri metropolitan area will be used for comparison with the predictions.

SECTION III

INTRODUCTION

BACKGROUND

This report describes the research which was initiated under a Public Health Service Grant No. APO 1278 and was continued under the U.S. Environmental Protection Agency Grant No. R801102. The work was undertaken in June 1971 under a three-year grant which terminated in January 1975. The primary objectives of the overall research program were the following:

- (1) Construct a physically realistic model for predicting radiative transfer in a polluted urban atmosphere by accounting for the radiative participation by both gaseous and particulate pollutants and perform sensitivity studies.
- (2) Develop a one-dimensional transport model for simulating the thermal structure and dispersion in an urban atmosphere and perform numerical experiments and sensitivity studies under different meteorological conditions.
- (3) Develop an unsteady two-dimensional transport model in a polluted urban atmosphere for simulating the radiative effects of air pollutants on the thermal structure and dispersion.

The first two objectives have been completed and the results are described in the papers and a thesis which are listed in the APPENDIX. Objective 3 has been completed; the model has been developed and checked by comparing its predictions for limiting situations with the results of other investigators and is discussed fully in this report. Improvements in the two-dimensional transport model and numerical simulations will be performed under a new U.S. Environmental Protection Agency Grant No. R803514.

The modification of the environment as a result of industrialization and urbanization has been increasing at an accelerating rate. This modification together with the injection of air pollutants into the atmosphere has many observable adverse effects on all aspects of human, animal, and plant life (Stern, et al., 1973). In addition to being a health hazard air pollution affects the environment and the quality of life. Many atmospheric scientists consider air pollution together with modification of the environment to be a potential cause of irreversible changes in the local and global climate.

The effects of air pollutants have been discussed recently by study groups (U.S. Council on Environmental Quality, 1970; SCEP, 1970; SMIC, 1971; Broderick, 1972) which have assessed the problem of air pollution on a global scale. Answers to questions concerning the accumulation, dispersion, and fate of air pollutants as well as their effects on the global heat balance and on the global weather were sought. The effects of high flying aircraft, the relationships between sources, routes and reservoirs, and the role of air chemistry were also considered. The main conclusion of these studies was that no definitive answer can be given since the phenomena are too complicated and too little is known about the complex interaction between the man-made and naturally produced air pollution in the atmosphere.

The way in which the gaseous and particulate pollutants can alter the temperature of the earth and the atmosphere is quite simple. The climate is controlled by the balance of radiant energy (Kondratyev, 1969). The earth's surface maintains its thermal energy balance by absorbing short-wave solar radiant energy and by re-radiating energy back to space at longer wavelengths. Air pollution can affect the spectral absorption and scattering characteristics of the atmosphere. Solar radiation is absorbed by gaseous pollutants and absorbed and scattered by particulate pollutants. This can tend to raise the temperature of the atmosphere and cool the surface. However, the increased absorption and emission of thermal radiation by pollutant gases increases the surface temperature. Thus, the pollutants on one hand have the effect of decreasing the earth's temperature by allowing less of the solar energy to reach the earth while on the other hand, they lead to an increase in the earth's temperature by increasing the downward longwave radiation. Some studies (Atwater, 1970; Mitchell, 1971) have shown that aerosols can produce warming or cooling of the entire earth-atmosphere system depending on the ratio of absorption to scattering. Estimates of the relative magnitudes of the opposing effects have been made in terms of a globally averaged radiative energy budget (SCEP, 1970; SMIC, 1971; Mitchell, 1971; Rasool and Schneider, 1971; Ensor, et al., 1971; Yamamoto and Tanaka, 1972; Braslau and Dave, 1973; Reck, 1974; Wang and Domoto, 1974).

On the local scale it has been conclusively established that the climate over cities differs from that found in the surrounding rural environs. Increasing research efforts devoted to comparative studies of rural and urban regions are well documented and reviews are available (Peterson, 1969; Landsberg, 1970, 1972; Frisken, 1972; Terjung, 1973; Oke, 1973a). One of the better known features of an urban environment is the existence of warmer temperatures in the urban area than in the surrounding rural regions. This phenomenon is known as an urban heat island. The generally accepted primary reasons for the formation of an urban heat island are (Peterson, 1969): (1) seasonal effects such as solar radiation, anthropogenic (man-made) heat sources; (2) the layer of gaseous and particulate pollutants over a city; and (3) the differences in the thermal properties, moisture, surface albedo, and surface roughness characteristics existing between urban and rural sites.

The effects of pollutants in the urban atmosphere have been receiving increased attention (Atwater, 1970, 1971, 1972a, 1972b, 1974; Bergstrom and Viskanta, 1973a, 1973b; Pandolfo, et al., 1971; Zdunkowski and McQuage, 1972) and two American Meteorological Symposia (Philadelphia, 1972 and Santa Barbara, 1974) were devoted to their discussion. As the recent survey by Oke (1973a) indicates the main attention has been focused on the modification by pollutants of solar and thermal fluxes reaching the earth's surface rather than effects of pollutants on the thermal structure and pollutant dispersion as well as the other meteorological variables in the atmosphere. Results obtained from the modeling efforts cannot yet be considered conclusive. Recent experimental investigations (Robinson, 1970; Kondratyev, 1972, 1973) conclude that the solid fraction of aerosols plays a very important role in the radiative transfer in the atmosphere, particularly in the absorption of short-wave radiation. The net effect of air pollutants on the radiative energy balance and the thermal structure in the atmosphere then depends on both the concentration and distribution of gaseous and particulate pollutants as well as concentration, size, distribution, and altitude range of the aerosols. Thus, it is clear that considerably more work on the complex problem of understanding the atmosphere and on the radiative transfer by gaseous and particulate pollutants is needed before short and long-term effects of man-made pollution can be predicted.

On a local scale, a small change in the radiative properties of the atmosphere due to the presence of air pollutants may alter the vertical distribution of temperature. In turn, this change in temperature near the surface can modify significantly the atmospheric stability (Smith, 1968). Obviously, any significant change in the vertical motion then alters the dispersion of the pollutants themselves. So in effect, the pollutant concentration distributions may well be a factor in affecting the processes that determine their own dispersion. This interaction (the interaction between radiation, the thermal structure, the flow field, and the pollutants) must be accounted for when modeling transport processes in the lower atmosphere (troposphere) over a polluted urban area (Kondratyev, 1973).

Pollutant dispersal requires the knowledge of wind speed, wind direction, turbulent intensity, and the thickness of the boundary layer. Urban areas are characterized by high levels of turbulence which cause what is commonly referred to as the "mixed" layer. The dynamics of this "mixed" layer are largely controlled by thermal effects. In fact, it is the efficacy of the thermally enhanced turbulence that is responsible for the near uniformity of potential temperature, wind speed, and pollutant distributions within the "mixed" layer. The primary variables in air pollution dispersal over an urban area are the wind speed vector and the height of the mixed layer. Major research efforts are currently underway to predict the height of the mixed layer and its variation from hour to hour, from day to day, and from season to season (Carson and Smith, 1974). However, relatively few studies have been made on the role of pollutants in modifying the growth of the mixed layer.

Attempts have been made to use the equations to simulate the structure of the urban planetary boundary layer and the various models which have been developed are reviewed by Oke (1973a) and need not be repeated here.

The most complete models consist of a soil layer, an analytical constant flux layer, and a numerical transition layer which is assumed to extend to the top of the planetary boundary layer. In constructing the models it is generally assumed that the fluid in the upper layer is in hydrostatic equilibrium, the flow is incompressible, and horizontal diffusion is negligible in comparison to horizontal advection. Eddy diffusion coefficients are typically specified from semi-empirical correlations, and many models utilize a surface energy balance to predict the surface temperature. Most of the analyses are for steady state. Few models have been developed for flow over an urban area (for example, Yamada, 1972; McElroy, 1972; Wagner and Yu, 1972; Bornstein, 1972; Yu, 1973) and most have neglected the radiative effects of water vapor, carbon dioxide and, of course, the pollutants (Wagner and Yu, 1972; Yu, 1973; Bornstein, 1974). Only Atwater (1970, 1971, 1972a, 1972b, 1974), Bergstrom and Viskanta (1973a, 1973b), and Pandolfo, et al. (1971) have accounted for radiative participation of both gaseous and particulate pollutants.

An improved understanding of the transport processes (including radiative transfer) in the urban atmosphere would be beneficial. This knowledge would be valuable in constructing urban air quality simulation models (AQSM). In turn, such models may be used for real-time air quality management, urban and regional air quality planning, and perhaps most importantly in designing and testing control strategies for meeting air quality standards.

MATHEMATICAL MODELING OF AIR POLLUTION

So far, it has not been shown with any assurance that climate is actually subject to man's influence and the debate continues due to the lack of observational data as well as physical understanding of the phenomena. The observations which are necessary to resolve the issue are exceedingly difficult due to the magnitude of the problem. It is also clear from the above discussion that no definitive answers can be given because too little is known about the complex interaction between man-made and naturally produced air pollution with the normal atmosphere. One means of studying the effects of air pollution on the transport processes in the atmosphere is to model the phenomena mathematically and to perform extensive measurements over a long period of time to obtain the needed data. Such extensive measurements have been initiated and are being carried out by the U.S. Environmental Protection Agency over St. Louis, Missouri under the RAPS program.

Mathematical modeling of complex phenomena has been well established in science and technology. In a mathematical and numerical model, effects can be isolated and studied as to their short, intermediate, and long term influences. The model can also be used to test, for example, the impact of new industrial development. Use of mathematical models (U.S. Presidential Council on Environmental Quality, 1970; SCEP, 1970; SMIC, 1971; Broderick, 1972; Boughner, 1972) and of intensification of measurement programs (United Nations Conference on the Human Environment, 1972) have been recommended for gaining the much needed understanding of transport processes in the polluted urban atmosphere.

While conceptually straightforward, modeling of the influence of air pollution on the thermal structure and pollutant dispersion in an urban environment is a very complex problem. No model is better than the needed input data, and the data on air pollution and urban parameters are either unavailable or not very reliable. In addition, even with the use of the most advanced high speed digital computers, simplifying assumptions are necessary in order to make the problem numerically tractable.

OBJECTIVES OF THE STUDY

The primary objective of this research program was to enhance understanding of the effects of pollutants on the urban environment. The research program aimed to determine the role of pollutants in modifying the thermal structure in the atmosphere which, in turn, affects the pollutant dispersal. The net effect of the most important pollutants on radiative flux and its divergence, temperature, and flow fields would be predicted. Irrespective of the precise details by which gaseous pollutants and particulate matter might influence the energy balance in the polluted atmosphere, one important aspect in understanding local weather modification and pollutant dispersion involves feedback mechanisms which could amplify or dampen the influence of factors such as atmospheric stability, lapse rate, surface temperature, planetary albedo, dynamics of the inversion layers, and others.

To this end, the specific aims of the total project were:

1. To construct an unsteady, one-dimensional transport model applicable to the urban atmosphere in which both gaseous and particulate pollutants are included; to simulate the interaction of natural atmospheric constituents and air pollutants with solar and thermal radiation in an urban planetary boundary layer; to simulate the thermal structure and pollutant dispersion in the boundary layer for a period of up to a few days; and to conduct sensitivity analyses to determine which parameters are significant in altering temperature and concentration profiles in polluted urban atmospheres.
2. To develop an unsteady, two-dimensional transport model in which the processes of advection, turbulent diffusion, and radiative transfer in the polluted urban atmosphere are accounted for and to simulate the wind, temperature, and concentration profiles in the urban planetary boundary layer for a period of up to a few days under different meteorological conditions to determine, for example, if radiative transfer is important enough to compete with turbulent transport and under what conditions.

The role of pollutants in modifying the thermal structure, i.e., stability, surface and elevated inversions, altered turbulence, and mixing height is of concern because the vertical temperature distribution affects, for example: (1) forecasting of pollution episodes, (2) calculation of pollutant dispersion, (3) micrometeorological weather prediction in urban areas, (4) prediction of visibility, and (5) identification of pollutants by remote sensing (optical, absorption, and inversion) methods. If it is determined that the radiative interaction of gaseous and particulate pollutants with the solar and atmospheric radiation is important, this may require

inclusion of radiative transfer in the air quality simulation models (AQSM) intended for the control and management of urban air resources.

The pollutants affect the radiative transfer and through it the total thermal energy budget of the urban atmosphere. Since under certain atmospheric conditions, radiative transfer may comprise a major fraction of the total energy budget in an urban planetary boundary layer, studies should be conducted to identify the conditions under which the effects of pollutant gases and aerosols contribute significantly to the energy budget in the urban atmosphere. It was also desirable to establish any feedback mechanisms between the pollutant concentrations and their own dispersion in the atmosphere. The relative role of the existing feedback mechanisms at present is by no means clear.

SCOPE

This report is divided into two parts. The first part of the report is concerned with the unsteady one-dimensional model and its development as well as the discussion of the numerical simulations. The details of the model and the numerous simulations which have been carried out are given by Bergstrom (1972b) as well as in some open literature publications and will not be repeated here. Only some of the more interesting results will be summarized and their salient features discussed. The second part of the report will be concerned with the construction of an unsteady two-dimensional transport model in the polluted urban atmosphere. The numerical method of solution of the governing equations will be discussed and some preliminary results which have been obtained will be presented. The shortcomings of the model, problems encountered, and suggestions for overcoming the inadequacies and problems are presented.

SECTION IV

ONE-DIMENSIONAL MODELING OF THERMAL STRUCTURE AND POLLUTANT DISPERSION IN AN URBAN ATMOSPHERE

The specific purpose of this section is to summarize recent work on the effects of gaseous and particulate pollutants on the thermal structure and the pollutant dispersion in an urban atmosphere. The short-term effects of air pollution upon the temperature distribution and pollutant dispersion in an urban atmosphere are predicted. This is accomplished by constructing an unsteady, one-dimensional transport model and then solving numerically the resultant equations. Radiative transfer is modeled by accounting for the absorption and scattering process of solar (short-wave) radiation as well as emission and absorption of thermal (long-wave) radiation. Results for a few typical simulations of temperature and concentration distributions in the urban boundary layer are presented for a period of up to two days. A more realistic two-dimensional model for simulating the effects of air pollution on the thermal structure and dispersion in the urban atmosphere is presented in Section V. A detailed treatment of the present topic is extremely difficult not only because of the lack of necessary data but also because a two-day simulation may be beyond the capability of most available computers in this country.

ANALYSIS

Physical Model

The physical model of the atmosphere is depicted in Figure 1. As shown, the atmosphere-earth system is assumed to be composed of four layers: (1) the "natural" atmosphere where the atmospheric variables are considered to be time independent; (2) the "polluted" atmosphere (the planetary boundary layer) where the atmospheric variables of horizontal, lateral and vertical velocity, temperature, and the water vapor and pollutant species concentrations are functions of height and time; (3) the soil layer where the temperature is a function of depth and time; and (4) the lithosphere where the temperature is assumed to be constant during a few-days simulation period. The forcing function of the model is the time dependent solar irradiation (insolation). During the day the solar radiant energy passing through natural and polluted atmospheric layers is depleted by absorption and scattering while at the surface this radiation is reflected and absorbed. This absorbed energy is partially transferred to the atmosphere by turbulent convection (including evaporation or condensation) and to the soil by conduction. The earth's surface emits energy in the form of long-wave (thermal) radiation. The atmosphere also absorbs, emits, and scatters thermal radiation. At night the emission of thermal radiation cools the atmosphere as well as the surface while energy is transferred from the atmosphere to the surface. The physical model of the atmosphere is thus one where the atmosphere and the surface warm up during the day due to the

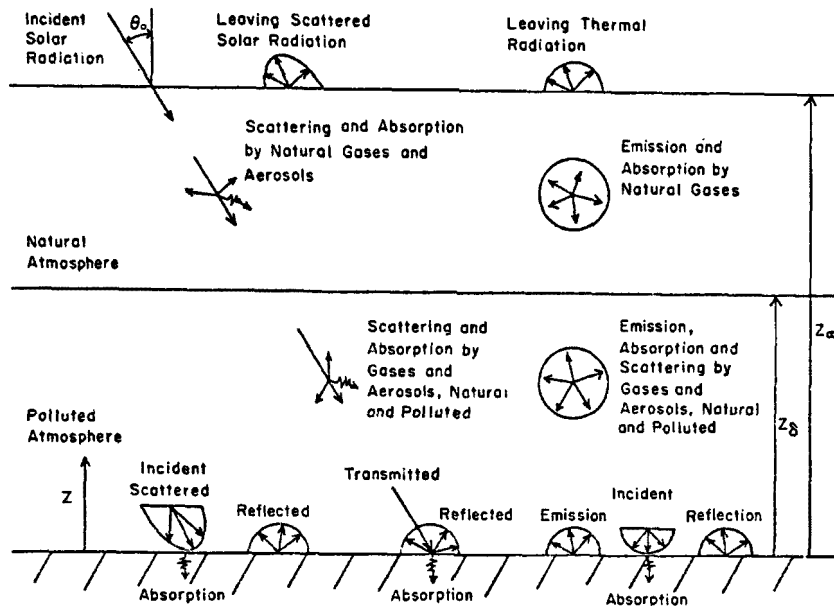


Figure 1. Physical Model for Solar and Atmospheric Thermal Radiation Transfer in a Polluted Urban Atmosphere

absorption of solar radiation while at night it cools due to the emission of thermal radiation. The distribution of thermal energy in the atmosphere depends upon the interaction between the turbulent vertical diffusion and the loss or gain of energy due to the radiative processes. Air pollution affects the energy balance by increasing both the scattering and absorption of solar radiation and the absorption and emission of infrared thermal radiation.

In the following analysis atmosphere is assumed to be in hydrostatic equilibrium. Furthermore, the atmosphere is considered to be horizontally homogeneous in such a way that both horizontal advection and diffusion can be neglected. This is probably valid for a region with a flat uniform terrain but, in general, would not be true for a heterogeneous urban area. The assumption neglects the change in the temperature structure of rural air as it is advected over a city. While this assumption can be criticized as unrealistic, it can be argued as somewhat representative of the worst possible case. Pollution episodes often occur in periods of stagnating high pressure centers with light winds. Thus, as far as the large scale processes are concerned, the neglect of horizontal advection is somewhat reasonable. On a smaller scale, however, this assumption does not account for the local horizontal pollutant transport. This is probably justified for large area sources of pollution but certainly not for large point sources such as industrial smoke stacks. The main justification of the horizontal homogeneity assumption is that it permits the development of a somewhat realistic yet relatively straightforward numerical model.

With this assumption it is possible to incorporate a fairly detailed description of radiative energy transfer without involving excessive computer time.

The one-dimensional model of energy transfer should therefore be considered as a first approximation (or a somewhat unrealistic worst case), while for more realistic modeling of an urban area a two- or a three-dimensional model is necessary. Even in a three-dimensional model the radiative transfer would probably have to be considered one-dimensional because of the excessive computer time requirements.

The horizontal homogeneity assumption implies that the mean vertical velocity component vanishes everywhere. This is equivalent to neglecting any upward flow generated by growth of the urban boundary layer (a result of the fully developed or horizontal homogeneity requirement) and to neglecting any free convection effects (vertical motion and/or cell development under lapse-free conditions) caused by the city other than turbulent enhancement.

Basic Equations

The governing equations for the model state mathematically the conservation principles of momentum, energy, and species and are the same set as those used by previous investigators (Estoque, 1963; Sasamori, 1970; Zdunkowski and McQuage, 1972). These equations for the one-dimensional, unsteady model are as follows:

$$z = z_{\infty}$$

Natural Atmosphere

$$u, v, \theta, C_w, C_p = \text{constant}$$

$$z = z_{\delta}$$

Polluted Atmosphere

Momentum (x-direction):

$$\rho \frac{\partial u}{\partial t} = \rho f(v - v_g) + \frac{\partial}{\partial z} \left[\left(\mu + \rho K_z^M \right) \frac{\partial u}{\partial z} \right] \quad (1)$$

Momentum (y-direction):

$$\rho \frac{\partial v}{\partial t} = -\rho f(u - u_g) + \frac{\partial}{\partial z} \left[\left(\mu + \rho K_z^M \right) \frac{\partial v}{\partial z} \right] \quad (2)$$

Momentum (z-direction):

$$0 = \frac{\partial p}{\partial z} + \rho g \quad (3)$$

Energy:

$$\rho C_p \frac{\partial \theta}{\partial t} = \frac{\partial}{\partial z} \left[\left(k + \rho C_p K_z^{\theta} \right) \frac{\partial \theta}{\partial z} \right] - \left(p_o/p \right)^{(\kappa-1)/\kappa} \frac{\partial F}{\partial z} \quad (4)$$

Species:

$$\frac{\partial C_n}{\partial t} = \frac{\partial}{\partial z} \left[\left(D_n + K_z^{C_n} \right) \frac{\partial C_n}{\partial z} \right] + \dot{C}_n, \quad n = 1, 2, 3 \quad (5)$$

Surface

$$z = 0$$

Soil Layer

Energy:

$$\frac{\partial T_s}{\partial t} = \alpha_s \frac{\partial^2 T_s}{\partial z^2} \quad (6)$$

$$T_s = \text{constant} \quad z = -z_\Delta$$

The conservation of energy equation in the atmosphere has been written in terms of the potential temperature θ . In order to completely formulate the problem it is necessary to specify the initial and boundary conditions, to predict the divergence of the radiative flux, and to relate the turbulent diffusivities to the other atmospheric variables.

At the edge of the outer flow the variables are solved subject to the boundary conditions

$$\chi(z, t) = \text{constant} \quad \text{at } z = z_\delta \quad (7)$$

Where χ represents the horizontal north velocity u , the horizontal west velocity v , the potential temperature θ and the concentration C_n of species n . This boundary condition is consistent with the notion that the large scale weather system is slowly moving. At the bottom of the soil layer the temperature is also taken as constant, i.e.,

$$T_s(x, t) = \text{constant} \quad \text{at } z = -z_\Delta \quad (8)$$

At the earth's surface the two velocity components are considered to vanish, i.e.,

$$u(z, t) = v(z, t) = 0 \quad \text{at } z = 0 \quad (9)$$

The surface temperature is predicted by assuming that the earth's surface cannot store energy and that it is opaque to radiation. Hence, the sum of the radiative, convective, latent, and conductive fluxes must vanish, i.e.,

$$\begin{aligned} (1-r_s)F_s^-(0, t) + e_+F_+^-(0, t) - e_+\sigma T^4(0, t) + \left(k + \rho c_p K^\theta \right) \frac{\partial \theta}{\partial z} \Big|_0 \\ + \rho L \left(D_w + K^w \right) \frac{\partial C_w}{\partial z} \Big|_0 - k_s \frac{\partial T_s}{\partial z} \Big|_0 + Q = 0 \quad \text{at } z = 0 \end{aligned} \quad (10)$$

where $F_s^-(0,t)$ and $F_t^-(0,t)$ represent the downward directed solar and thermal fluxes, respectively. Thus, the first and second terms represent the absorption of solar and thermal (long-wave) radiation by the surface, respectively. The third term accounts for the emission of thermal radiation by the surface and the fourth and fifth terms represent the turbulent thermal energy flux and the latent energy flux leaving the surface. The fifth term is the conductive energy flux to or from the soil, and the last term represents the anthropogenic (man-made) urban heat source.

The surface water vapor concentration is prescribed by Halstead's moisture parameters (Pandolfo, et al., 1971) in an approximate manner by the expression

$$C_w(0,t) = MC_{sat}(0,t) + (1-M)C_w(z_1,t) \quad \text{at } z = 0 \quad (11)$$

where z_1 is the first grid point above the surface and C_{sat} is the water vapor concentration at saturated conditions. The values of the parameter M range from 1 for water [$C_w(0,t) = C_{sat}$] to 0 for dry soil [$C_w(z_1,t) - C_w(0,t) = 0$]. The fraction of area which is saturated with water, the moisture parameter M , depends on the soil type, root distribution, water table depth, and other variables (Halstead, et al., 1957). In addition, the soil in urban areas is partly covered by buildings, pavement, etc., and this fraction covered cannot be readily estimated. It is therefore recognized that Eq. (11) may not model evaporation from the soil surface accurately enough. More detailed models for predicting the temperature distribution in the soil and the evaporation from the earth's surface are available, i.e., Sasamori (1970). Unfortunately, hydraulic and thermal properties of porous soil such as moisture potential, effective permeability (hydraulic conductivity), and moisture content as well as the thermal diffusivities are not well known for the soil types and textures encountered in urban areas (Eagelson, 1970).

The surface boundary condition for the pollution concentration when a surface source is present is given by specifying the "surface" pollutant mass flux, m_p , that is

$$m_p = -\left(D_p + K^p\right) \frac{\partial C_p}{\partial z} \bigg|_0 \quad \text{at } z = 0 \quad (12)$$

It should be emphasized that the surface is not the location where the pollutants are introduced into the atmosphere, and this formulation then has certain physical limitations. Again, as with the moisture parameter M , there is little quantitative data on sources of individual pollutants at the surface.

Radiative Transfer Model

The urban atmosphere is again considered to be cloudless, plane-parallel, and to consist of two layers: (1) the urban (surface, planetary) boundary layer where most pollutants are concentrated, and (2) the free atmosphere. The idealized model was illustrated in Figure 1. The top of the free

atmosphere is transparent to both solar and thermal radiation. From below the boundary layer is bounded by an opaque earth's surface which not only emits but also reflects radiation. The emission characteristics and the albedo of the earth's surface in the model are arbitrary but prescribed functions of wavelength. The radiative transfer between the free atmosphere and the planetary boundary layer is coupled. The gaseous and particulate atmospheric constituents are considered to absorb, emit, and scatter radiation. No consideration, however, is given to individual point sources of pollutants. The following physical processes are considered in predicting radiative transfer in the atmosphere: (1) attenuation of solar radiation by gaseous absorbers such as ozone, water vapor, carbon dioxide, and other gases in the natural atmosphere; (2) Rayleigh scattering by molecules and Mie scattering by a natural aerosol in the natural atmosphere; (3) absorption of solar radiation by natural and pollutant gases, Rayleigh scattering by molecules and Mie scattering by both natural and pollutant aerosols in the polluted planetary boundary layer, and finally, (4) emission of thermal radiation by both natural and pollutant gases and aerosols in the free and polluted atmospheres are accounted for. The radiative transfer model is considered one-dimensional; therefore, the local radiative flux divergence at a given horizontal position is determined from the vertical temperature, water vapor, pollutant and aerosol concentration distributions. A more detailed two-dimensional radiative transfer model is considered to be impractical and too time-consuming for numerical simulations. It must be recognized that multidimensional radiative transfer is exceedingly complex and inclusion of it would overshadow many of the more important problem areas of this research. In the two-dimensional transport model described in Section V radiative transfer is considered to be quasi-two-dimensional.

The radiant energy flux divergence, $\partial F/\partial z$, which appears in the energy equation physically represents the net loss (or gain) of radiant energy per unit of volume. The conservation of radiant energy equation can be written as

$$\frac{\partial F}{\partial z} = \int_0^{\infty} \kappa_v \left[4\pi I_{bv}(z) - G_v(z) \right] dv \quad (13)$$

where the spectral incident radiant energy is defined as

$$G_v(z) = \int_0^{2\pi} \int_{-1}^{+1} I_v(z, \mu, \phi) d\mu d\phi \quad (14)$$

and the radiative flux as

$$F_v(z) = \int_0^{2\pi} \int_{-1}^{+1} I_v(z, \mu, \phi) \mu d\mu d\phi \quad (15)$$

The first term on the right-hand side of Eq. (13) represents emission and the second term accounts for absorption of radiant energy. The spectral intensity, I_ν , defining the radiation field is predicted from the equation of transfer in the direction, μ, ϕ as (Chandrasekhar, 1960)

$$\begin{aligned} \mu \frac{\partial I_\nu(z, \mu, \phi)}{\partial z} = & - \left[\kappa_\nu(z) + \sigma_\nu(z) \right] I_\nu(z, \mu, \phi) + \kappa_\nu(z) I_{b\nu}(z) \\ & + \frac{\sigma_\nu(z)}{4\pi} \int_{\mu'=0}^{\phi'=2\pi} \int_{\mu'=-1}^{\mu'=1} p_\nu(z, \mu', \phi' \rightarrow \mu, \phi) I_\nu(z, \mu', \phi') d\mu' d\phi' \end{aligned} \quad (16)$$

In writing this equation it is assumed that the atmosphere is in local thermodynamic equilibrium, the index of refraction is equal to unity and the radiative transfer is quasi-steady, i.e., $(1/c)\partial/\partial t \ll \mu(\partial/\partial z)$.

The boundary conditions necessary to solve the equation of transfer (16) are the specification of the intensity at the top of the atmosphere and at the earth's surface. At the top of the atmosphere it is assumed that the sun is the only source of radiation present and at the surface of the earth it is assumed that the reflection and emission are diffuse and the radiation characteristics of the earth's surface are known. This can be written as

$$I_\nu^-(z_\infty, \mu, \phi) = F_{\infty, \nu}^-(\mu - \mu_0) \delta(\phi - \phi_0), \quad \mu < 0 \quad (17)$$

and

$$I_\nu^+(0, \mu, \phi) = (r_\nu/\pi) F_\nu^-(0) + \epsilon_\nu I_{b\nu}(0), \quad \mu > 0 \quad (18)$$

where δ is the Dirac delta function and μ_0, ϕ_0 is the direction of the incidence of the solar flux. The solution of the radiative transfer equation was accomplished (Bergstrom, 1972b; Bergstrom and Viskanta, 1973c) by dividing the entire electromagnetic spectrum into a solar part ($0.3\mu \leq \lambda < 4\mu$) and a thermal part ($4\mu \leq \lambda \leq 100\mu$). In the solar part the integrodifferential equation of radiative transfer was solved analytically using the spherical harmonics approximation. The solutions based on the P_3 -approximation of the spherical harmonics method were found to be in good agreement with the results of other more detailed methods. These results are discussed in detail by Bergstrom and Viskanta (1973c, 1974).

The total radiative flux and flux divergence in the thermal spectrum were predicted by using the total emissivity data for water vapor (Kuhn, 1963) and carbon dioxide [Shekhter (Atwater, 1970)] and neglecting multiple scattering. The data of Kuhn was used because the overlap of the carbon dioxide and water vapor bands had been accounted for in these data. It was assumed that the influence of gaseous pollutants is confined to the 8-12 μ m spectral region due to the relative opacity of the water vapor and carbon dioxide bands.

The spectral absorption and scattering characteristics of the aerosol in a polluted atmosphere must be specified. A truly accurate treatment is extremely complex and not practical because of lack of data and averaging difficulties. The absorption and scattering coefficients and the scattering distribution function were predicted using Mie electromagnetic theory by specifying the size distribution (Deirmendjian's Haze L distribution; Deirmendjian, 1969) and by assuming that the aerosol was composed of absorbing (carbon-like) and nonabsorbing (quartz-like) particles. While the latter assumption can be criticized as arbitrary, the resulting absorption and extinction coefficients do correspond to the measured mean indices of refraction measured by Fisher and Hänel (Hänel, 1972) for a dry aerosol over an industrialized area. The details of the model have been given elsewhere (Bergstrom, 1972a; Bergstrom, 1973).

Turbulent Diffusivities

The governing equations also require the specification of the turbulent diffusivities. The diffusivity for an arbitrary quantity ξ in the j -direction is defined as

$$K_j^\xi = -\overline{\xi'v_j'} / (\partial \overline{\xi} / \partial x_j) \quad (19)$$

where the primes (') represent instantaneous values and the bars ($\overline{}$) denote time averaged quantities and v_j and x_j are the velocity and unit direction vectors in the j -th direction. It is recognized that specification of the eddy diffusivities (K 's) is perhaps one of the most difficult problems associated with the modeling of the planetary boundary layer. The modeling of turbulence in the atmosphere has been a subject of a recent symposium (Frankiel and Munn, 1974) and a review of the eddy exchange coefficients is available (Oke, 1973a). In view of the excessive computer time requirements to model turbulence using higher order models (Donaldson, 1973; Mellor, 1973; Wyngard, Cote and Kao, 1974), it was considered impractical to incorporate higher-order turbulence models in the type of study being attempted in this program. Therefore, the semiempirical expressions for the eddy diffusivities developed by Pandolfo, et al. (1971) were used. In this connection it should be mentioned that other investigators (Sasamori, 1970; Estoque, 1973) have obtained realistic results using eddy diffusivity formulations which are dependent on the "constant flux" layer correlations.

Also, the accuracy of the various models has not been determined. Comparison with observations has shown limitations in the assumptions of the numerical models and has given little or no indications of the level of accuracy of the turbulent models. Therefore, while the empirical expressions of Pandolfo, et al. and others are "crude" approximations to actual turbulent motions, no other method has demonstrated conclusively that it is "better" for simulations of atmospheric motion under diabatic conditions.

The eddy diffusivity relations employed in the calculations are presented in Table I. The diffusivities were assumed to be valid in the entire planetary boundary layer. The decay of turbulence in the upper part of the

TABLE 1. EDDY DIFFUSIVITY CORRELATION DUE TO PANDOLFO, ET AL., (1971)

$$0 \leq Ri < Ri_c: K^M = K^\Theta = K^C_w = (k\ell)^2 \left[\frac{\partial U}{\partial z} \right] (1 + \alpha Ri)^2$$

$$Ri_+ < Ri < 0: K^M = (k\ell)^2 \left[\frac{\partial U}{\partial z} \right] (1 - \alpha Ri)^{-2}$$

$$K^\Theta = K^C_w = K^M / (1 - Ri)^2$$

$$Ri \leq Ri_+: K^\Theta = K^C_w = (h/k^2)\ell^2 \left[\left(\frac{g}{T} \right) \left(\frac{\partial \theta}{\partial z} \right) \right]^{\frac{1}{2}}$$

$$K^M = (h/k)^{-1/3} Ri^{-1/6} K^\Theta$$

where

$$k = 0.4, Ri_c = 1/|\alpha|, Ri_+ = -1/[7|\alpha|], \alpha = -3$$

$$h = k^2 \left[\left(|Ri_+| \right)^{1/3} + \left(1 + |Ri_+|^2 \right) \right]^{-3/2}$$

planetary boundary layer was accounted for following Blackadar (1962) and Wu (1965) by replacing the height, z , with a modified mixing length ℓ where

$$\ell = \frac{z}{1 + z/\lambda} \quad (20)$$

and λ is a constant.

Method of Solution

The governing partial differential equations, Eqs. (1) through (6), cannot be solved analytically, and therefore a finite-difference technique was used. The details are given elsewhere (Bergstrom, 1972b). Suffice it to note that the implicit Crank-Nicholson method was employed with a nonuniform grid spacing. A total of 22 grid points were used. The first grid point was placed at a height of 1 m and the last at 2000 m. A variable time step was used to keep the largest stability parameter below a certain set value. Convergence was investigated by doubling the number of grid points and reducing the time increments. Doubling the grid points altered the surface temperature by 0.1 C after a two-day simulation period. This corresponded to only a few percent change in the daily surface temperature but increased the required computer time by about a factor of four.

The calculation of the divergence of the radiative flux in the solar part of the spectrum was the most time consuming part of the model and was evaluated at longer time steps than the other variables. The values of $\partial F/\partial y$ were then extrapolated between computations. Each two-day simulation required approximately 5 minutes of CDC 6600 computer time.

RESULTS AND DISCUSSION

The effects of air pollution on the thermal structure and dispersion were predicted by numerically simulating the temperature, velocity, water vapor, and aerosol as well as typical gaseous pollutant concentrations in an urban area for a period of up to two days. Since there were a great many independent parameters the number of possible situations that could be simulated was very large. Therefore, only several selected conditions were considered and only some of those are discussed here. The pollutant conditions studied were those for an urban summer and winter both with and without an elevated inversion present. The pollutant parameters varied were the amount of aerosol, the fraction of absorbing aerosol, the amount of pollutant gas, and the choice of pollutant gas. In total 32 numerical experiments were performed and are summarized in Table 2. The details are given elsewhere (Bergstrom, 1972b). Before discussing the results it is desirable to compare the predictions of the radiative and total energy transfer models against other analyses and against measured data in order to establish some degree of their reliability and to increase the confidence level of the predicted results.

Radiative Transfer in a Polluted Atmosphere

Since the concentration, composition, and size distribution of the aerosol are not very well known and vary considerably, it usually is very difficult to compare the predicted solar flux and its divergence to experimental data. Therefore, the results predicted by various methods were compared against each other for typical conditions of interest in order to determine their relative agreement. The techniques chosen were the P_1 - and P_3 -approximations of the spherical harmonics method, the 20th order of the discrete ordinates method (Chandrasekhar, 1960; Mudgett and Richards, 1971), and an iterative method (Herman and Browning, 1965).

Radiative fluxes and flux divergences were predicted for a homogeneous atmosphere containing only an air pollution aerosol at a typical concentration. The radiative properties of the aerosol were evaluated according to the model of Bergstrom (1972a). The agreement between the radiative fluxes for different solar zenith angles predicted by the different methods was found to be surprisingly good while the discrepancy was slightly greater for the predicted flux divergences (Bergstrom, 1972b; Bergstrom and Viskanta, 1973c). The computational time requirements for the different solution schemes showed much more drastic results. The computation time for a given wavelength ranged from 1 to 2 seconds on a CDC 6400 computer for P_1 - and P_3 -approximations of the spherical harmonics method, 20 seconds for the 20th order Gaussian quadrature of the discrete ordinates method, and 200 seconds for the iterative procedure. While it was difficult to assess the absolute accuracy of each method, the small relative difference (a maximum difference

TABLE 2. LIST OF NUMERICAL SIMULATIONS

Situations: A. Urban Summer
 B. Urban Summer Elevated Inversion
 C. Urban Winter
 D. Urban Winter Elevated Inversion

<u>Simulation Number</u>	<u>Situation</u>	<u>Aerosol Pollutants</u>	<u>Gaseous Pollutants</u>	<u>Source* Strength $\mu\text{g}/\text{m}^2\text{-s}$</u>
1	A	Nonparticipating	Nonparticipating	3
2	B	"	"	"
3	C	"	"	"
4	D	"	"	"
5	A	20% Carbon	Ethylene	"
6	B	"	"	"
7	C	"	"	"
8	D	"	"	"
9	A	20% Carbon	None	"
10	B	"	"	"
11	C	"	"	"
12	D	"	"	"
13	A	None	Ethylene	"
14	B	"	"	"
15	C	"	"	"
16	D	"	"	"
17	A	20% Carbon	Sulfur Dioxide	"
18	B	"	"	"
19	C	"	"	"
20	D	"	"	"
21	A	"	Ethylene	1
22	B	"	"	"
23	C	"	"	"
24	D	"	"	"
25	A	Nonabsorbing	"	3
26	B	"	"	"
27	C	"	"	"
28	D	"	"	"
29	A	30% Carbon	"	"
30	B	"	"	"
31	C	"	"	"
32	D	"	"	"

*Aerosol source strength is given. The gaseous source strength was adjusted so that an aerosol concentration of $100 \mu\text{g}/\text{m}^3$ corresponded to a gas concentration of 1 ppm (volume).

of about 2 percent for the flux and about 10 percent for the flux divergence) gave some degree of confidence in the reliability of the techniques. Therefore, in the subsequent computations the P_3 -approximation is used throughout. The order of the approximation could be readily increased if this was warranted in future studies. Unfortunately, the computation time would be increased significantly.

As a specific example, the results for the spectral solar flux and flux divergence predicted by the P_3 -approximation were compared against those obtained by Eschelbach (1972). The method employed by Eschelbach is similar to that used by Herman and Browning (1965) and the error is claimed to be less than 1 percent. The atmospheric aerosols were assumed to have a power law distribution and indices of refraction of $1.5-0.02i$. The vertical concentration distribution for both Rayleigh scatterers (σ_R) and atmospheric aerosols (β_H , where $\beta = \sigma + \kappa$) was assumed to be exponential as (Eschelbach, 1972)

$$\sigma_R = \sigma_R \Big|_{z=0} \exp(-z/H_R) \quad (21)$$

and

$$\beta_H = \beta_H \Big|_{z=0} \exp(-z/H_H) \quad (22)$$

with $H_R = 8$ km and $H_H = 1.25$ km. The single scattering albedo, ω , and percentage of Rayleigh scattering for a wavelength of $0.55 \mu\text{m}$ used in the computations are given elsewhere (Bergstrom and Viskanta, 1974).

The normalized downward directed surface fluxes and upward directed fluxes at the top of the atmosphere are illustrated in Figure 2. The fluxes are shown as a function of the cosine of the solar zenith angle for three different turbidity factors,

$$T = (\tau_{R\infty} + \tau_{H\infty})/\tau_{R\infty} \quad (23)$$

Since $\tau_{R\infty}$ is constant, increasing T increases the aerosol optical thickness $\tau_{H\infty}$. The normalized total (scattered plus transmitted) flux is shown in Figure 2a. The ratio $F_{\lambda}^{\downarrow}(0)/\mu_0 F_{0\lambda}$ represents the total transmittance of the atmosphere to the incoming solar radiation flux ($\mu_0 F_{0\lambda}$) at the top of the atmosphere. The values predicted by Eschelbach (1972) are denoted by pluses (+). As illustrated, the points for which data are available are in very good agreement. This is quite surprising due to the simplification made in the P_3 -approximation. The normalized upward directed fluxes at the top of the atmosphere illustrated in Figure 2b represent the total reflectance or "albedo" of the earth-atmosphere system. The results are also in very good agreement with the predictions of Eschelbach (1972). Equally valid results have been obtained for the flux divergence. Additional comparisons are given by Bergstrom and Viskanta (1974).

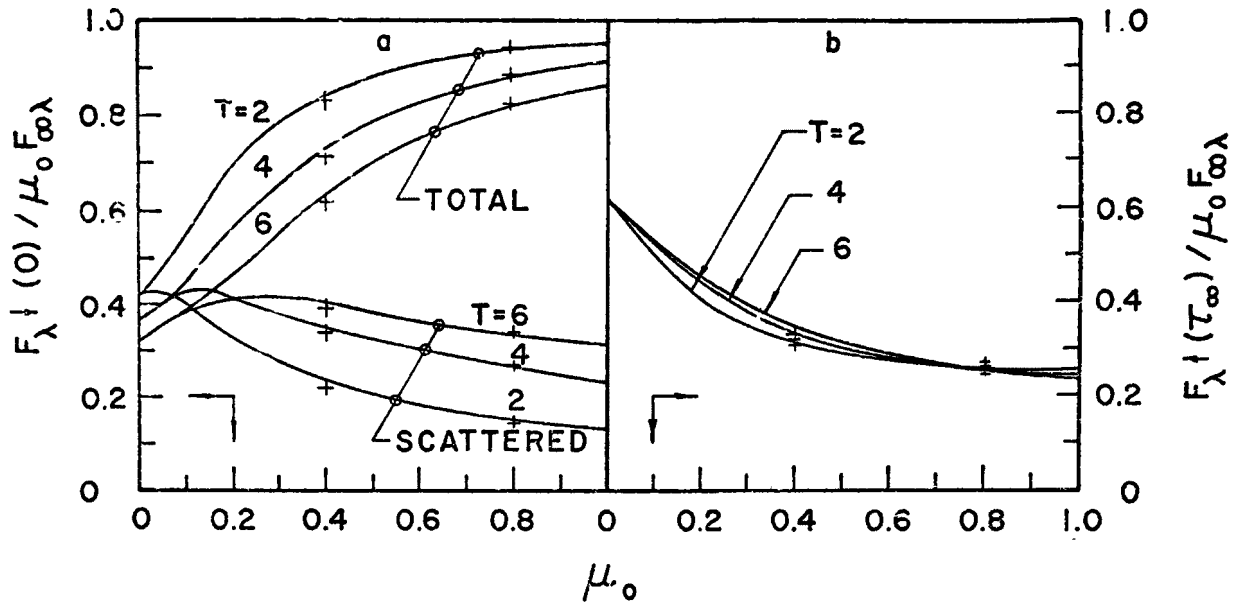


Figure 2. Effect of Turbidity Factor T on the Normalized Downward Directed Scattered and Total Surface Fluxes (a) and the Normalized Upward Directed Flux at the Atmosphere (Earth-Atmosphere Albedo) (b) for $\lambda = 0.55 \mu\text{m}$ and $\rho^d = 0.25$

The results obtained (Bergstrom, 1972b; Bergstrom and Viskanta, 1974) show that the lower orders of the spherical harmonics approximation to the equation of radiative transfer predict solar fluxes and flux divergences which are in good agreement with more detailed methods of solution for both homogeneous and nonhomogeneous atmospheres. The approximations result in a considerable saving of computational effort (from one to two orders of magnitude) over other more detailed methods. This saving is of great important in applications to time dependent problems and where integration over wavelength by necessity must be made for the flux and the radiative flux divergence.

Solar heating and infrared cooling rates due to different individual pollutant gases for both uniform and nonuniform pollutant concentration distributions have been computed and sensitivity studies conducted (Bergstrom, 1972b; Bergstrom and Viskanta, 1973c). Infrared cooling rates for a mixture of water vapor, carbon dioxide, and possible pollutant gases have been obtained. The results, for example, show that cooling rates for a mixture of H_2O , CO_2 , and C_2H_4 (ethylene) as a pollutant gas can be smaller than those for the mixture of water vapor and carbon dioxide alone. The downward directed thermal radiative flux, however, is increased. The results also show that large cooling rates may occur for nonuniform pollutant concentration distributions just above the point of maximum concentration. There are, however, numerical problems in predicting accurately the radiative flux divergence in the regions where the pollutant concentration changes sharply. This is analogous to large cooling rates which occur at cloud tops

(Korb and Zdunkowski, 1970) and is due to the large change in the net radiative flux above the point of maximum concentration.

Test Simulation--O'Neill Observations

The Great Plains Turbulence Study (the O'Neill Study; Lettau and Davidson, 1957) was held in 1954 and until recently was the most complete set of measurements of the temperature, velocities, humidity, and radiation fluxes reported. The results of the study have been analyzed in numerous publications and both Estoque (1963) and Sasamori (1970) have simulated the conditions for the fifth observational period. Since no comparable set of data existed for an urban area this situation was chosen to test the numerical model. The input data and values for the physical constants were taken from observed or published sources.

The simulation was started at 12:30 on August 24, 1954 (which was the beginning of the data). The temperature profiles at 12:30, 18:30, 24:30, 06:30, and 08:30 are illustrated in Figure 3. These distributions show the cooling of the surface, development of the nighttime inversion, breakup of the inversion, and development of the super adiabatic profiles. Comparison of the predicted temperature profiles with those determined by Sasamori (1970) and those observed show good agreement (Bergstrom, 1972b; Figure 6.2). Both analytical models predict a surface inversion (as did Estoque, 1963) which was not observed. However, Deardorff (1967) has suggested that the advection of cold air during the night may have counteracted any surface heating effects which were present at the O'Neill site.

The predicted and observed surface temperatures as a function of time are shown in Figure 4. As illustrated the predicted maximum surface temperatures are somewhat high; however, the general trend is well described. A comparison between predicted surface fluxes and those inferred by Suomi (Lettau and Davidson, 1957) showed fairly good agreement (Bergstrom, 1972b; Bergstrom and Viskanta, 1973a). Particularly encouraging is the finding that the radiative fluxes are within 10-20 percent of the observed. The natural aerosol conditions were not measured and were assumed to correspond to that of high visibility (Elterman, 1970). Both the solar and thermal radiant fluxes are underestimated. Sasamori (1970) also underpredicted the solar flux due to the uncertainties of the atmospheric conditions.

For the purposes of this study the analysis has shown to compare reasonably well with other one-dimensional studies as well as observed data and therefore establishes a high degree of confidence in the present analysis. The advantages of the model are that a constant flux layer is not assumed and the solar radiative flux does not have to be known *a priori* at the surface but is computed.

Urban Summer

The purpose of this experiment was to simulate the summer conditions of an urban area. The same initial variables as the O'Neill study with urban values of the parameters z_0 , M , Q (anthropogenic heat source parameter), α_s , and k_s were selected. The values for these parameters are summarized

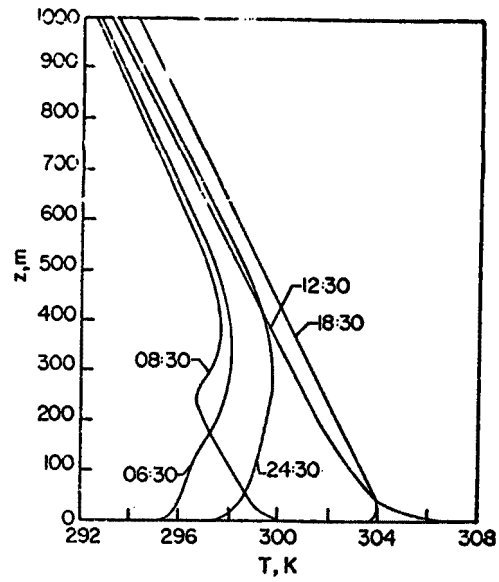


Figure 3. Temperature Profiles for the Test (The O'Neill) Simulation

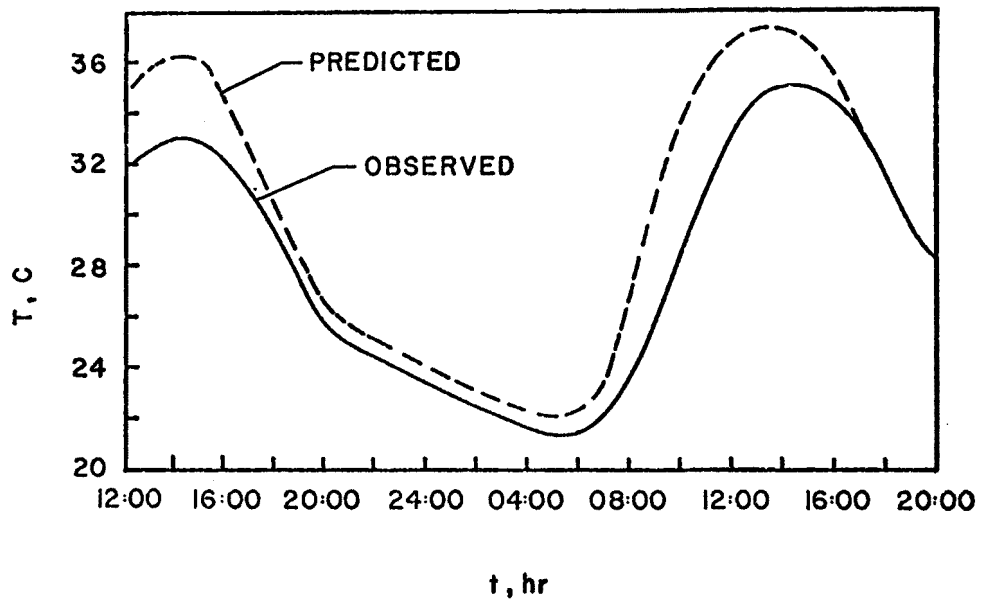


Figure 4. Comparison of Predicted and Observed (Lettau and Davidson, 1957) Surface Temperatures for Test Simulation

in Table 3. The general influences of these quantities on the urban surface temperature have been well documented, for example, Pandolfo, et al. (1971, p. 46, Figure 3.4-1) and Atwater (1972a, Figures 1 to 3), and they need not be repeated here.

The pollution parameters employed in the simulations are also shown in Table 3. The pollution source was taken to be that of an industrialized area in the Hartford, Connecticut study (Pandolfo, et al., 1971) and was found to give reasonable pollutant concentrations. A surface source was used since this was shown by Uthe (1971) to be approximately valid for the study of St. Louis, Missouri. As mentioned, pollution aerosol composition of quartz and carbon was selected from the aerosol model of Bergstrom (1972a). Ethylene was at first selected to simulate gaseous pollutants since Ludwig, et al., (1969) considered it to be representative of a typical hydrocarbon and because it was shown to have strong absorption characteristics in the 8 μ m to 12 μ m range. Obviously, other individual gases such as ammonia or gas mixtures could have been used to simulate the actual polluted conditions; however, in this initial study a more detailed description of gaseous pollutants was considered to be unwarranted. Also, ethylene was felt to be a "worst" case selection.

The results for the temperature and pollutant concentrations distributions as a function of both height and time are shown in Figures 5a and 5b, respectively, for the simulation with nonparticipating pollutants (Simulation 1). The temperatures are warmer at night than for the corresponding O'Neill study due to the change from a rural to an urban area. There is essentially no inversion and the warming trend during the computational period is enhanced. Temperature and pollutant concentration profiles for a simulation with radiatively participating pollutants (Simulation 5) are illustrated in Figures 5c and 5d, respectively. Note that the general trends are the same as the first simulation but the magnitude of the temperatures is different. The differences in the temperatures and pollutant concentrations are illustrated in Figures 5e and 5f, respectively. The difference is defined as the quantity in the simulation with nonparticipating pollutants minus the quantity in simulation with the radiatively participating pollutants. As shown, the temperatures are warmer at night by a maximum of 2.2C and cooler during the day by a maximum of 0.4C. Thus, the net effect is a reduction in diurnal temperature variation of 2.6C from a total of about 8 to 10C.

The surface solar and thermal radiant energy fluxes for the two experiments are presented in Table 4. It is clear from the table that the pollutants reduce the solar flux and increase the thermal flux. This indicates the reason why the surface temperature is cooler during the day and warmer during the night in the simulation with participating pollutants. The solar flux is reduced by about 10 percent on the first day and 20 percent on the second day (see Table 5 for results of winter simulations). This is well within the range of observed reduction of solar fluxes in an urban area (Peterson, 1969). The downward thermal radiation flux is increased by about 10 percent. However, the flux is also a function of the temperature profile, and the temperatures are somewhat warmer at night and cooler during the day in Figure 5c. This increase agrees well with the observations of

TABLE 3. URBAN AND POLLUTION PARAMETERS

(a) Urban Parameters		
z_o	100 cm	Pandolfo, et al., 1971
M	0	Pandolfo, et al., 1971
Q	9.09×10^4 erg/cm ² -s	McElroy, 1971, and Pandolfo, et al., 1971
α_s	2.2×10^{-2} cm ² /s	Pandolfo, et al., 1971
k_s	4.6×10^5 erg/cm-s-C	Pandolfo, et al., 1971
r_s	0.1	Ludwig, et al., 1969
(b) Pollution Parameters		
m_p^*	3 μ gm/m ² -s	Pandolfo, et al., 1971
Aerosol	20% by weight carbon	Bergstrom, 1972a
Gas	Ethylene	Ludwig, et al., 1969

*The aerosol source strength was used as listed in the table. The gaseous pollutant source strength was adjusted so that an aerosol concentration of 100 μ g/m³ equaled a gaseous pollutant concentration of 1.0 ppm at the surface.

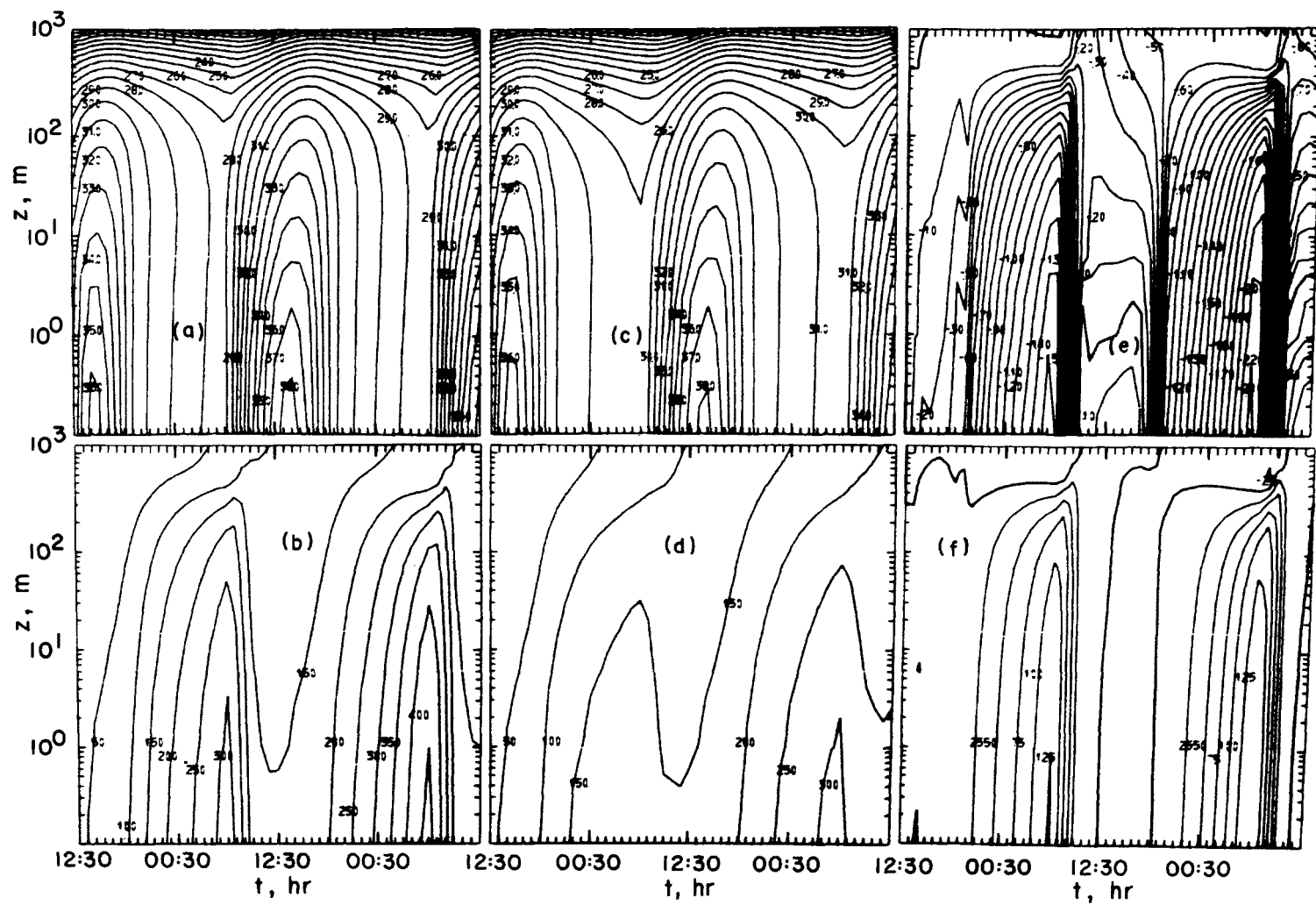


Figure 5. Isopleths for Simulations 1 and 5; Top Row are Temperatures (in C) and Bottom Row are Concentrations (in $\mu\text{g}/\text{m}^3$); Column 1 is Simulation 1, Column 2 is Simulation 5, and Column 3 is the difference Between Simulations 1 and 5

TABLE 4. COMPARISON OF THE SOLAR AND THE DOWNWARD THERMAL RADIANT FLUXES AT THE SURFACE FOR THE URBAN SUMMER SIMULATION 1 WITHOUT RADIATIVELY PARTICIPATING POLLUTANTS AND FOR SIMULATION 5 WITH RADIATIVELY PARTICIPATING POLLUTANTS

Time	Solar, $F(0)$, erg/cm ² -s		Thermal, $F^-(0)$, erg/cm ² -s	
	1	5	1	5
12:30	8.22×10^5	8.22×10^5	3.95×10^5	3.95×10^5
14:30	7.07×10^5	7.00×10^5	4.02	4.33
16:30	3.87×10^5	3.72×10^5	4.02	4.38
18:30	5.37×10^4	4.91×10^4	3.95	4.34
20:30			3.89	4.31
22:30			3.85	4.30
24:30			3.83	4.29
02:30			3.81	4.28
04:30			3.78	4.27
06:30	5.37×10^4	4.21×10^4	3.76	4.25
08:30	3.87×10^5	3.14×10^5	3.85	4.32
10:30	7.07×10^5	6.09×10^5	3.96	4.43
12:30	8.28×10^5	7.20×10^5	4.05	4.53
14:30	7.07×10^5	5.91×10^5	4.10	4.62
16:30	3.87×10^5	2.87×10^5	4.09	4.61
18:30	5.37×10^4	3.65×10^4	4.02	4.51
20:30			3.95	4.50
22:30			3.92	4.47
24:30			3.88	4.45
02:30			3.85	4.43
04:30			3.83	4.41
06:30	5.37×10^4	3.22×10^4	3.80	4.39
08:30	3.87×10^5	2.44×10^5	3.83	4.32
10:30	7.07×10^5	5.07×10^5	4.00	4.54
12:30	8.28×10^5	6.13×10^5	4.09	4.66

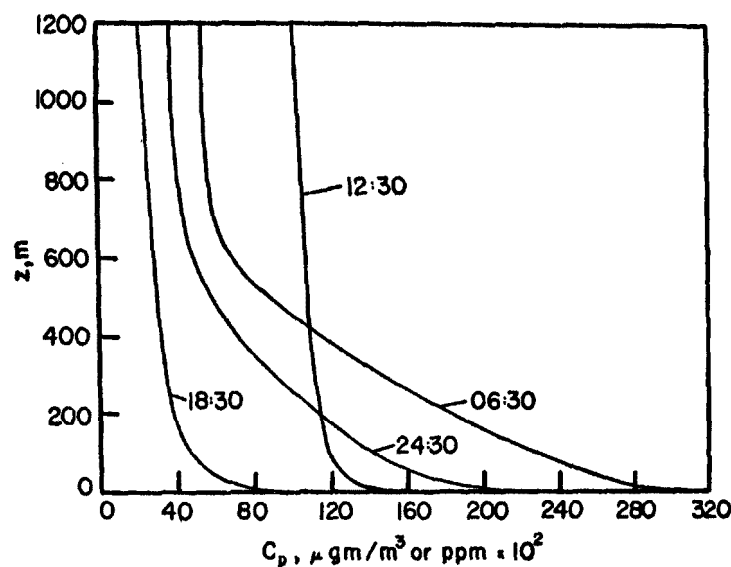


Figure 6. Pollutant Concentration Distributions for Summer Conditions with Radiatively Nonparticipating Pollutants (Simulation 1)

Oke and Fluggle (1972) who measured an increase of about 10 percent in the downward thermal flux in Montreal, Canada as compared to the surrounding countryside. Thus, the alterations in the radiant flux appear to be quite realistic and agree with available experimental evidence. However, it must be noted that Oke and Fluggle suggested that the increase in thermal flux could be due to the warmer temperatures and not necessarily to the presence of pollutants.

The effect of the radiation characteristics of the pollutants on the pollution concentrations is larger. The maximum surface concentration at night is reduced by $125 \mu\text{g}/\text{m}^3$ while there is little difference during the day between the concentrations with (Simulation 5) and without (Simulation 1) radiatively participating pollutants as shown in Figures 5b and 5d, respectively. The difference (simulation with minus simulation without radiatively participating pollutants) between the values in Figures 5b and 5d is shown in Figure 5f. This change is about 40 percent and represents a significant difference. The results of Figure 6 show more clearly that the pollutant concentrations increase at night due to the lower level of turbulence and reach a maximum in the early morning. This maximum is reduced by the good mixing of the next afternoon caused by the strong instability of the lower atmosphere. Since there is no allowance made in the model for horizontal advection, the pollutant level builds up and the same cycle is repeated again the next night. This type of pollutant dispersion is realistic. The worst times for dispersion of pollutants are in the late evening and early morning while the afternoon is generally the best. The breakup of morning haze layers is often observed (Utne, 1971).

The reduction in the pollutant concentration is due to the fact that the surface temperatures are warmer at night and the atmosphere is less stable. The diffusion of pollutants is therefore enhanced and the night buildup is thus reduced. The presence of pollutants affects the atmospheric radiation and alters the thermal structure. This influence changes the stability and enhances the ability of pollutants to disperse vertically.

Urban Summer Elevated Inversion

Since pollution episodes usually occur when an elevated inversion is present, the urban summer situation was investigated with a layer of stable air above 750 m. Because the vertical velocity was assumed to be zero, it was not possible to include a subsidence production term to maintain the inversion. Thus, this situation physically represents an elevated inversion which has been produced and the production process ceased. Experiments (not presented here) using the same starting time and velocities as the urban summer simulation (Simulation 1) showed that the stable region was destroyed by the strong afternoon mixing within one hour. Therefore, in order to investigate the effect of pollutants under inversion conditions, the simulations were started in the evening (17:00) and the velocities reduced to $\frac{1}{4}$ the values of the O'Neill data. The temperatures* at 6-hour intervals for Simulation 2 are shown in Figure 7. As shown, a radiative inversion develops at night due to the reduction in wind speed and corresponding lower diffusivities. During the next day the mixing destroys the stable layer while the elevated stable region inhibits the upward convective energy transport causing the surface temperature to be greater than in the simulation without the inversion (Simulation 1). The reduction in wind speed also tends to increase the surface temperature (see Figure 3). The results of the numerical experiment are very similar to those of the O'Neill simulation in that a radiative inversion develops, deepens, and is finally destroyed. The destruction of the surface stable region has occurred by 12:00 and the elevated stable region has been moved upward to a height of 900 m.

The corresponding temperature distributions for Simulation 6 with radiatively participating pollutants are shown in Figure 7b. Comparison of Figures 7a and 7b reveals that the radiative properties of the 20 percent carbon aerosol and ethylene pollutant gas have a pronounced effect on the temperature distribution. The surface inversion does not develop since the increase in thermal radiation increases the surface temperature about 2C. There is cooling at two different levels: (1) at the base of the nighttime stable layer at 100 m, and (2) at 650 m at the height of the elevated inversion. Both of these colder regions result from the thermal radiation cooling by the pollutants which are trapped beneath the stable regions. The temperature profiles show that a weaker elevated inversion forms at about 100 m instead of the radiative surface inversion. This weak elevated inversion has also been predicted by Atwater (1970) and Pandolfo, et al. (1971). This

*Temperature and concentration isopleths similar to those shown in Figure 5 are given by Bergstrom (1972b), but they are somewhat more difficult to interpret and are therefore not presented here.

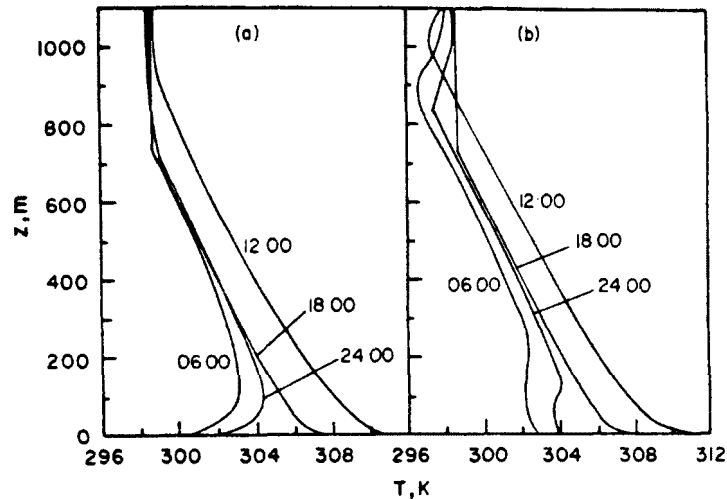


Figure 7. Temperature Distributions for Urban Summer Inversion Conditions:
 (a) Simulation 2 with Radiatively Nonparticipating Pollutants and
 (b) Simulation 6 with Radiatively Participating Pollutants
 Consisting of 20% by Weight Carbon Aerosol and Ethylene as
 Pollutant Gas

inversion then moves upward and weakens further during the early morning hours. The base of the stable region at 750 m also cools and is moved upward during the night.

The changes in the surface radiative flux for these two situations are similar to simulations previously discussed and are therefore not presented. The downward thermal radiative fluxes were larger while the solar radiative flux were 10 to 20 percent smaller in the simulation in which the radiative effects of pollution were considered.

The corresponding concentration profiles at six hour intervals are given in Figures 8a and 8b for the simulation without (Simulation 2) and with (Simulation 6) radiatively participating pollutants, respectively. As shown (Figure 8a) the pollutants build up near the surface owing to the presence of the surface stable layer. The elevated stable region forms a sharp boundary at 750 m. During the next day the pollution concentration near the surface is decreased as the destruction of the stable layer permits vertical mixing. At the same time the boundary due to the stable region is moved upward to above 800 m. Figure 8b indicates that there are two distinct concentration layers during the night. The first layer is from the surface to an altitude of about 100 m while the second is from 100 m to the base of the elevated inversion. These layers cause the radiative cooling which modifies the stable regions and changes the concentration profiles. At night the lower stable region is lifted from below 100 m to about 140 m in Figure 8b. The upper level stable layer is moved from 740 m to 820 m and by noon of the following day the stable region has moved upwards to a height of 1000 m in Figure 8a as compared to 820 m in Figure 8b. This clearly shows the significance of the radiative properties of air pollutants in modifying elevated inversions and changing the concentration levels.

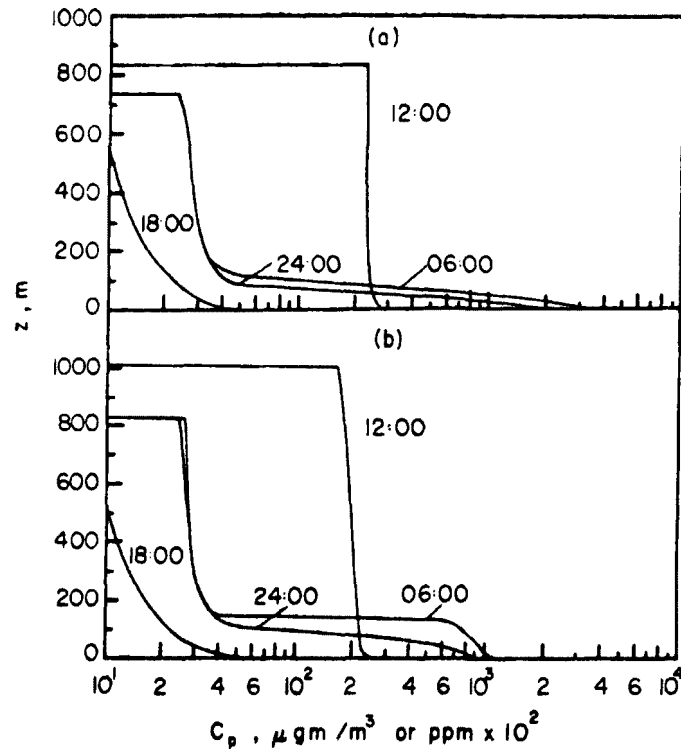


Figure 8. Concentration Profiles for Summer Inversion Conditions:
 (a) Simulation 2 with Radiatively Nonparticipating Pollutants,
 and (b) Simulation 6 with Radiatively Participating Pollutants
 Consisting of 20% by Weight Carbon Aerosol and Ethylene as
 Pollutant Gas

Urban Winter

In order to evaluate the influence of the change of season on the influence of air pollution on the thermal structure and pollutant dispersion an urban winter condition was simulated. The initial and free atmosphere conditions are given by Bergstrom (1972b). The only major changes are in the solar declination, initial temperature and humidity, and starting time. The solar declination is that of Nebraska in January. The initial temperature profile is presumed adiabatic at 17:00 with a surface temperature of about 15C. The free atmosphere conditions were taken from Atwater (1970) and the urban and pollution parameters were the same as before. The temperature isopleths for Simulation 3 without radiatively participating pollutants, for Simulation 7 with radiatively participating pollutants, and the difference between Simulations 7 and 3 are shown in Figures 9a, 9c, and 9e, respectively. The corresponding concentration isopleths are presented in Figures 9b, 9d, and 9f, respectively.

The difference between day and night temperatures without radiatively participating pollutants (Figure 9a) is only 4C which is less than that during the summer. This is in agreement with other investigators

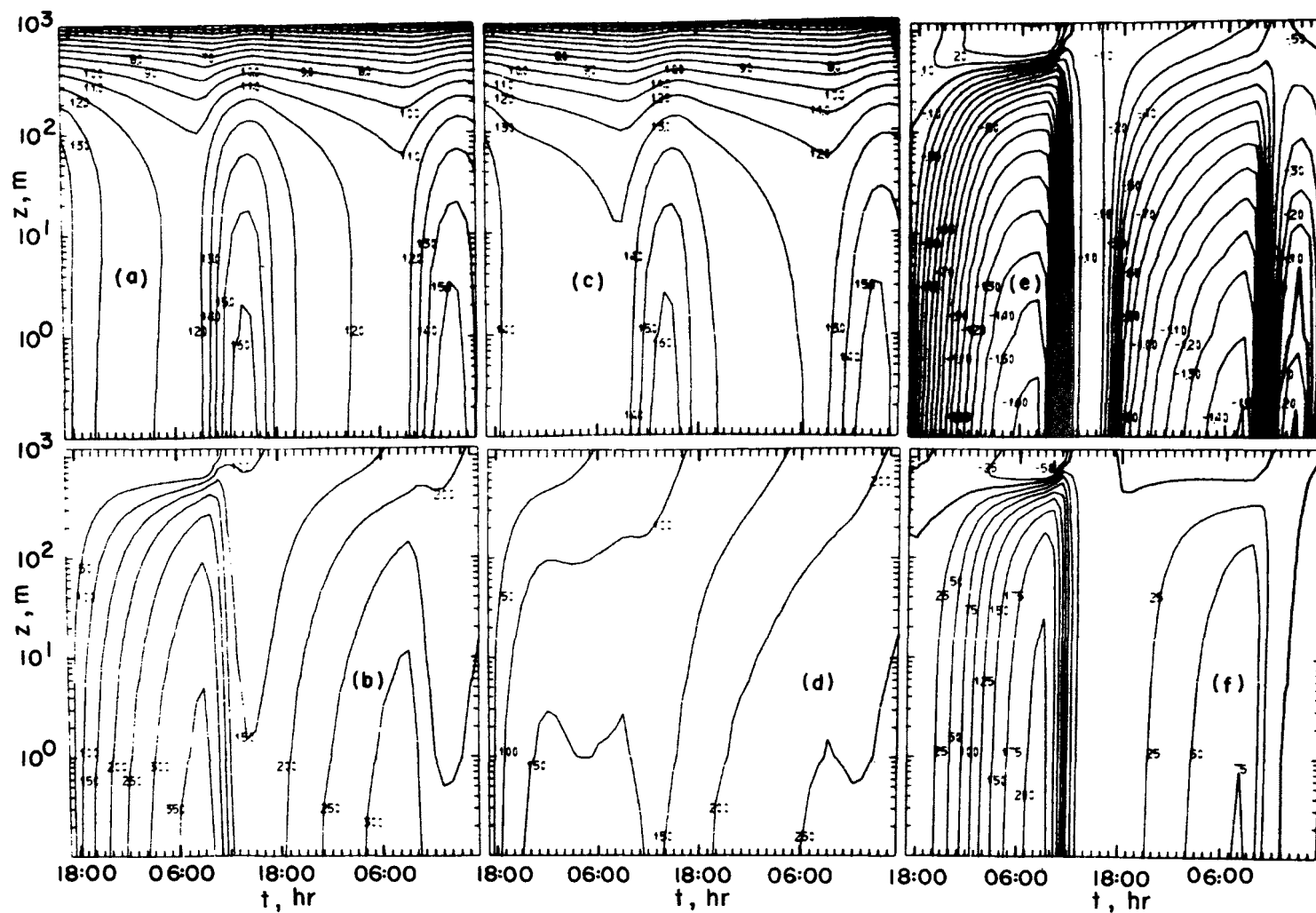


Figure 9. Isopleths for Simulations 3 and 7; Top Row are Temperatures in C (Celsius) and Bottom Row are Concentrations (in $\mu\text{g}/\text{m}^3$); Column 1 is Simulation 3, Column 2 is Simulation 7, and Column 3 is the Difference Between Simulations 3 and 7

(Pandolfo, et al., 1971). During the first night and next day the temperature differences in Figure 9c are warmer than in Figure 9a near the surface, the maximum being -1.6°C and the difference decreasing during the day to -0.1°C . The cycle is repeated during the second day as the temperatures are 0.2°C smaller during the second day in Figure 9c. At 20:00 and at an altitude of about 600 m the temperatures in Figure 9c are lower than in Figure 9a due to the infrared cooling by pollutants.

The surface fluxes for the solar radiation and the downward thermal radiation are shown in Table 5. The thermal radiation flux for the simulation with radiatively participating pollutants increases quite rapidly and is 8 percent higher within 2 hours. The average increase of thermal radiation flux is about 20 percent while the solar radiation is reduced by about 10 to 30 percent. This decrease in the solar flux is larger than the summer simulations (see Table 4) and is due to the fact that the average solar elevation angle is lower in the winter. The larger increase in the thermal radiation flux is apparently due to the lower specific humidities in the winter situation. The rate of increase of the thermal radiation flux slows down as the spectral region becomes relatively opaque.

The concentration differences are also similar to the urban summer simulation. The maximum concentration is reduced at night whereas the differences in concentration (Figure 9f) are very slight during the day. At an altitude of about 600 m during the first night the concentrations are higher when radiative participation of pollutants is accounted for. This results from the upward movement of the stable region due to the radiative cooling.

Urban Winter Elevated Inversion

In these simulations the conditions are identical to the experiments described in the previous subsection except that the temperatures are isothermal above 600 m. This situation roughly corresponds to conditions observed by Reagan and Herman (1971). Temperature and concentration isopleths are not presented here because their interpretation is more difficult, but they can be found elsewhere (Bergstrom, 1972b). The temperature and pollutant concentration profiles at six hour intervals are given in Figures 10 and 11. Comparison of Figures 10a and 10b reveals that the surface temperatures are warmer for Simulation 8 with radiatively participating pollutants than for Simulation 4 with nonparticipating ones.

In the experiment without radiatively participating pollutants the stable layer remains at about 600 m during the night, is moved up to about 1 km during the next day and remains there during the next night and is destroyed in the final day. The surface temperatures in the experiment with the radiatively participating pollutants are warmer than in the corresponding experiment (Simulation 3) without the inversion since stable layer prevented any turbulent energy transport from the planetary boundary layer to the free atmosphere. The maximum surface temperature during the second day is 15°C as compared to 19°C with and without radiatively participating pollutants, respectively.

TABLE 5. COMPARISON OF THE SOLAR AND THE DOWNWARD THERMAL RADIANT FLUXES AT THE SURFACE FOR THE URBAN WINTER SIMULATION 3 WITHOUT RADIATIVELY PARTICIPATING POLLUTANTS AND FOR SIMULATION 7 WITH RADIATIVELY PARTICIPATING POLLUTANTS

Time	Solar, $F(0)$, erg/cm ² -s		Thermal, $F_{\downarrow}^-(0)$, erg/cm ² -s	
	3	7	3	7
17:00	4.869×10 ⁴	4.87×10 ⁴	2.76×10 ⁵	2.76×10 ⁵
19:00			2.74	3.13
21:00			2.72	3.19
23:00			2.70	3.22
01:00			2.69	3.24
03:00			2.68	3.24
05:00			2.67	3.25
07:00			2.67	3.25
09:00	4.879×10 ⁴	3.92×10 ⁴	2.66	3.25
11:00	2.738×10 ⁵	2.18×10 ⁵	2.71	3.29
13:00	3.838×10 ⁵	3.08×10 ⁵	2.75	3.38
15:00	2.738×10 ⁵	2.07×10 ⁵	2.77	3.35
17:00	4.879×10 ⁴	3.56×10 ⁴	2.74	3.34
19:00			2.71	3.33
21:00			2.70	3.32
23:00			2.69	3.32
01:00			2.68	3.31
03:00			2.67	3.31
05:00			2.66	3.30
07:00			2.65	3.30
09:00	4.879×10 ⁴	2.99×10 ⁴	2.65	3.30
11:00	2.738×10 ⁵	1.64×10 ⁵	2.69	3.33
13:00	3.837×10 ⁵	2.37×10 ⁵	2.72	3.36
15:00	2.738×10 ⁵	1.57×10 ⁵	2.73	3.38
17:00	4.879×10 ⁴	2.75×10 ⁵	2.71	3.37

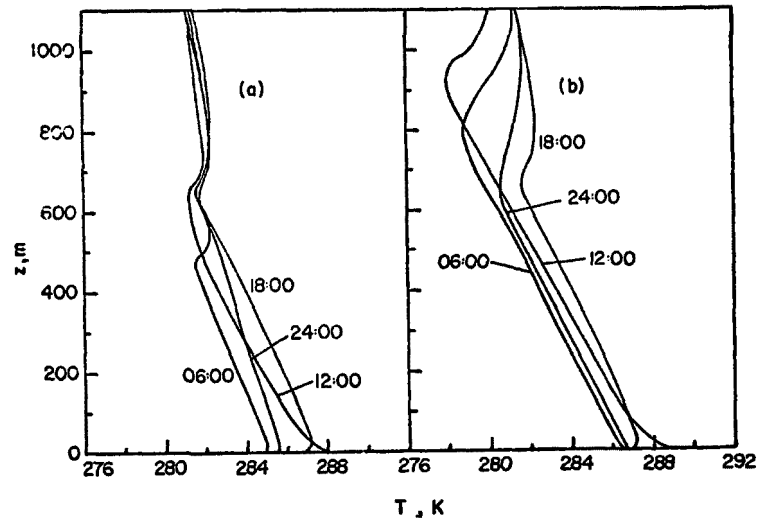


Figure 10. Temperature Distributions for Urban Winter Inversion Conditions:
 (a) Simulation 4 with Radiatively Nonparticipating Pollutants and
 (b) Simulation 8 with Radiatively Participating Pollutants
 Consisting of 20% by Weight Carbon Aerosol and Ethylene as
 Pollutant Gas

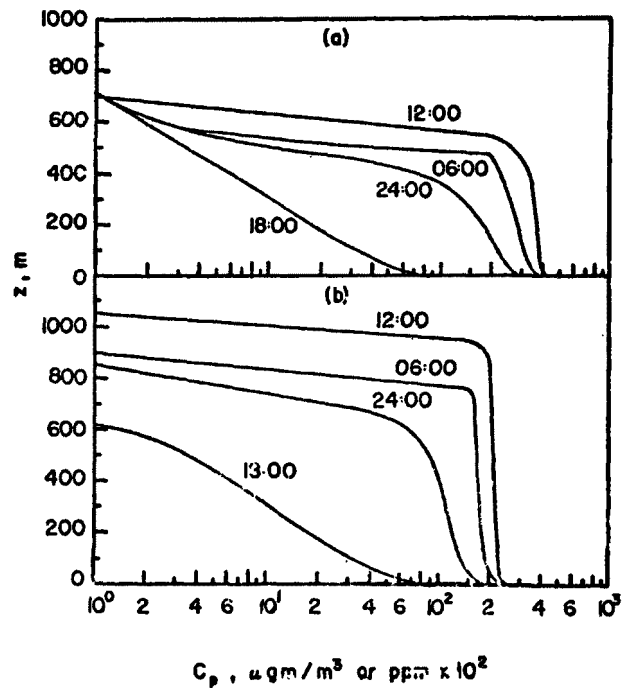


Figure 11. Concentration Profiles for Winter Elevated Inversion Conditions:
 (a) Simulation 4 with Radiatively Nonparticipating Pollutants, and
 (b) Simulation 8 with Radiatively Participating Pollutants
 Consisting of 20% by Weight Carbon Aerosol and Ethylene as
 Pollutant Gas

As in the summer simulation the radiative properties of air pollution (specifically the strong radiative cooling which occurs at the base of a sharp concentration gradient) cause the elevated stable region to move upward. Figure 10b shows that during the night the stable region is moved upward to about 1 km. The temperature and concentration differences illustrate this motion (Bergstrom, 1972b) since the temperatures are lower and concentrations are higher in the experiment with radiatively participating pollutants at about 500 m during the first night (from about midnight to about 08:00 in the morning). Consequently, this lifting of the stable layer results in a much lower surface pollutant concentration ($450 \mu\text{g}/\text{m}^3$ for the aerosol and 4.5 ppm for the gas versus $750 \mu\text{g}/\text{m}^3$ for the aerosol and 7.5 ppm for the aerosol with and without radiatively participating pollutants, respectively, at 06:00 in the morning). Again, the results clearly show the significance of the radiatively participating air pollutants in modifying elevated inversions and changing the concentration levels.

Effects of Other Pollution Parameters

In the previous subsection the various pollution parameters such as the radiative characteristics of the pollutant aerosol or gas were kept constant. The effects of pollutant aerosol alone, the effects of the gaseous pollutant alone, the choice of the gaseous pollutant, the source strength, and increased as well as decreased aerosol absorption on the thermal structure and pollution dispersion for the summer elevated inversion conditions have also been studied (Bergstrom, 1972b). This situation (urban summer elevated inversion) was selected for the simulations because the most serious pollution episodes occur under these conditions. Here, only the effects of the choice of gaseous pollutant and decreasing aerosol absorption are summarized while the isopleths and a more detailed discussion of the results are given by Bergstrom (1972b).

As explained before, ethylene was chosen since it can be considered to be a representative hydrocarbon and is a strong absorber in the 8 to 12 μm region. This choice, however, may be criticized as an oversimplification of an urban atmosphere. Therefore, to investigate the sensitivity of the predicted effects to the choice of gaseous pollutant, sulfur dioxide was considered. The emittance of sulfur dioxide (SO_2) as published by Chan and Tien (1971) was used. Comparison of results (Bergstrom, 1972b; Figures 6.4 and 6.11) show that when SO_2 is chosen as the pollutant gas, the influences due to the gaseous pollutant on the thermal structure are smaller than when C_2H_4 is considered as a gaseous pollutant. This is due to the fact that sulfur dioxide is a weaker absorber than ethylene. The surface temperatures are 0.75C warmer during the second night than for Simulation 2 with radiatively nonparticipating gaseous pollutant and the stable layer is moved slightly upward. However, the infrared cooling is not large enough to form a noticeable elevated inversion at 100 m. Thus, sulfur dioxide has the same qualitative effects as ethylene and only a magnitude of the results is altered. This finding is quite significant since a high concentration of sulfur dioxide beneath stable regions is often observed (Hoffert, 1972). However, it should be mentioned that while the concentrations of the gaseous pollutant are reasonable for hydrocarbons (Bergstrom, 1972b) they are somewhat too high for sulfur dioxide.

Since the radiative properties of aerosols are not well known, the amount of absorption by the aerosol was varied to determine their relative influence on the results. In this simulation it was assumed that the aerosol was nonabsorbing (i.e., only scattering). The effects due to aerosol absorption were clearly shown (Figures 6.4 and 6.15 of Bergstrom, 1972b). The temperatures during the day in Experiment 26 for a nonabsorbing aerosol are lower than those for Experiment 6 with an absorbing aerosol at altitudes higher than 10 m. This is due to the solar heating of the aerosols and is as large as 0.9C. The surface temperatures during the day are somewhat higher for the simulation with the nonabsorbing aerosol (Simulation 26) since then a larger fraction of the incident solar radiation reaches the surface.

Summary of Surface Temperature Differences and Surface Concentration

The differences in the surface temperatures for the urban summer simulations in the absence of an elevated stable layer are shown in Figure 12. For the conditions with ethylene alone the temperature is 1.5C warmer during the first night, reduces to 0.8C warmer during the day, and rises to 2.3C warmer during the next night. The simulation with only an aerosol present is essentially the same as the one with nonparticipating pollutants during the first night (1C cooler during the day, slightly cooler during the next night, and 2C cooler during the last day). This shows quite clearly the warming tendency of the gas (infrared properties) and the cooling tendency of the aerosol (solar properties). At night the presence of gaseous pollutants in the atmosphere increases the downward thermal radiative flux at the surface (see Table 4) and consequently raises the temperature while during the day the flux reaching the surface is reduced as a result of the attenuation of the incoming solar radiation, and the surface temperature is decreased.

The other temperature differences (Figure 12) lie between these two extremes. For the simulation with both ethylene and aerosol it is almost as warm during the night as with ethylene alone, but the surface is cooler during the day. The reduction of the source strength by one-third shows that temperature differences are decreased but not proportionately. In the simulation with sulfur dioxide the surface is cooler than in the simulations with ethylene due to the reduction in absorptance, but the influence of sulfur dioxide is still apparent. The effect of increased absorption by the aerosol increases the cooling of the surface; compare curves 3 and 4. Thus, in these simulations the aerosol and the gas had somewhat compensating effects. However, whether the effects cancel or one dominates over the other is clearly a function of the radiative properties of the gaseous and particulate pollutant and the atmospheric conditions. It should be mentioned that considerations by other investigators of the influence of aerosols on the temperature of the atmosphere have indicated that for most combinations of aerosol properties and surface reflectance the effect of increasing aerosol concentrations is one of cooling the earth-atmosphere system. However, there are combinations of aerosol absorption and surface reflection characteristics for which the effect of the aerosol is that of warming the earth-atmosphere system (Yamamoto and Tanaka, 1972) and since

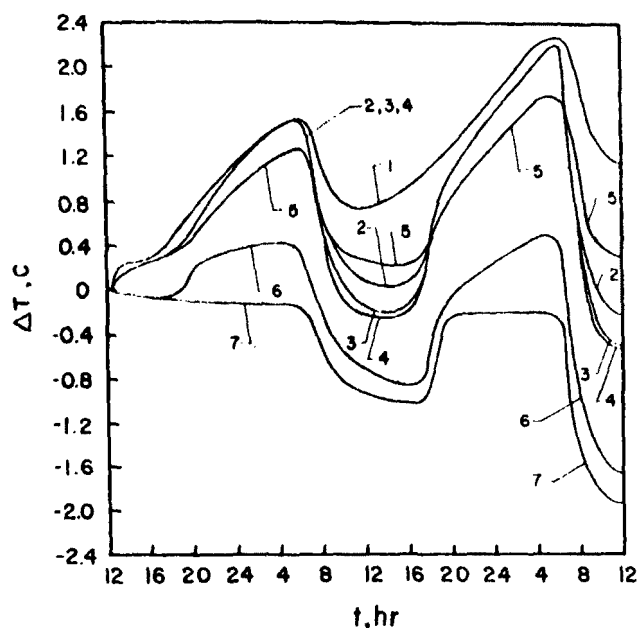


Figure 12. Surface Temperature Difference (Simulation with Radiatively Participating Pollutants Minus Simulation with Radiatively Nonparticipating Pollutants) for Summer Conditions:

Curve	Pollutant Gas	Aerosol	m_p ($\mu\text{g}/\text{m}^2\text{-s}$)
1	C_2H_4	Nonparticipating	1
2	C_2H_4	Nonabsorbing	1
3	C_2H_4	20% Carbon	1
4	C_2H_4	30% Carbon	1
5	C_2H_4	20% Carbon	1/3
6	SO_2	20% Carbon	1
7	Nonparticipating	30% Carbon	1

the absorption properties of the aerosols are not well known, this issue is still in doubt.

The surface pollutant concentrations as a function of time are shown in Figure 13 for the summer simulation without an elevated stable region. In all the simulations the concentration builds up to a peak during the night and is reduced during the morning and then increases again. Since no pollutant can escape from the planetary boundary layer, the average concentration increases during the two days. The highest pollutant concentrations are found in the simulations in which only the aerosol radiative properties are accounted for (Curve 1). These are only slightly higher than the values with radiatively nonparticipating pollutants (Curve 2). The concentrations for the simulation with sulfur dioxide show that the nighttime results are decreased due to the slightly warmer surface temperatures.

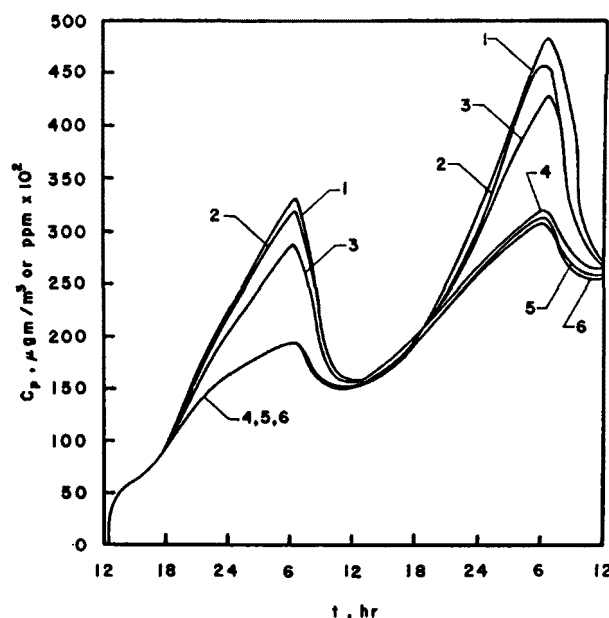


Figure 13. Surface Pollutant Concentration Variation with Time for Summer Conditions:

Curve	Pollutant Gas	Aerosol	m_p ($\mu\text{g}/\text{m}^2\text{-s}$)
1	Nonparticipating	20% Carbon	
2	Nonparticipating	Nonparticipating	
3	SO ₂	20% Carbon	
4	C ₂ H ₄	30% Carbon	
5	C ₂ H ₄	Nonabsorbing	
6	C ₂ H ₄	Nonparticipating	

There is a large reduction in pollutant concentrations in the simulations with ethylene as the pollutant gas owing to the decreased stability at night. The presence of the aerosols leads to a slight increase in the concentration.

The surface pollutant concentrations are shown in Figure 14 for the winter simulation without an elevated stable region. The general trend is the same as for the summer except in this case there is no perceptible difference between the results of the simulations without radiatively participating pollutants and that with 20 percent by weight carbon aerosol only. The reduction in concentration due to ethylene during the first night is somewhat larger than in the summer case (the surface temperature difference was also larger). Again, the variation in the aerosol absorption properties only had a slight effect during the day. In both Figures 13 and 14 the surface concentrations during the day were only slightly different for the

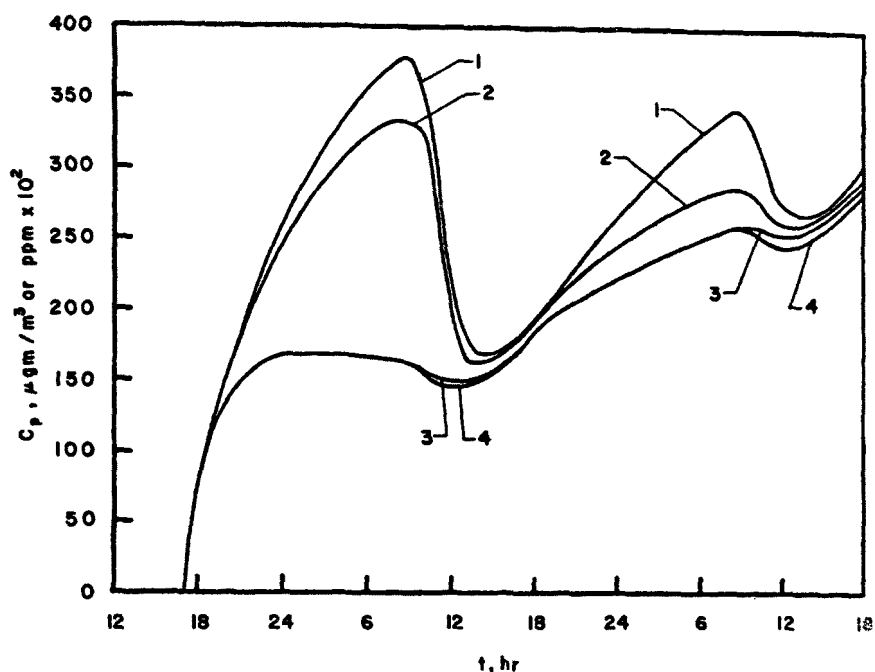


Figure 14. Surface Pollutant Concentration Variation with Time for Winter Conditions:

Curve	Pollutant Gas	Aerosol	m_p ($\mu\text{g}/\text{m}^2\text{-s}$)
1	Nonparticipating	Nonparticipating	1
1	Nonparticipating	20% Carbon	1
2	SO ₂	20% Carbon	1
3	C ₂ H ₄	30% Carbon	1
4	C ₂ H ₄	Nonabsorbing	1

various simulations. However, the concentrations at night were substantially different showing the influence of the infrared radiative properties of air pollutants.

The maximum daytime and nighttime differences from the radiatively non-participating Simulations 1 to 4 (see Table 2) are presented in Table 6. The results are similar to those already discussed and are only briefly commented upon. The temperature difference is negative at night in every instance when gaseous pollutants are considered to be radiatively participating and is due to warmer surface temperatures. The differences increase (become less negative) during the day and sometimes become positive as a result of the cooling effect of the aerosols. The concentration differences are always positive at night (the dispersion of pollutants is enhanced) and is negative only in five instances during the day (four of which are simulations where the pollutant gases are considered transparent). This

TABLE 6. MAXIMUM SURFACE DAYTIME (D) AND NIGHTTIME (N) TEMPERATURE AND POLLUTION CONCENTRATION DIFFERENCES (SIMULATION 1-SIMULATION 5, ETC.)

Simulation	Situation	$\Delta T, ^\circ C$				$\Delta C_p, \mu g/m^3$			
		N	D	N	D	N	D	N	D
5	A	-1.5	0.1	-2.2	0.4	125	0	125	0
6	B	-2.1	0.5	-2.8	0.9	>1000	0	>1000	0
7	C	-1.6	-0.1	-1.5	0.1	200	0	75	0
8	D	-1.6	-0.1	-3.0	-1.1	150	50	225	150
9	A	0	1.0	0	1.75	0	0	0	- 50
10	B	0	1.75	0.5	2.0	0	-200	- 200	-300
11	C	0	0.5	0	1.25	0	0	0	0
12	D	0	0.5	0	1.25	0	0	0	-100
13	A	-1.5	-0.75	-2.25	-1.5	100	0	150	0
14	B	-2.0	0	-3.0	-1.0	>1000	0	>1000	0
15	C	-1.5	-0.75	-1.5	-1.25	200	0	50	0
16	D	-1.5	-0.75	-3.25	-2.25	150	50	250	150
17	A	-0.25	0.75	-0.50	1.50	0	0	0	0
18	B	-0.25	0.5	-0.75	1.25	750	0	900	- 50
19	C	-0.25	0.5	-0.25	1.00	0	0	0	0
20	D	-0.25	0.5	-0.5	1.00	0	50	0	50
21	A	-1.25	0	-1.75	-0.5	---	---	---	---
22	B	-1.5	0	-2.5	0	---	---	---	---
23	C	-1.25	-0.25	-1.0	-0.5	---	---	---	---
24	D	-1.0	-0.25	-2.5	-1.25	---	---	---	---
25	A	-1.5	0	-1.75	0	100	0	150	0
26	B	-2.0	0.5	-2.75	0.5	>1000	50	>1000	0
27	C	-1.5	-0.25	-1.25	0	200	0	50	0
28	D	-1.5	0	-2.75	-1.0	150	50	200	150
29	A	-1.5	0	-2.25	0.5	100	0	100	0
30	B	-2.0	0.5	-2.75	1.0	>1000	50	>1000	50
31	C	-1.5	0	-1.5	0.25	200	0	50	0
32	D	-1.5	-0.25	-3.25	-1.5	150	50	200	150

illustrates the importance of the gaseous pollutants in influencing the pollutant dispersion. The table also clearly shows that the magnitude of the effect of air pollution on the temperature and pollutant concentrations is dependent upon the meteorological conditions, specific types of pollutants present, and their concentration distributions.

SECTION V

TWO-DIMENSIONAL MODELING OF THERMAL STRUCTURE AND POLLUTANT DISPERSION IN THE URBAN ATMOSPHERE

The results of simulations previously discussed have shown that a one-dimensional (vertical transport only) model is not adequate to describe the transport phenomena in the planetary urban boundary layer due to the neglect of advection. Therefore, work was initiated to develop a more realistic (two-dimensional) model for the thermal structure and pollutant dispersion. A two-dimensional transport model has been constructed for the prediction of the time dependent velocity, temperature, humidity, and pollutant concentration profiles. It should be emphasized that the flow field in the urban area is three-dimensional and would require a very fine grid for accurate simulation over the city. The increased computational time would be too expensive for numerical simulations on most present day computers. Since the primary objective of this research was to simulate the thermal structure, and two-dimensional model should provide a more realistic description than the one-dimensional one even though some details of the complicated urban flow field have been ignored. The temperature distribution should not be extremely sensitive to the wind profile. Advection, turbulent diffusion, and radiative transfer as well as radiative participation of pollutants are all included. Surface and elevated pollutant sources are considered, but chemical reactions and particle deposition have been neglected. In addition, pollutant removal processes have been neglected including washout by precipitation. The physical model and the numerical method of solution are described and some preliminary numerical results are presented in this section.

ANALYSIS

Physical Model

As in the case of the one-dimensional model, the earth-atmosphere system is assumed to be composed of four layers: (1) the "free" ("natural") atmosphere where the meteorological variables are considered to be time independent; (2) the "polluted" atmosphere (the planetary boundary layer) where the meteorological variables such as horizontal, vertical, and lateral wind velocities, temperature, water vapor and pollutant concentrations are functions of height, distance along the urban area, and time; (3) the soil layer where the temperature is assumed to be a function of depth and time only, and where the physical properties of the soil such as thermal conductivity and diffusivity, surface albedo, and thermal emittance vary with the distance along the horizontal axis; and (4) the lithosphere where the earth's temperature is assumed to be constant during a few day simulation period. The atmosphere is assumed to be cloud-free. The variation in topography of the urban area is not accounted for, i.e., the terrain

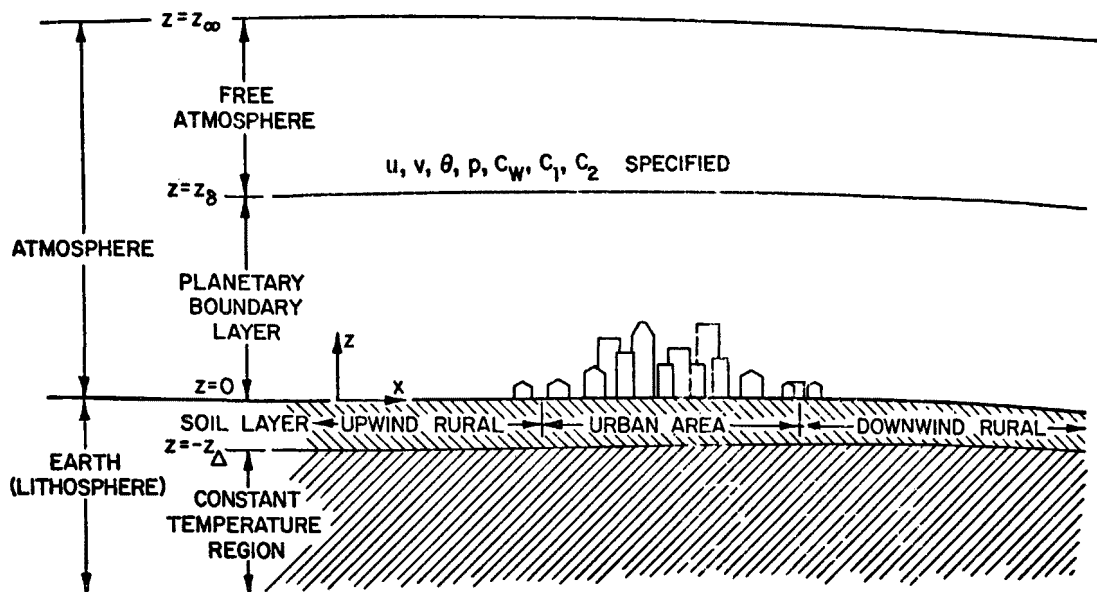


Figure 15. Physical Model and Coordinates

is assumed uniform even though the region modeled starts in a rural area, includes the city, and ends again in a rural area, see Figure 15.

In the free atmosphere the meteorological variables, including the geostrophic winds, are assumed to be constant. The primary forcing function for the model is the time-dependent solar irradiation.

In the polluted planetary boundary layer the transport of momentum, energy, and species is assumed to take place by vertical and horizontal advection as well as vertical and horizontal turbulent diffusion. In addition, energy is also transport by solar (short-wave) and thermal (long-wave) radiation. The interaction of both gaseous and particulate pollutants as well as natural atmospheric constituents with solar and thermal radiation is accounted for; however, the radiative energy transport in both the solar and thermal parts of the spectrum is assumed to be quasi-one-dimensional and will be described in greater detail in another subsection.

The coupling between the planetary boundary and soil layers is affected by energy and species balances at the atmosphere-soil interface. The horizontal variation of the urban parameters such as man-made heat and pollutant sources, surface solar albedo (reflectance) and thermal emittance, surface roughness, thermal diffusivity and conductivity of the soil and moisture parameter are prescribed but arbitrary functions of position along the urban area. The variation of these parameters with the time of day (i.e., solar angle for reflectance and emittance) is neglected. It is well recognized that the anthropogenic pollutant and heat emissions, for example, vary during the diurnal cycle. A more realistic modeling of the sources during the day

must await observational data. The surface temperature and pollutant concentrations are determined from energy (including heat conduction in the soil) and mass balances at the interface.

In the soil layer heat conduction is considered to be one-dimensional and only the variation of the physical properties of the soil with the distance along the urban area is accounted for. The water content in the soil is assumed to be constant. Data on the hydraulic properties of soil such as moisture potential, effective permeability, thermal liquid diffusivity, liquid and vapor diffusivities as well as the fraction of the area covered by concrete and buildings are not available (Eagelson, 1970) to warrant more detailed modeling of the moisture migration phenomena in the soil characterizing the urban area.

Governing Equations

The conservation equations of mass, momentum, energy, and species for a planetary boundary layer are well known (Haltiner and Martin, 1957; Plate, 1971). Turbulent eddy diffusivities (K-theory) are used to close the problem. The detailed discussion of the conservation equations appropriate for an unsteady two-dimensional planetary boundary layer is given by Johnson (1975). The final equations of the model are:

$$z = z_{\infty}$$

Natural Atmosphere

$$u, v, \theta, C_w, C_p = \text{constant}$$

$$z = z_{\delta}$$

Polluted Atmosphere

Mass:

$$\frac{\partial(\rho u)}{\partial x} + \frac{\partial(\rho w)}{\partial z} = 0 \quad (24)$$

Momentum (x-direction):

$$\begin{aligned} \rho \left(\frac{\partial u}{\partial t} + u \frac{\partial u}{\partial x} + v \frac{\partial u}{\partial z} \right) &= \rho f(v - v_g) + \frac{\partial}{\partial x} \left[\left(\mu + \rho K_{y,x}^M \right) \frac{\partial u}{\partial x} \right] \\ &+ \frac{\partial}{\partial z} \left[\left(\mu + \rho K_{x,x}^M \right) \frac{\partial u}{\partial z} \right] \end{aligned} \quad (25)$$

Momentum (y-direction):

$$\rho \left(\frac{\partial v}{\partial t} + u \frac{\partial v}{\partial x} + w \frac{\partial v}{\partial z} \right) = -\rho f(u - u_g) + \frac{\partial}{\partial x} \left[\left(\mu + \rho K_{y,x}^M \right) \frac{\partial v}{\partial x} \right]$$

$$+ \frac{\partial}{\partial z} \left[\left(\mu + \rho K_{y,z}^M \right) \frac{\partial v}{\partial z} \right] \quad (26)$$

Momentum (z-direction):

$$0 = + \frac{\partial p}{\partial z} + \rho g \quad (27)$$

Energy:

$$\begin{aligned} \rho c_p \left(\frac{\partial \theta}{\partial t} + u \frac{\partial \theta}{\partial x} + v \frac{\partial \theta}{\partial z} \right) = & \frac{\partial}{\partial x} \left[\left(k + \rho c_p K_x^\theta \right) \frac{\partial \theta}{\partial x} \right] \\ & + \frac{\partial}{\partial z} \left[\left(k + \rho c_p K_z^\theta \right) \frac{\partial \theta}{\partial z} \right] - \left[\frac{\partial F_z}{\partial z} - \dot{q} \right] \left(\frac{p_o}{p} \right)^{(\kappa-1)/\kappa} \end{aligned} \quad (28)$$

Species:

$$\begin{aligned} \frac{\partial C_n}{\partial t} + u \frac{\partial C_n}{\partial x} + w \frac{\partial C_n}{\partial z} = & \frac{\partial}{\partial x} \left[\left(D_n + K_x^{C_n} \right) \frac{\partial C_n}{\partial x} \right] \\ & + \frac{\partial}{\partial z} \left[\left(D_n + K_z^{C_n} \right) \frac{\partial C_n}{\partial z} \right] + \dot{C}_n \end{aligned} \quad (29)$$

Surface

$$z = 0$$

Soil Layer

Energy:

$$\frac{\partial T_s}{\partial t} = \alpha_s \frac{\partial^2 T_s}{\partial z^2} \quad (30)$$

$$T_s = \text{constant} \quad \text{at} \quad z = -z_\Delta$$

The upstream is taken in a rural area upwind of the city under consideration. At this location ($x = 0$) it is assumed that only background pollution is present and that the flow is fully developed, parallel and possessing no vertical velocity component. The meteorological variables at this point are predicted from the one-dimensional model given in Section IV.

At the edge of the outer flow, the meteorological variables are specified and held constant during the simulation; that is,

$$\chi(t, x, z) = \text{constant} \quad \text{at} \quad z = z_\delta \quad (31)$$

where χ represents the horizontal east velocity u , the horizontal north velocity v , the potential temperature θ , and the species concentration C_n . Implicit in those assumptions is the idea that the planetary boundary layer thickness remains essentially constant. At the bottom of the soil layer the temperature remains constant,

$$T_s(t, x, z) = \text{constant} \quad \text{at } z = -z_\Delta \quad (32)$$

At the earth's surface the velocities vanish,

$$u(t, z, x) = v(t, x, z) = w(t, z, x) = 0 \quad \text{at } z = 0 \quad (33)$$

Along the earth's surface (any x) the surface temperature at any instant of time t is predicted from an energy balance:

$$\begin{aligned} [1 - r_s(x)]F_s^-(x, 0) + e_t(x)F_t^-(x, 0) - e_t(x)\sigma T^4(x, 0) + \\ \left(k + \rho c_p K_z^\theta \right) \frac{\partial \theta}{\partial z} \Big|_0 + L_p \left(D_w + K_z^w \right) \frac{\partial C_w}{\partial z} \Big|_{z=0} - k_s(x) \frac{\partial T_s}{\partial z} \Big|_{z=0} \\ + Q(x) = 0 \quad \text{at } z = 0 \quad (34) \end{aligned}$$

This boundary condition is identical to that for the one-dimensional model [Eq. (10)] except the physical characteristics of the soil, and the urban parameters are functions of position. In the above equation the first two terms account for absorption of the solar and thermal radiation; the third term represents thermal emission; the fourth and fifth terms account for sensible and latent heat transfer by molecular and turbulent diffusion, respectively; the sixth term represents soil heat conduction; and the final term represents the anthropogenic heat sources.

The water vapor concentration C_w at the surface at any instant of time is prescribed by Halstead's moisture parameter M (Pandolfo, et al., 1971), see Eq. (11). In writing this equation the anthropogenic water vapor sources have been neglected (Bornstein and Tam, 1975).

The boundary condition for the pollutant concentration C_p , $p = 1, 2, \dots, N$, when a surface source is present is written by specifying the surface pollutant mass flux, m_p , i.e.,

$$m_p = - \left(D_p + K^p \right) \frac{\partial C_p}{\partial z} \Big|_{z=0} \quad \text{at } z = 0 \quad (35)$$

Downwind of the city (i.e., in the rural area) it is assumed that all of the meteorological and air pollution variables change very slowly, or

$$\frac{\partial \chi}{\partial x} = 0 \quad \text{at } x = L \quad (36)$$

This condition physically implies that the downstream rural area is far away from the city center and that nearly fully developed conditions have been reached.

Radiative Transfer Model

The radiative transfer model used is identical to that described in Section IV. However, since the water vapor content as well as the radiation characteristics of the earth surface vary along the horizontal direction, and since both the gaseous as well as the particulate pollutants are being advected downwind, it is obvious that the radiative transfer is not one-dimensional. Certainly, the radiation field in the urban atmosphere is three-dimensional. Because the analysis of multidimensional radiative transfer is very complex, it does not appear to be warranted at the present time. Hence, it is assumed that the radiative transfer can be approximated by a quasi-two-dimensional field based on the vertical temperature, water vapor, and pollutant distributions at several predetermined horizontal positions. The radiative fluxes were then evaluated at a few prescribed horizontal locations while interpolation was used to determine the radiative fluxes between the locations.

Turbulent Diffusivities

Specification of eddy diffusivities associated with the numerical modeling of the planetary boundary layer is a very difficult problem and has been a subject of a recent review (Oke, 1973a). In the numerical calculations, it was assumed that the semiempirical equations for the eddy diffusivities in the vertical (z) direction as given in Section IV were valid for the entire boundary layer. Implicit in those correlations are the definitions:

$$K_{x,z}^M \equiv K_{y,z}^M \equiv K^M, \quad K_z^\theta \equiv K^\theta \quad \text{and} \quad K_z^C = K^C.$$

Following the procedures adopted by other investigators (Olfe and Lee, 1971; McPherson, 1968) the eddy diffusivities in the horizontal direction are taken as constant, i.e.,

$$K_{x,x}^M = K_{y,x}^M = K_x^\theta = K_x^C \equiv K_x.$$

Even though K_x was small, inclusion of this horizontal turbulent diffusion improved the stability of the numerical method particularly under very stable meteorological conditions which occurred late at night and early in the morning.

It is recognized that the semiempirical eddy diffusivity equations which are used are based on similarity theories for equilibrium surface layers

and may not be applicable for nonequilibrium boundary layers. For example, when air flows over an inhomogeneous terrain the flow field changes and it takes time for the turbulence to "adjust." Available predictions (Shir, 1972) show that the adjusting process is rather slow, and the transition region, i.e., the region where the air is adjusting to the new surface condition, is a significant portion of the boundary layer above the new surface layer. In this region the eddy diffusivity is not only a function of height, but also a function of downwind distance from the change in conditions as well as parameters representing the different surface conditions.

Method of Solution

The finite-difference scheme used to obtain the numerical solution of the model equations was the alternating direction implicit (A.D.I.) method (Ames, 1969). The method has recently been applied (Roache, 1972) to many fluid flow problems.

The unsteady, two-dimensional conservation equations of momentum, energy, and species can be written in the following general form:

$$\frac{\partial \phi}{\partial t} + u \frac{\partial \phi}{\partial x} + w \frac{\partial \phi}{\partial z} = \frac{\partial}{\partial z} \left(K_z \frac{\partial \phi}{\partial z} \right) + K_x \frac{\partial^2 \phi}{\partial x^2} + \beta \quad (37)$$

In this equation, ϕ may represent the horizontal velocity $u(x,z,t)$, the lateral velocity $v(x,z,t)$, the potential temperature $\theta(x,z,t)$, or the n th species concentration $C_n(x,z,t)$. The turbulent eddy diffusivities (K 's) and the source term β , i.e., the Coriolis force term in the momentum equations or the divergence of the radiative flux in the energy equation, are known functions over the entire two-dimensional field.

The alternating direction implicit (A.D.I.) algorithm is a two-step method which employs two finite-difference equations which are used at successive time steps of increment $\Delta t/2$. The first equation is written explicitly in the x -direction while the second is written explicitly in the z -direction so that the results of the first time step are utilized in the second time step. The finite difference approximations for the spatial derivatives and the numerical algorithm are discussed in detail by Johnson (1975) and only the selection of a suitable grid and time steps is summarized here.

The grid spacing should be so selected as to optimize computer storage requirements with respect to the accuracy of the results. Taylor and Delage (1971) have shown that the accuracy of the solution depends on the type of vertical grid spacing. The spacing should be finer near the surface and courser aloft. Therefore, to improve the resolution near the surface, a logarithmic-uniform grid spacing was chosen in the vertical (z -direction). The logarithmic spacing extended from the earth surface to about 1 km and from there to the top of the boundary layer (~ 2 km) the spacing was uniform. This was accomplished by using the transformation: $\zeta = A \ln[(z+B)/B]$, where A and B were arbitrary constants. Equidistant spacing was chosen for the horizontal (x) direction.

The number of grid points and their spacing in the vertical (z) and the horizontal (x) directions can be varied. The only limitation is the computer core storage and computational time requirements. The results reported here have been obtained using 22 nodes in the vertical direction and 17 in the horizontal. With the many dependent variables (and numerous auxiliary functions) that need to be evaluated and stored at different times, the storage requirements exceed 128,000 bytes (octal) on the NCAR's CDC 7600 digital computer [maximum high speed core storage is 150,000 bytes (octal)]. A much finer grid spacing would necessitate using the slower disk storage (large core memory) and thereby increase the computer time requirements.

Three distinct time steps (one for the two-dimensional momentum equations, one for the other two-dimensional transport equations, and one for the one-dimensional transport equations) must be selected and a balance must be made between computational time and the actual time steps employed. Table 7 shows the values of some of the variables computed for different values of the time steps used to solve the respective finite difference equation. In this table, $\Delta t_{\text{Transport}}$ is the time step used to solve all unsteady two-dimensional conservation equations except the x- and y-momentum equations while $\Delta t_{\text{Momentum}}$ is the time step used for solution of the unsteady two-dimensional x- and y-momentum equations. Likewise, $\Delta t_{\text{C.N.I.}}$ is the time step used to solve all unsteady, one-dimensional transport equations by the Crank-Nicholson scheme at the upwind boundary. As can be seen in Table 7, the solutions to the partial differential equations appear to approach a limiting value as the time steps approach zero, thus implying convergence.

In order to obtain some appreciation for the sensitivity of the model numerical experiments were performed using different horizontal grid spacing and different vertical coordinate distributions. The details of these studies are given by Johnson (1975). It was found that the results were considerably more sensitive to the vertical spacing than to either the time step or the horizontal spacing particularly at the surface. This should be expected since the gradients near the surface are quite large and hence sensitive to the vertical grid size. Two numerical experiments were also performed to check the model for downwind error propagation. This was accomplished by positioning a small city at different horizontal locations (Johnson, 1975). If the numerical scheme was behaving correctly, then the upwind and downwind results would be independent of the horizontal location of the center of the city. The results showed that the meteorological variables downwind of the city are independent of the horizontal position of the city and yield identical results regardless of the location of the urban center.

RESULTS AND DISCUSSION

The unsteady two-dimensional transport model developed has been tested and some numerical experiments have been performed. Some of these preliminary results are presented and discussed in this section of the report. Shortcomings of the model are indicated and improvements are suggested.

TABLE 7. EFFECT OF TIME STEP ON SELECTED METEOROLOGICAL VARIABLES AT THE CENTER OF THE CITY ($z_0 = 1$ m), $z = 1$ m, and $t = 1$ hr; SIMULATION STARTED AT 12:00, COMPUTER-CDC 6600 (C_1 DENOTES THE AEROSOL AND C_2 THE POLLUTANT GAS CONCENTRATIONS)

Meteorological Variable		Time Steps		
	$\Delta t_{\text{Transport}}$	45.0 s	20.0 s	15.0 s
	$\Delta t_{\text{Momentum}}$	22.5 s	15.0 s	7.5 s
	$\Delta t_{\text{C.N.I.}}$	11.25 s	7.5 s	3.75 s
θ	(K)	305.256	306.315	306.318
u	(m/s)	1.0009	0.9415	0.9414
v	(m/s)	1.0067	0.9417	0.9419
w	(cm/s)	4.6918	4.3644	4.3606
C_w	(kg/m ³)	0.02068	0.01994	0.01994
C_1	($\mu\text{g}/\text{m}^3$)	546.80	544.15	544.30
C_2	($\mu\text{g}/\text{m}^3$)	546.80	544.15	544.30
Computational Time	(s)	182.4	215.8	316.2

Prior to modeling the unsteady thermal structure and pollutant dispersion in the urban atmosphere the model was used to simulate some of the experimental observations of the Great Plains Turbulence Study (Lettau and Davidson, 1957). Since the test simulations using the one-dimensional model have already been discussed in Section IV, the details are omitted here but they are given elsewhere (Johnson, 1975). The results obtained were very similar to those already discussed. It was found that perturbation of the surface roughness parameter z_0 from 0.01 to 0.05 cm caused a slight change in the peak surface temperature. On the other hand, changing Halstead's moisture parameter from $M = 0.01$ to $M = 0.1$ significantly increased the evaporation and resulted in a much cooler (about 7C) surface temperature during the day.

Parameters and Initial Conditions Used in the Simulations

In the preliminary numerical experiments the city of St. Louis, Missouri was modeled and the simulations were performed for typical summer conditions. The simulations discussed in the report are summarized in Table 8. The effects of wind speed, choice of gaseous pollutant, pollutant source flux, and the type of pollutant source flux and urban heat flux distributions along the urban area were studied. The horizontal grid spacing Δx was selected to be 1.5 km. With 17 nodal points, the total horizontal extent of the area modeled was only 24 km, somewhat smaller than the size of the St. Louis Metropolitan area. Since for most of the simulations, the geostrophic wind speeds were relatively low, the vertical grid spacing with the first point located at 5 m above the ground was used.

The urban surface parameters and their assumed variation along the area are presented in Table 9. The horizontal distribution was established by selecting the values of the parameters at the rural and urban center locations and, for the lack of any other data or information, a Gaussian distribution curve was fitted between the rural and urban positions. In the table, the values of k_g and α_g were obtained by computing the urban-rural values of thermal admittance from a recent study carried out over St. Louis by Dabberdt and Davis (1974) with the soil heat capacity data of Pandolfo, et al. (1971). The thermal emittance, e_t , were obtained from Wolfe (1964) and these values were representative of foliage, concrete, asphalt, and bricks. The solar reflectance of the surface, r_s , were obtained from albedo measurements obtained by Dabberdt and Davis (1974) over St. Louis. The surface roughness parameter of 1 m at the urban center was taken from Pandolfo, et al. (1971). This same value was also used in the simulations with the one-dimensional model. The rural value of 20 cm was selected because it was considered to be a more realistic value of the undulating countryside surrounding the St. Louis metropolitan area. Finally the moisture parameter M was estimated for the model using the results of Johnson (1975) as a basis.

Figure 16 illustrates the assumed Gaussian and rectangular distributions for the anthropogenic heat source Q along the urban area. The pollutant source fluxes had similar type of distributions. To compare the results, the areas under the two curves had to be equal. This was accomplished by first evaluating the area under the rectangular distribution and then determining the Gaussian distribution by adjusting the value of the standard deviation.

TABLE 8. SUMMARY OF SIMULATIONS PERFORMED TO STUDY THE EFFECTS OF RADIATIVE PARTICIPATION ON POLLUTANT DISPERSION AND THERMAL STRUCTURE IN ST. LOUIS, MISSOURI, DURING THE SUMMER, COMPUTER-CDC 7600

Simulation Number	Distribution Q, m_1, m_2	u_g (m/s)	v_g (m/s)	Pollutant Gas	Mean Pollutant Source Flux ($\mu\text{g}/\text{m}^2\text{-s}$)	Radiative Interaction
1	Gaussian	12	8	C_2H_4	2.5	Nonparticipating
2	Gaussian	12	8	C_2H_4	2.5	Participating
3	Gaussian	6	4	C_2H_4	2.5	Nonparticipating
4	Gaussian	6	4	SO_2	2.5	Participating
5	Gaussian	6	4	C_2H_4	2.5	Participating
6	Gaussian	6	4	C_2H_4	5.0	Participating
7	Rectangular	6	4	C_2H_4	2.5	Nonparticipating
8	Rectangular	6	4	C_2H_4	2.5	Participating

TABLE 9. VARIATIONS OF THE URBAN SURFACE PARAMETERS ALONG THE HORIZONTAL DIRECTION ASSUMED FOR THE SIMULATIONS

Node No.	Horizontal Location, x(km)	r_s	e_t	k_g (W/m-K)	α_s ($\text{m}^2/\text{s}) \times 10^7$	M	z_o (m)
1	0	0.180	0.900	0.100	25.00	0.1000	0.200
2	1.5	0.166	0.913	0.153	20.11	0.0886	0.307
3	3.0	0.153	0.924	0.200	15.24	0.0780	0.440
4	4.5	0.142	0.933	0.296	10.67	0.0687	0.591
5	6.0	0.132	0.941	0.372	6.70	0.0608	0.744
6	7.5	0.126	0.946	0.438	3.62	0.0549	0.877
7	9.0	0.121	0.949	0.483	1.67	0.0512	0.968
8	10.5	0.120	0.950	0.500	1.00	0.0500	1.000
9	12.0	0.121	0.949	0.483	1.67	0.0512	0.968
10	13.5	0.126	0.946	0.438	3.62	0.0549	0.877
11	15.0	0.132	0.941	0.372	6.70	0.0608	0.744
12	16.5	0.142	0.933	0.296	10.67	0.0686	0.591
13	18.0	0.153	0.924	0.200	15.24	0.0780	0.440
14	19.5	0.166	0.913	0.153	20.11	0.0886	0.307
15	21.0	0.180	0.900	0.100	25.00	0.1000	0.200
16	22.5	0.180	0.900	0.100	25.00	0.1000	0.200
17	24.0	0.180	0.900	0.100	25.00	0.1000	0.200

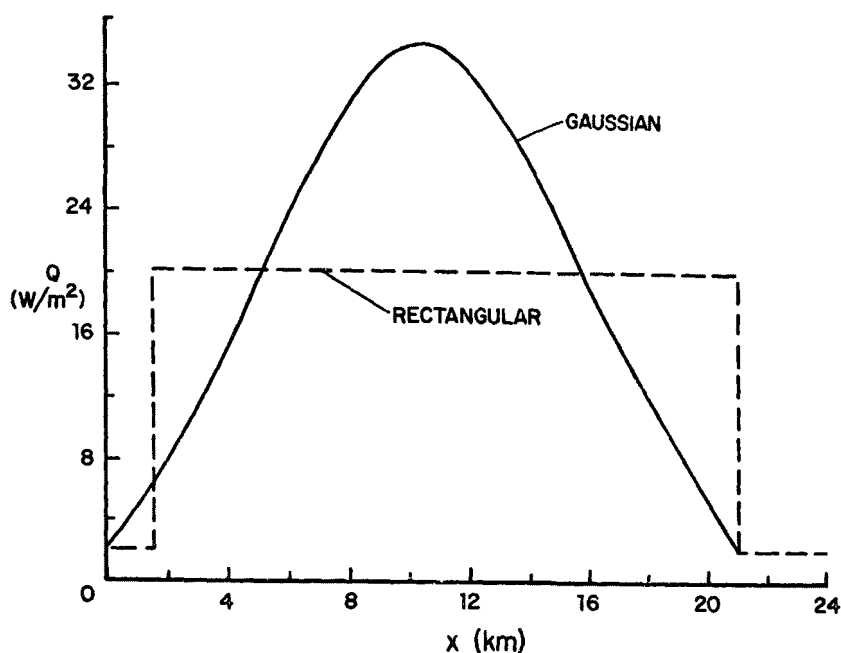


Figure 16. Comparison of Rectangular and Gaussian Anthropogenic Heat Source Distributions Along the City

The pollutant source flux was modified to yield typical concentrations observed in the urban atmosphere (Stern, et al., 1972). The mean man-made urban heat source parameters (based on the rectangular distribution) of 20 W/m^2 was characteristic of Columbus, Ohio (McElroy, 1972) while the rural value of 2 W/m^2 was obtained for the whole of West Germany (Oke, 1973a).

The simulations were started at noon (12:00) solar time and continued for a 24-hour period. The initial conditions used in Simulations 1 and 2 were identical to those employed for the one-dimensional model and were imposed over the entire model (no x-variation). The data were taken from Lettau and Davidson (1957) for August 24, 1954. For the remaining simulations (3 through 8), the initial horizontal and lateral velocity fields were simply divided by two while the other variables remained the same. The pollutant concentration profiles were initialized to a constant background value of 50 ppm. In the experiments, the large-scale synoptic gradients were zero thus allowing the use of time-independent boundary condition at the top of the planetary boundary layer for temperature, pressure, water vapor, and pollutant concentrations. The lower soil boundary beneath the surface ($z = -z_{\Delta} = -50 \text{ cm}$) was held constant at a temperature of 295.5 K (Pandolfo, et al., 1971), and the soil layer grid spacing was 5 cm. The time step for the momentum equations was 22.5 s while the upwind boundary condition time step was 11.25 s. Both time steps were held constant. The time step for the transport equations was equal to 45 s during the day (05:00 to 20:00) and during the night (20:00 to 05:00) the value was raised to 90 s. The computational time per 24-hour simulation on the NCAR CDC 7600 computer took about 8 minutes.

Some Difficulties Encountered

Many problems were encountered when the entire model was assembled and simulations were attempted. Only a few of the more important ones will be mentioned here. A more detailed discussion is given by Johnson (1975).

Late in the afternoon when the atmosphere changed from free convection conditions to forced convection conditions (the turbulent diffusivity equations changed from the free convection to the forced convection correlations), a difficulty arose in that the diffusivities were not continuous (see Table I). As the Richardson number approached Ri_T from the left (negative side) the diffusivities predicted for free convection conditions were smaller than those predicted when Ri_T was approached from the right under forced convection conditions. This caused a pollutant buildup at the surface near sundown that was physically unrealistic. As yet, this problem has not been corrected, and all that can really be said is that an improved turbulence model is required.

Late at night it was found that the atmosphere became quite stable especially in the simulations with the lower geostrophic winds ($u_g \approx 2.4$ m/s, $v_g \approx 1.6$ m/s) and a very deep surface inversion resulted. The Richardson numbers computed for these cases were found to exceed Ri_C which caused the diffusivities predicted from the Pandolfo, et al. (1971) eddy diffusivity-Richardson number correlations to be meaningless. In order to overcome this difficulty, the cubic polynomial developed by O'Brien (1970) and used by Bornstein (1973) was employed for diffusivity prediction in the transition layer. This polynomial can be written as (Bornstein, 1973; p. 45)

$$K(z) = K(H^*) + \left[\frac{z-H^*}{H^*-h} \right]^2 \left\{ \left[K(h) - K(H^*) + (z-h) \left[\left(\frac{\partial K}{\partial z} \right)_h \right. \right. \right. \right. \\ \left. \left. \left. + 2 \left(\frac{K(h)-K(H^*)}{H^*-h} \right) \right] \right] \right\} \quad (38)$$

where H^* is an assumed level, $K(H^*)$ takes on a constant small value, and h is the top of an assumed constant flux layer.

The original diffusivity model was employed in the entire boundary layer except under stable conditions. Stable conditions were assumed to exist when the average Richardson number in the lowest 25 meters of the atmosphere was greater than zero. When this condition was reached, the original diffusivity model was used only near the surface while the polynomial was employed in the transition layer. Otherwise, the original diffusivity model was used throughout the entire boundary layer. If the Richardson number exceeds 3/8, it was automatically reset to this value so that unreasonable values would not be predicted under very stable conditions from the Pandolfo, et al. (1971) correlations.

Late at night when very stable conditions existed, slight oscillations in the horizontal (u) velocity component appeared near the surface. At this

time the velocity was quite small (≈ 1 m/s) at the first grid point near the surface and small oscillations with a magnitude of about $\pm 5\%$ were observed which always disappeared soon after sunrise. It should also be mentioned that these oscillations did not show up in the v or w velocity components unless they had already become very large in u . It was felt that these oscillations were related to discretization errors which become quite prevalent when attempting to predict small numbers with high accuracy. Other investigators have noted the presence of similar oscillations and some attribute them to the finite-difference approximations (Yu, 1973; p. 27). Yu (1973) has employed a three-point horizontal filter to suppress the high frequency components of these oscillations which are thought to be the principal cause of these horizontal instabilities.

Components of the Energy Budget at the Surface

The surface temperature is a very important parameter as far as the "forcing" of the model is concerned. For this reason, the surface energy budget, Eq. (34), and the budget components are considered first. Figures 17 and 18 illustrate the variation along the urban area of the energy budget components at the surface for Simulation 3 at midnight (24:00) and noon (12:00) of the next day, respectively. Inspection of Figure 17 shows that the emitted (q_e) and the absorbed thermal (q_{at}) fluxes are the dominant components. The turbulent (q_t), the latent (q_l), the ground conduction (q_g), and the anthropogenic heat (Q) fluxes are significantly smaller. The results indicate that for the meteorological conditions of Simulation 3 thermal radiation dominates in establishing the surface temperature at midnight and in the early morning of the next day. The variations of the various energy budget components along the urban area are found to be relatively small.

At noon (Figure 18) the absorbed solar flux (q_{as}) is the largest term in the energy balance and the anthropogenic heat source (Q) is the smallest. At the urban center ($x = 10.5$ km) the heat conduction term into the soil (q_g) amounts to about 10 percent of the absorbed solar flux. All of the components of the energy budget that were computed are important, and they must be included in the surface energy budget in order to correctly predict the surface temperature.

The only two components of the energy budget which depend to any great degree on the wind speed are the turbulent (q_t) and the latent (q_l) fluxes. Their diurnal variation is illustrated in Figures 19 and 20. The results show that, as expected, these two fluxes are quite sensitive to the wind speed. The turbulent flux is higher at the urban center than at the upwind rural location because of increased turbulent mixing over the city. Johnson (1975) has found that the latent flux is quite sensitive to the Halstead's moisture parameter. Since the parameter is larger at the upwind rural location than at the urban center (see Table 9) the latent heat flux is also larger there. The results also show that for the conditions of Simulation 3 condensation occurs at the surface late at night.

The energy budget components at the surface for simulations with radiatively participating pollutants and the differences between the radiatively non-interacting and interacting pollutants are discussed in a later section.

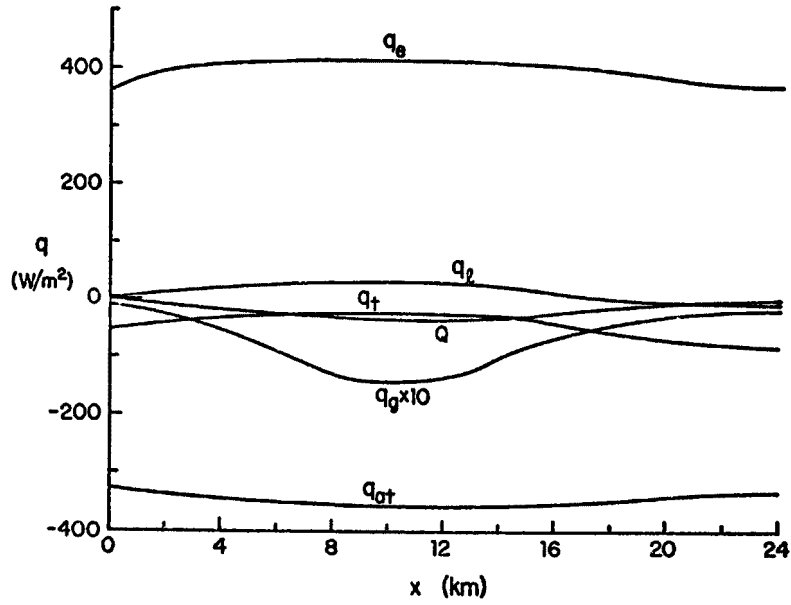


Figure 17. Variation of the Surface Energy Flux Components (q_t --Turbulent, q_l --Latent, q_e --Emitted, q_{at} --Absorbed Thermal, q_g --Ground Conduction, Q --Anthropogenic Heat Source) for Simulation 3 at 24:00 of the First day

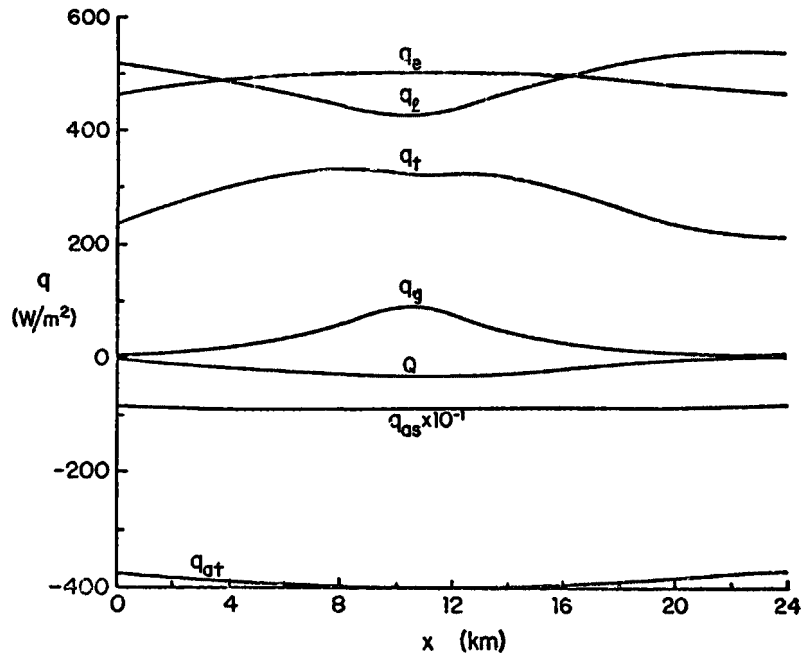


Figure 18. Variation of the Surface Energy Flux Components (q_t --Turbulent, q_l --Latent, q_e --Emitted, q_{as} --Absorbed Solar, q_{at} --Absorbed Thermal, q_g --Ground Conduction, Q --Anthropogenic Surface Heat Source) for Simulation 3 at 12:00 of the Second Day

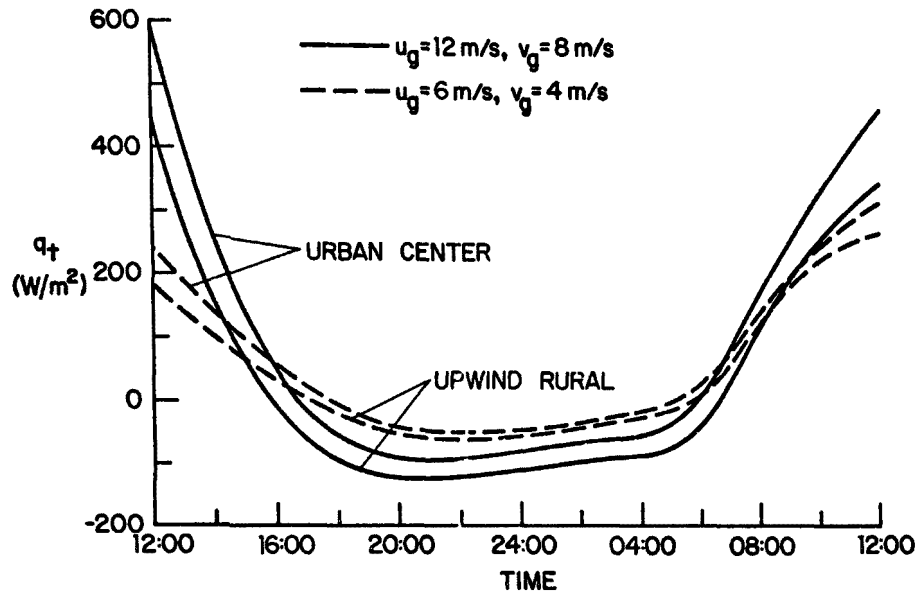


Figure 19. Effect of Wind Speed on the Diurnal Variation of the Turbulent Heat Flux at the Surface for Simulations 1 and 3

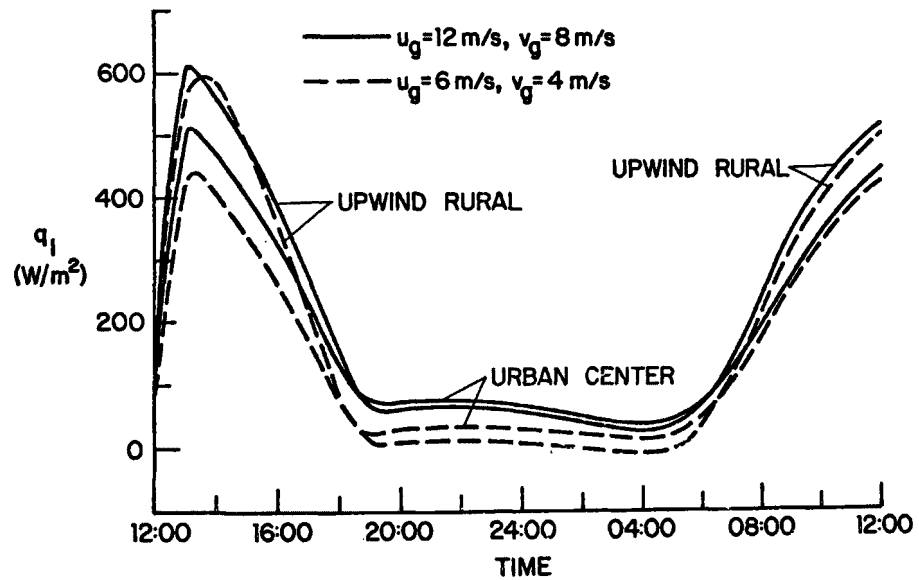


Figure 20. Effect of Wind Speed on the Diurnal Variation of the Latent Heat Flux at the Surface for Simulations 1 and 3

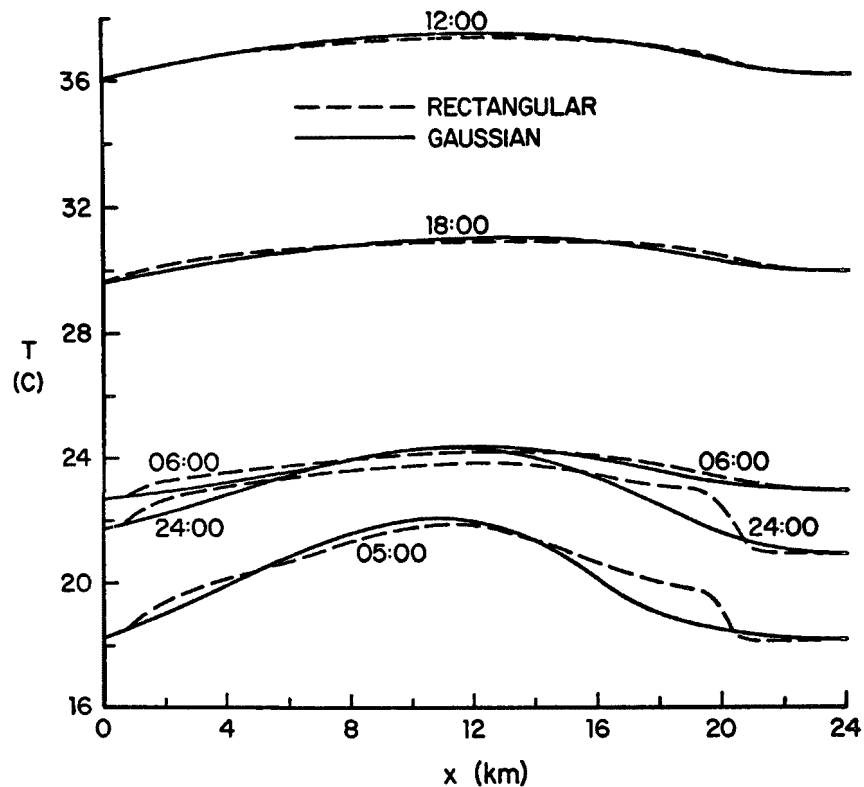


Figure 21. Comparison of Surface Temperatures for Gaussian (Simulation 3) and Rectangular (Simulation 7) Distributions of Anthropogenic Heat and Pollutant Sources Along the City

Surface Temperature

Simulations with Radiatively Nonparticipating Pollutants

A comparison of the surface temperatures for the Gaussian (Simulation 3) and the rectangular (Simulation 7) distributions of anthropogenic heat sources is illustrated in Figure 21. The figure shows that the difference between the two results is only about 1°C and the maximum difference occurs late at night (05:00) when the anthropogenic heat source is a significant component of the energy budget. At noon (12:00) the surface temperatures in the city differ by only about 0.1°C. The surface temperatures predicted along the urban area are consistent with the urban heat source distribution, see Figure 16.

The diurnal variation of the surface temperature for Simulations 1 and 3 is illustrated in Figures 22 and 23, respectively. Temperatures at four positions along the urban area--"upwind rural" (node 1, $x = 0$ km), "upwind residential" (node 4, $x = 4.5$ km), "urban center" (node 8, $x = 10.5$ km), and "downwind residential" (node 12, $x = 16.5$ km)--are shown in the figures. Inspection of the figures reveals that the amplitudes of the diurnal surface temperature variations are smaller for the higher wind speeds (Simulation 1).

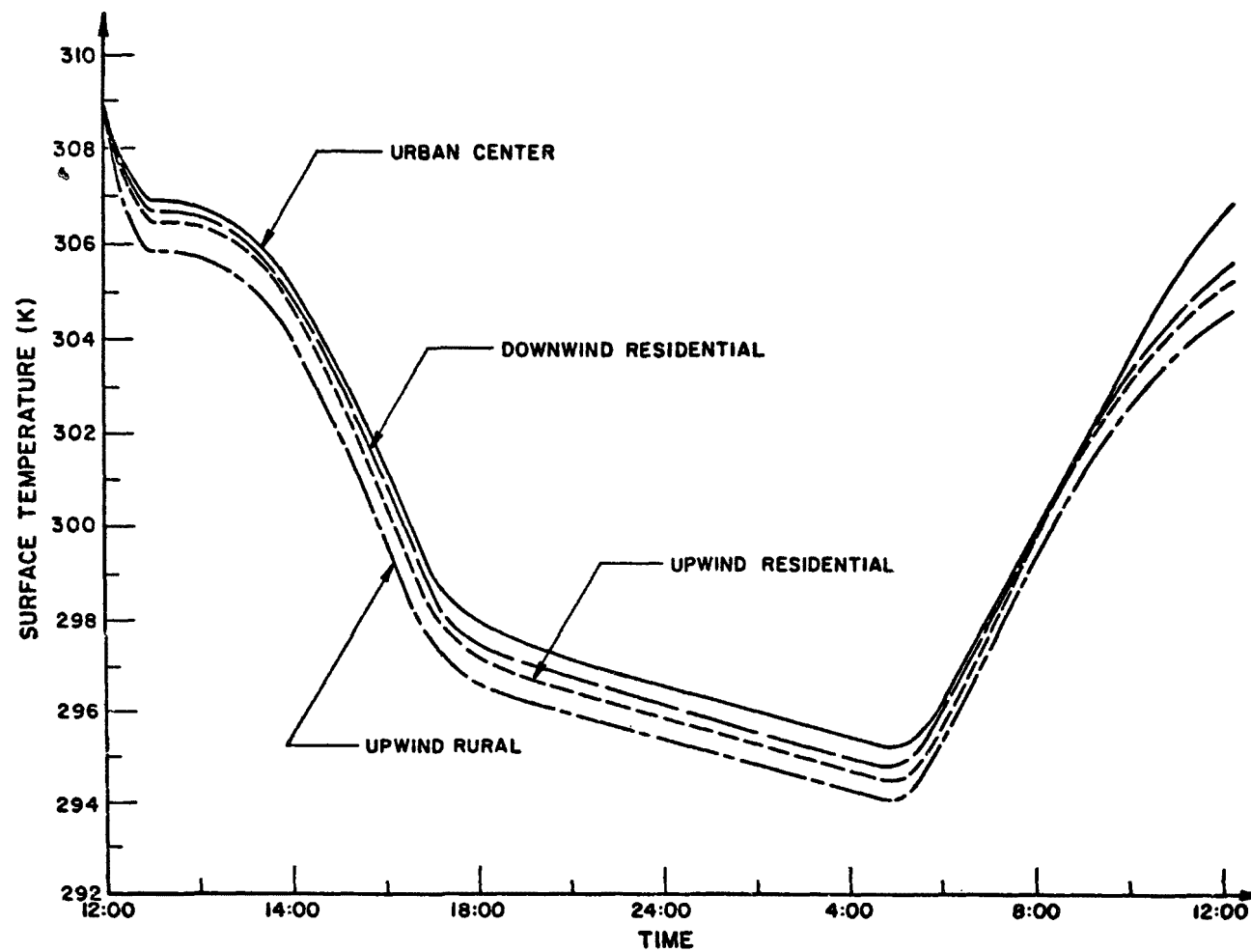


Figure 22. Variation of Surface Temperature with Time for Simulation I;
 $u_g = 12 \text{ m/s}$, $v_g = 8 \text{ m/s}$

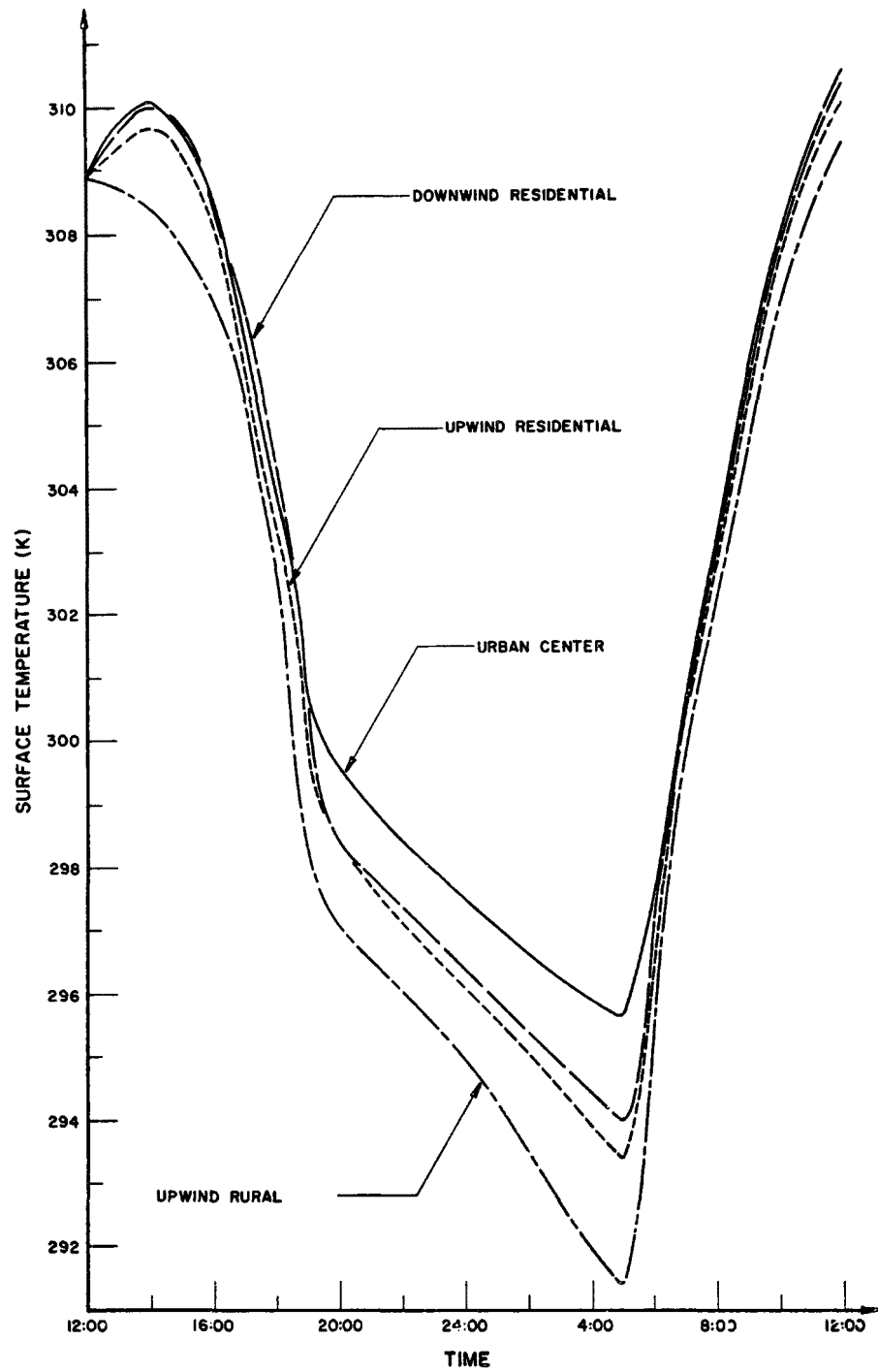


Figure 23. Variation of Surface Temperature with Time for Simulation 3;
 $u_g = 6 \text{ m/s}$, $v_g = 4 \text{ m/s}$

This is due to the fact that the turbulent and latent energy fluxes are larger and dominate surface energy balance, see Figures 19 and 20. The minimum temperature occurs just before sunrise (between 05:00 and 06:00). The surface temperature drops sharply during the late afternoon and rises rapidly after sunrise. During the first few hours of the simulation an initial transient is noted in the surface temperatures presented in Figures 22 and 23. This is due to the fact that the assumed initial velocity, temperature, and water vapor concentration profiles were too "far" away from the quasi-steady solution induced by the diurnal cycle, and it took about 2 to 3 hours for the system to adjust. The temperatures after a 24-hour simulation period are about 2C cooler in Simulation 1 (Figure 22) and about 1C warmer in Simulation 3 (Figure 23) than the assumed initial surface temperatures. The surface temperatures at the downwind residential location are slightly warmer than at the upwind residential location. This is attributed to the heating of air as it flows over the warm city. For higher wind speeds (Simulation 1, Figure 22) the maximum surface temperature difference (about 1.4C) between the urban center and upwind rural locations occurs in the evening at 19:00 and remains almost constant throughout the night. On the other hand, for the lower wind speeds (Simulation 3, Figure 23) the maximum difference occurs just before the sunrise, and the difference is considerably higher.

The main conclusion of these results is that the model predicts an urban heat island for Simulation 3 having a magnitude of about 4C just before sunrise and about 1.4C at noon. For a simulation with lower wind speeds ($u_g = 3$ m/s and $v_g = 2$ m/s) which are not reported here, the maximum urban heat island reached an intensity of about 8C. The simulated results compare well with nighttime and daytime observed temperature excesses between the urban and rural locations (Peterson, 1969; Oke, 1973b; DeMarrais, 1975).

Simulations with Radiatively Participating Pollutants

The local surface temperature differences along the city between Simulations 2 and 1 (see Table 8 for parameters) and between Simulations 5 and 3 are presented in Figures 24 and 25, respectively. The difference is defined as the local surface temperature for a simulation with radiatively participating pollutants minus the surface temperature for a simulation without radiatively participating pollutants. The temperature differences are a result of the complex interactions of the flow of air over a rough urban area, the anthropogenic heat and pollutant sources, and the radiative participation of the aerosol and gaseous pollutants. Individual influences cannot be readily attributed. As expected, the results show that the differences between the simulations with radiatively participating and nonparticipating pollutants are considerably smaller for higher wind speeds ($u_g = 12$ m/s, $v_g = 8$ m/s; Figure 24) than for lower wind speeds ($u_g = 6$ m/s, $v_g = 4$ m/s; Figure 25). The surface temperature difference is largest during the night, reaches a maximum before the sunrise (05:00), and is smallest at noon.

Comparison of the local surface temperatures along the city for a simulation with radiatively participating pollutants having a surface source flux of $2.5 \mu\text{g}/\text{m}^2\text{s}$ (Simulation 5) and one having a surface flux of $5.0 \mu\text{g}/\text{m}^2\text{s}$

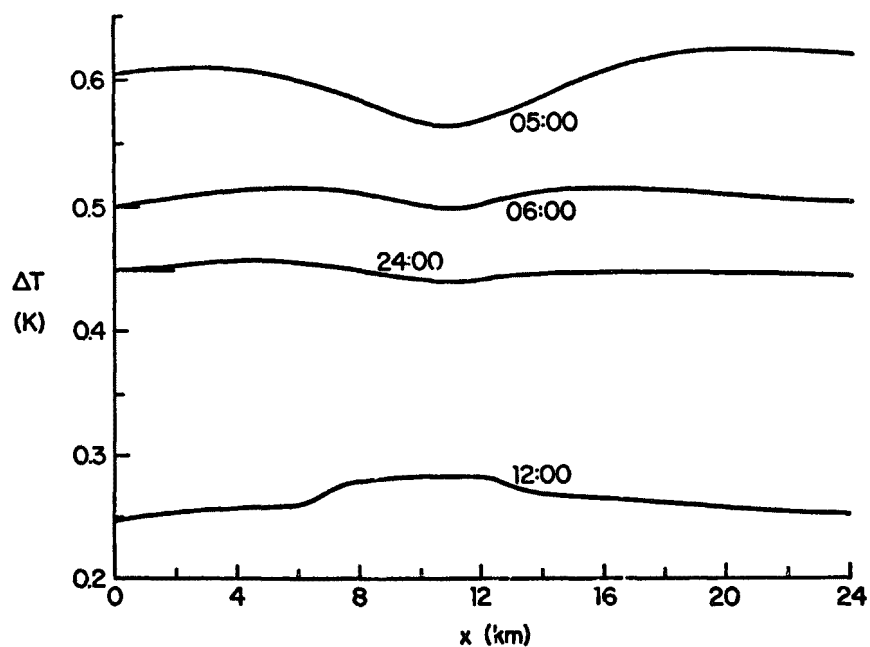


Figure 24. Surface Temperature Difference (Simulation 2 minus Simulation 1)
Along City; $u_g = 12$ m/s, $v_g = 8$ m/s

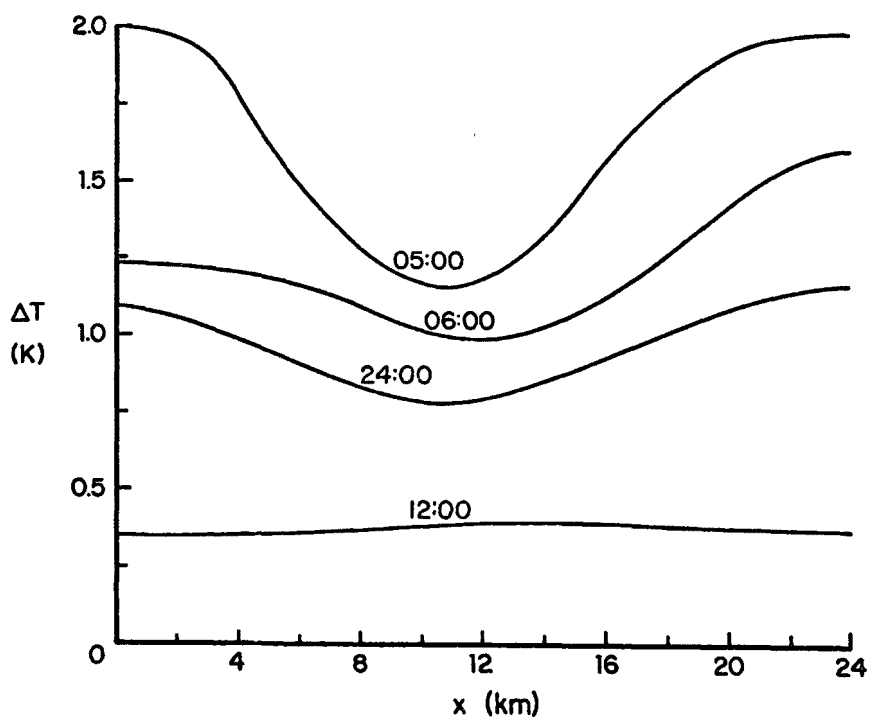


Figure 25. Surface Temperature Difference (Simulation 5 minus Simulation 3)
Along City; $u_g = 6$ m/s, $v_g = 4$ m/s

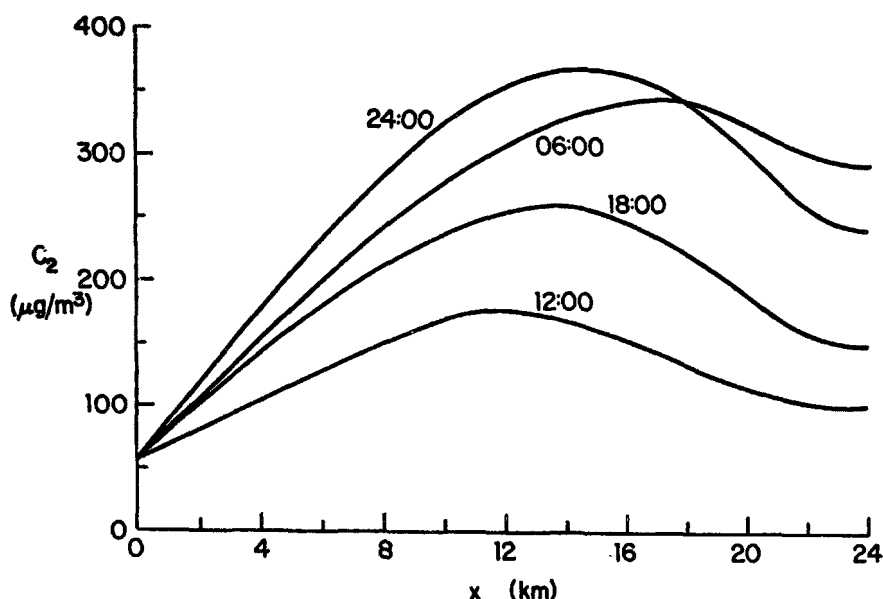


Figure 26. Variation of Surface Pollutant Concentration Along the City for Simulation 3; $u_g = 6$ m/s, $v_g = 4$ m/s

(Simulation 6) showed that there is little difference between the surface temperatures for the two simulations. The differences were greatest downwind of the city center just before sunrise and were less than 0.30°C higher for Simulation 6 than for Simulation 5. The reason for this small difference (see Table 10) is that the thermal absorbed flux (q_{at}) which enters the energy budget at the surface is not altered significantly by the radiatively participating pollutants. The reason for this is that even though the pollutant source flux at the surface for Simulation 6 is twice that for Simulation 5, the total mass loading of aerosol and pollutant gas in the atmosphere is only about 12 percent larger for Simulation 6. This finding will be discussed later.

Surface Concentrations

The variation of the surface pollutant gas concentrations along the urban area for Simulation 3 is shown in Figure 26. The pollutants build up during the night and reach a maximum surface concentration just before sunrise. After sunrise the atmosphere becomes unstable and by noon the surface concentrations are significantly reduced. At the center of the city ($x = 10.5$ km), for example, the gaseous pollutant concentration at the surface increases to $404 \mu\text{g}/\text{m}^3$ before sunrise (05:00) and by noon (12:00) is reduced to $175 \mu\text{g}/\text{m}^3$. Because of the effective vertical dispersion during the day, the maximum concentration occurs in the immediate vicinity of the peak pollutant surface source flux ($x = 10.5$ km), while at night and early in the morning the maximum concentration occurs downwind of the urban center because of the horizontal advection. The downwind residential and rural pollutant concentrations predicted appear to be too high. This may be due to the fact that a zero gradient pollutant concentration condition

TABLE 10. DIURNAL VARIATION OF THE ABSORBED THERMAL FLUX AT THE SURFACE (q_{at} in W/m^2) FOR SIMULATIONS 3, 5, AND 6 AT THE UPWIND RURAL AND THE CENTER OF THE CITY LOCATIONS

Time	<u>Simulation 3</u>		<u>Simulation 5</u>		<u>Simulation 6</u>	
	Upwind Rural	Urban Center	Upwind Rural	Urban Center	Upwind Rural	Urban Center
12:00	363.4	383.6	381.5	402.7	381.5	402.7
14:00	370.1	396.3	387.7	417.3	387.7	418.5
16:00	370.6	395.6	388.8	416.2	388.8	417.5
18:00	360.1	383.5	377.7	403.6	377.6	404.7
20:00	343.9	368.7	362.8	389.2	362.7	390.3
22:00	338.4	362.3	356.8	382.0	356.7	382.7
24:00	333.9	357.6	352.8	377.3	352.4	377.9
02:00	329.1	353.6	348.7	373.7	348.6	374.3
04:00	324.2	349.7	344.8	370.5	344.8	371.7
06:00	328.4	351.2	348.0	372.1	348.0	372.9
08:00	345.6	367.5	363.8	388.0	363.7	388.9
10:00	362.3	386.3	380.1	406.7	380.1	407.8
12:00	374.9	400.8	392.2	420.9	392.1	422.1

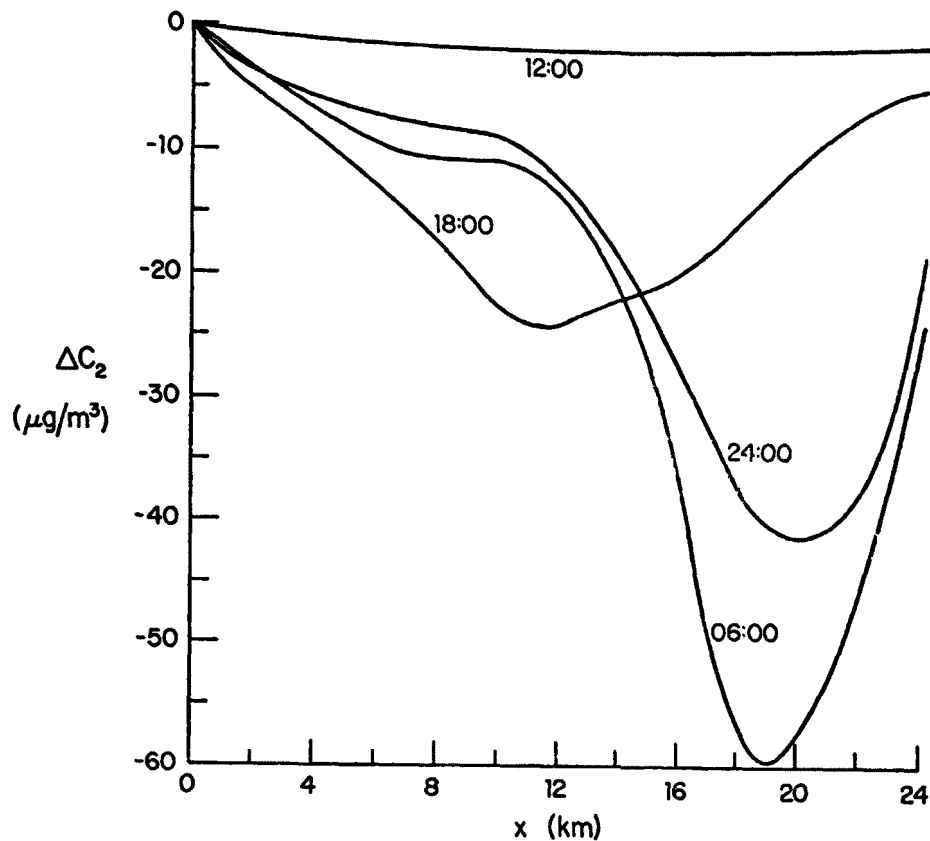


Figure 27. Surface Pollutant Concentration Differences (Simulation 5 minus Simulation 3) Along the City

$(\partial C_2 / \partial x)$ was imposed at the downwind rural position ($x = 24$ km) or maybe because no sinks were considered. The surface pollutant concentrations predicted also appear high. The modeling of pollutant sources is considered to be the most important reason for this result. Modeling of the spatial and diurnal variation of the pollutant sources produced by human activity is very difficult because of the lack of data. Use of a constant (time independent) pollutant source is, of course, unrealistic. It is well known that each of the different pollutants have their own diurnal variation (Peterson, 1970, 1972; Turner, 1968). For example, the production of carbon monoxide can be related to the daily automobile traffic count (Lin and Goodin, 1975). Furthermore, location of the source at the surface ignores the fact that pollutants are injected directly into the atmosphere at some height and not at the surface. Pollutants must diffuse from the vicinity of the surface before they can be dispersed throughout the atmosphere. Since the turbulent diffusivities are generally small near the surface, high pollutant concentrations naturally result.

The difference between the surface pollutant concentrations for Simulation 5 with radiatively participating pollutants and Simulation 3 with radiatively nonparticipating ones are illustrated in Figure 27. The results show that

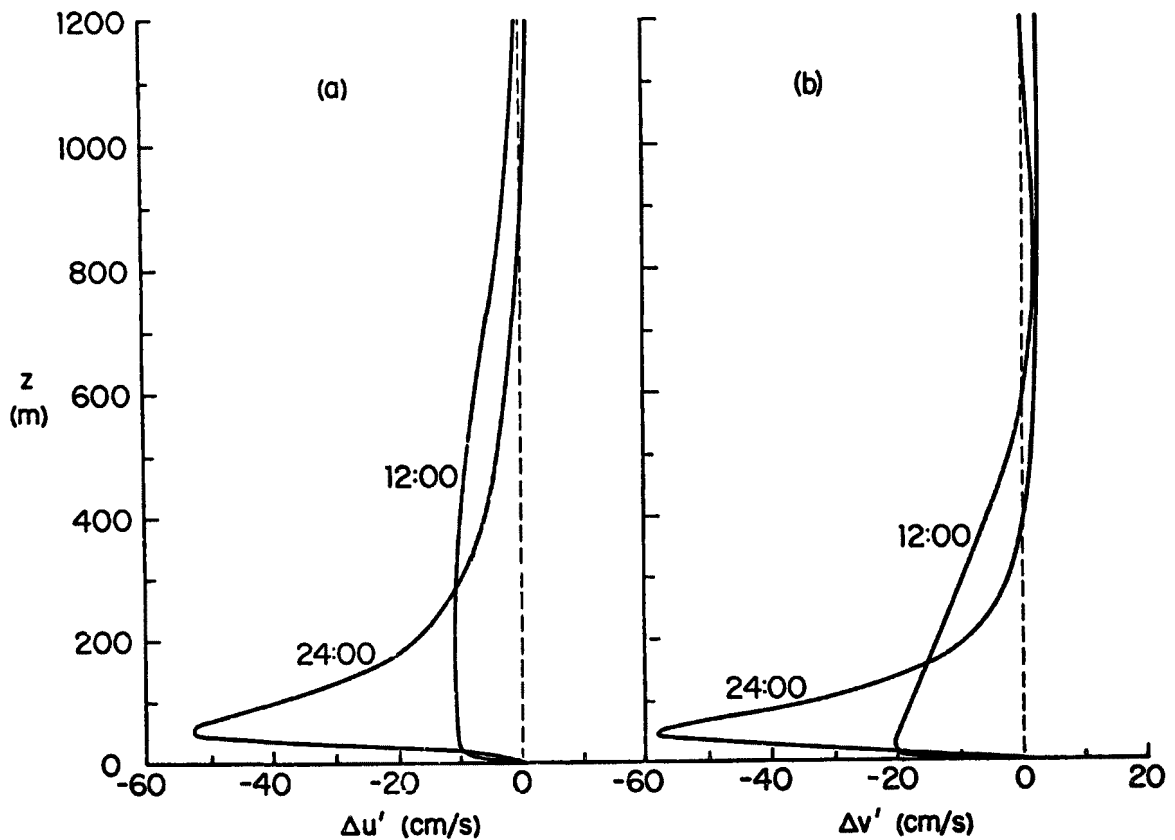


Figure 28. Perturbation Velocities (Velocity at the Urban Center minus Velocity at the Upwind Rural Location) for Simulation 3

the radiative participation of pollutants in the atmosphere enhances their own dispersion and reduces the pollutant surface concentrations. The reduction is greatest at night and amounts to about 10 percent. However, the pollutant mass loading for these simulations, see Table II, is relatively small compared to that used by Bergstrom (1972b). On the basis of results obtained with the one-dimensional model and presented in Figure 13, it is expected that the reduction would be larger for greater mass loadings and more restrictive dispersion conditions such as would arise, for example, under lower wind speeds and stable upper layer temperatures.

Velocity Distribution

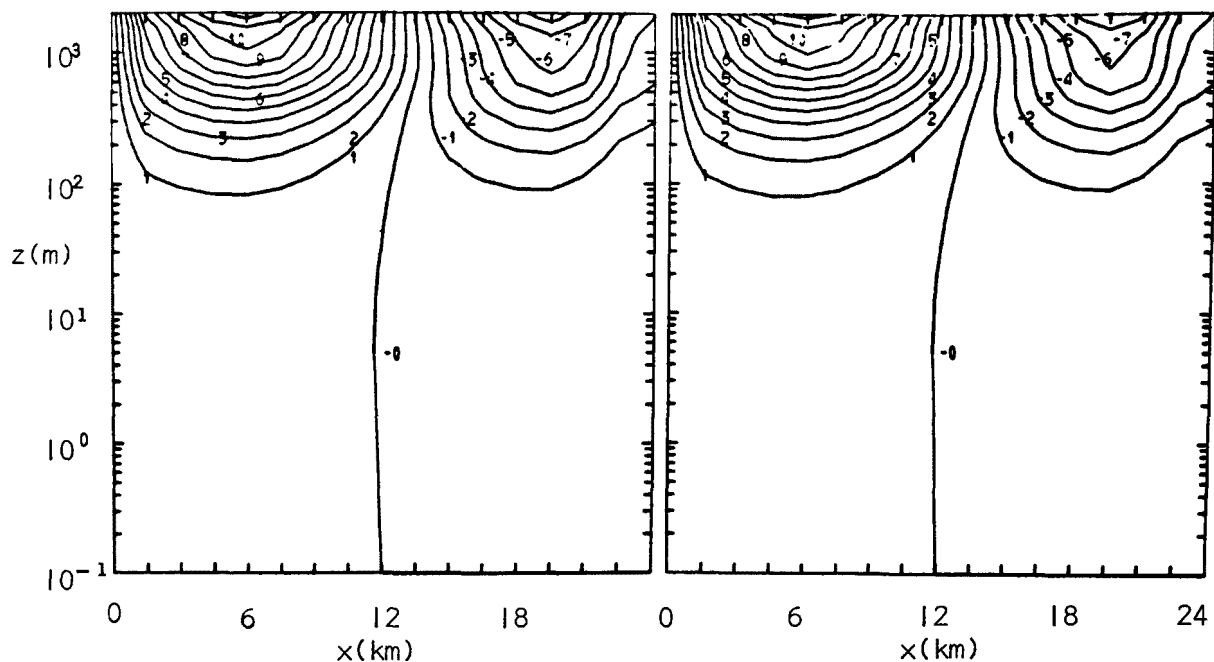
Results of simulations show that prevailing flow decelerates on encountering the roughness elements of the city and accelerates on leaving the urban area. This is indicated in Figure 28 where the perturbation velocities (velocity at the urban center minus the velocity at the upwind rural location) are presented at two different times during the course of Simulation 3. The differences are greatest at night and the maximum is seen to occur at or below 50 meters. The trends found are consistent with those found by other investigators modeling flow over rough strips (Estoque and Bhumralkar, 1970) or over an urban area (Bornstein, 1972; Wagner and Yu, 1972).

TABLE 11. COMPARISON OF AEROSOL MASS LOADINGS (M_1) FOR VARIOUS SIMULATIONS

Source	Time (hr)	u_g (m/s)	v_g (m/s)	M_1 ($\mu\text{g}-\text{km}/\text{m}^3$)
Simulation 3	05:00	6	4	119.9
Simulation 4	05:00	6	4	119.9
Simulation 5	05:00	6	4	119.8
Simulation 6	05:00	6	4	132.0
Bergstrom (1972b)	05:00	12	8	161.0
Simulation 3	12:00	6	4	122.0
Simulation 4	12:00	6	4	122.0
Simulation 5	12:00	6	4	121.5
Simulation 6	12:00	6	4	136.2
Bergstrom (1972b)	12:00	12	8	211.1

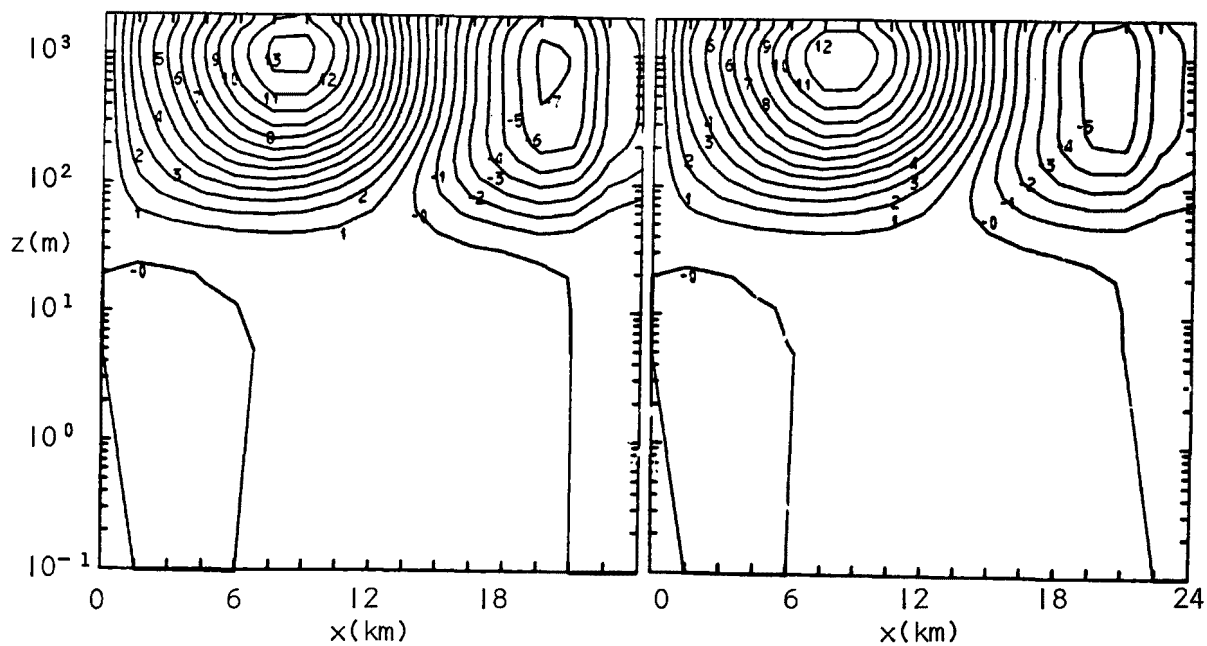
TABLE 12. SURFACE TEMPERATURES (IN K) AT THE CENTER OF THE CITY ($x = 10.5$ km) FOR SIMULATIONS 3, 4, 5, AND 6 AT SELECTED TIMES

Time (hr)	<u>Simulation Number</u>			
	3	4	5	6
18:00	304.01	304.05	304.39	304.39
24:00	297.50	297.62	298.28	298.30
05:00	295.58	295.77	296.72	296.74
06:00	297.48	297.65	298.49	298.51
09:00	306.67	305.73	306.24	306.25
12:00	310.58	310.61	310.98	310.98



(a) Nonparticipating Simulation 3; $t = 24:00$ hr

(b) Participating Simulation 5; $t = 24:00$ hr



(c) Nonparticipating Simulation 3; $t = 12:00$ hr

(d) Participating Simulation 5; $t = 12:00$ hr

Figure 29. Comparison of Vertical Velocity Isopleths (in cm/s) for Simulations with Radiatively Nonparticipating (Simulation 3) and Radiatively Participating (Simulation 5) Pollutants

As a consequence of the decrease in horizontal wind speed the continuity of mass requires upward vertical motion ahead of the urban center and downward motion downwind of the urban area, Figure 29. The magnitude of the vertical velocity is, however, small and is generally confined to the upper regions of the boundary layer. The net effect of the radiatively participating pollutants is a relatively minor factor in establishing the flow over the urban area.

Temperature Distribution

Radiatively Nonparticipating Pollutants

Figure 30 illustrates the isopleths of the two-dimensional potential temperature fields at six hour intervals for Simulation 3. At 18:00 the boundary layer is nearly adiabatic, especially in the upwind rural area, with a thermal plume having a temperature of about 305K forming at a height of about 100 m downwind of the city center ($x = 10.5$ km). This plume is not felt downwind, and the upwind and downwind rural temperatures near the surface are virtually identical. A surface temperature inversion develops at night over the urban area. The inversion is seen to be deeper over the rural area than over the city. This is indicative of the nocturnal urban heat island which decreases the stability of the atmosphere. The magnitude of this island is larger at night than during the day. This type of behavior is well documented (Peterson, 1969; Oke, 1973a). For Simulation 1 with higher wind speeds ($u_g = 12$ m/s and $v_g = 8$ m/s) the surface inversion was found to be less deep, and the magnitude of the nocturnal heat island was smaller.

The variation of temperature in the atmosphere during the diurnal cycle is more clearly illustrated in Figure 31 in which a comparison of the upwind rural and urban center potential temperature profiles are presented for Simulation 3. During the night a surface inversion develops and is seen to be larger in the upwind rural location than at the urban center. The inversion reaches a maximum before sunrise (05:00) and by 06:00 the breakup of the stable surface layer is noted. The surface inversion erodes rapidly after sunrise due to heating by absorption of solar radiation and by 09:00 all traces of the inversion have then disappeared. The low-level nocturnal temperature structure over the center of the city differs significantly from that in upwind rural location. The profiles also indicate distinct regions of stability particularly at night, and this is in agreement with observations of Clarke and McElroy (1974) over the city of St. Louis, Missouri. Of course, pollutants injected into the layers having different stabilities are dispersed at different rates.

The potential temperature isopleths over the urban area for Simulation 7 having a rectangular distribution of anthropogenic heat sources are presented in Figure 32. A comparison of Figures 30 and 32 reveals that the difference between the two simulations is quite small. The maximum difference occurs just before sunrise when the contribution of urban heat source Q to the surface energy balance is the largest. Due to the assumed shape of Q (see Figure 16), the temperature profiles for Simulation 7 define the urban area more sharply.

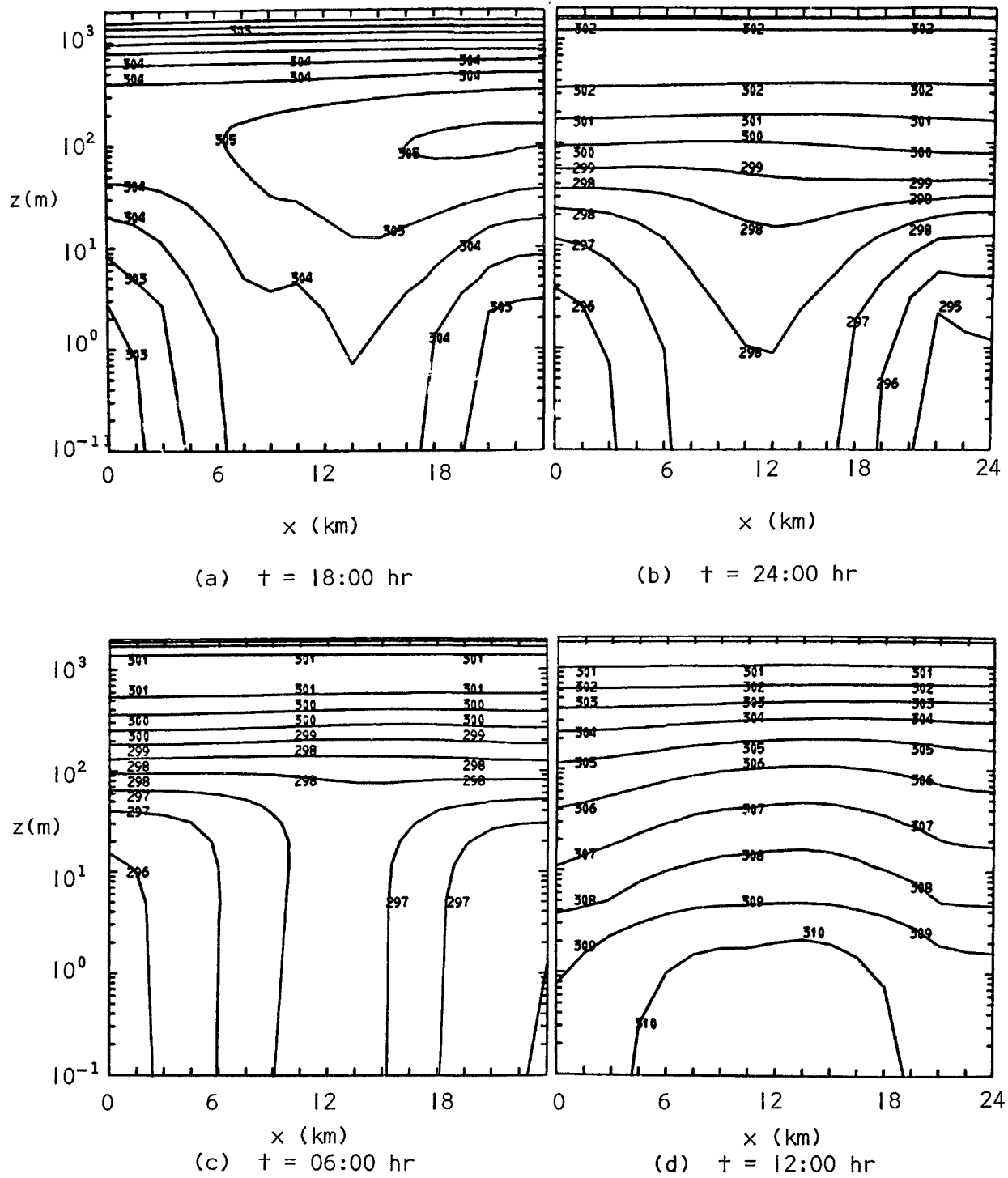


Figure 30. Potential Temperature Isopleths (in K) for Simulation 3; Note that the Last Digit Denoting the Temperature of the Isotherms at 18:00, 24:00, and 06:00 Hours has been Truncated

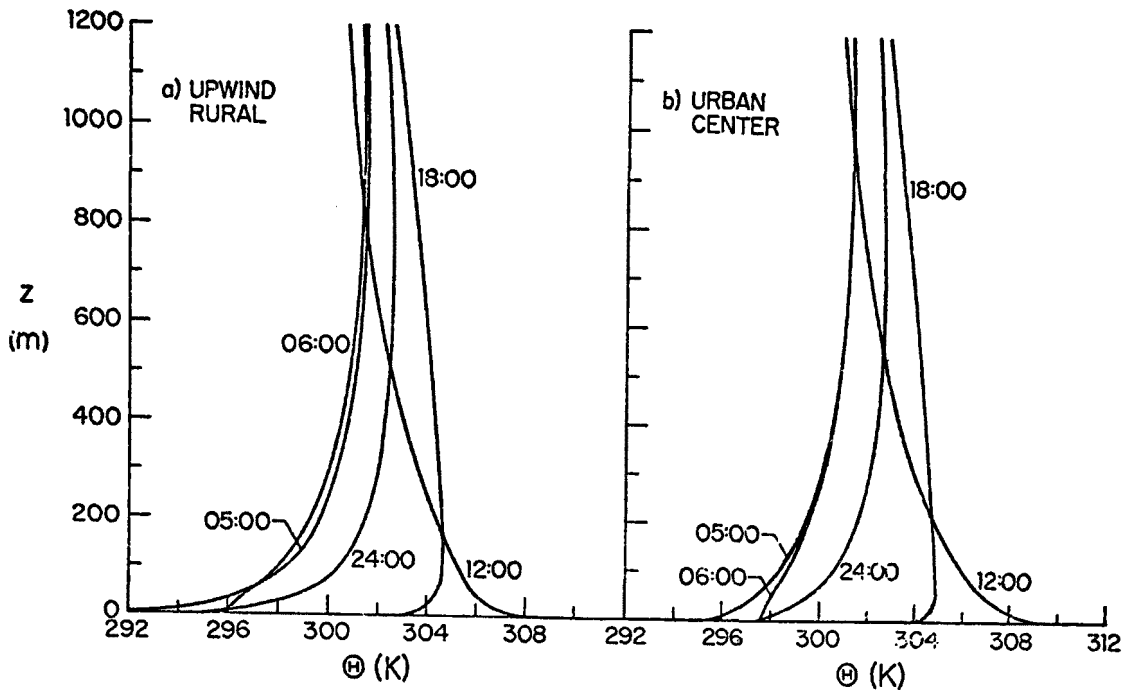


Figure 31. Potential Temperature Distribution for Simulation 3

Radiatively Participating Pollutants

A comparison of potential temperature isopleths for the four simulations (3 through 6) having a Gaussian distribution of anthropogenic heat and pollutant sources at times 24:00, 06:00, and 12:00 are given in Figures 33, 34, and 35, respectively. A summary of the surface temperatures at the urban center for several different times during the diurnal cycle is given in Table 12. The results show that the maximum surface temperature difference between Simulation 3 with radiatively nonparticipating pollutants and Simulations 4, 5, and 6 with radiatively participating pollutants occurs late at night before sunrise (05:00) and reaches 1.16 K. Note also that there is surprisingly little difference between temperatures for Simulations 5 and 6 which have surface pollutant sources of 2.5 and 5.0 $\mu\text{g}/\text{m}^2\text{s}$, respectively. This indicates that at night for Simulation 5 the gaseous pollutant concentration distribution and the total mass in the atmosphere are such that a "saturation" condition may have been reached, and an additional increase in pollutant concentration (Simulation 6) does not affect the net thermal (long-wave) radiative transfer in the atmosphere. This may also be due to the fact that the total mass of the representative pollutant gas (ethylene, C_2H_4) present in the atmosphere was only about 12 percent greater than for Simulation 5 (see Table 11). During the day the aerosols and gaseous pollutants appear to have compensating effect on the surface energy balance and therefore on the surface temperature. The aerosols decrease the solar flux while the gaseous pollutants increase the thermal flux incident on the surface. Careful comparison of the potential temperature isopleths presented in Figures 33, 34, and 35 reveals that the maximum temperature difference between the simulations with radiatively interacting

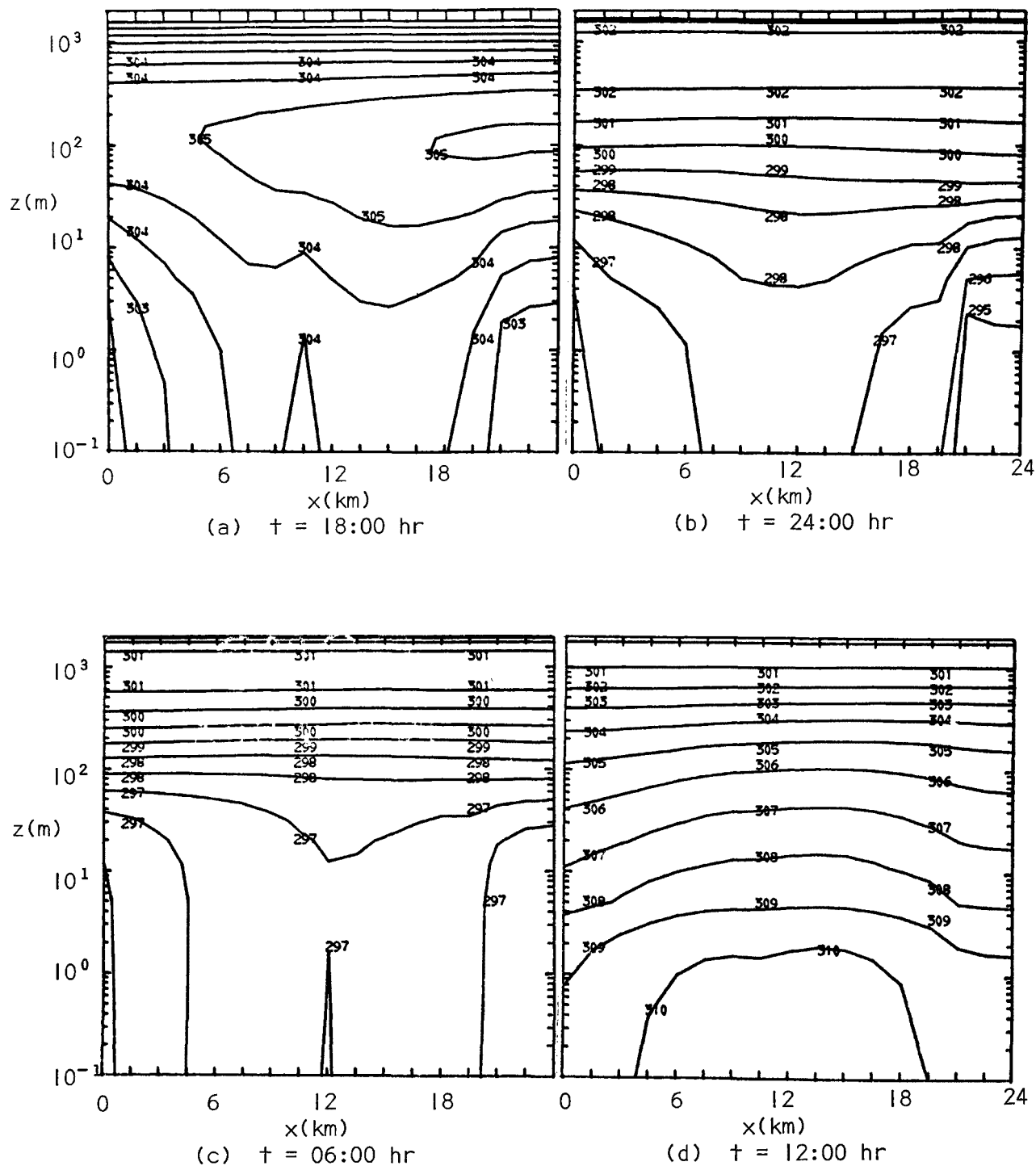
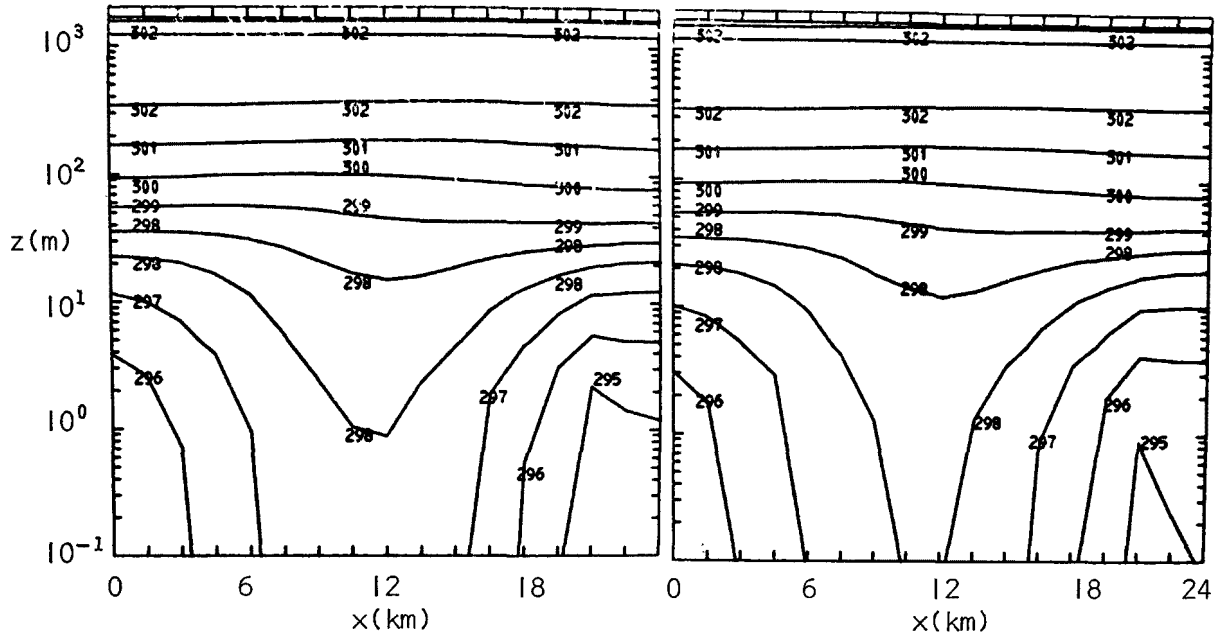
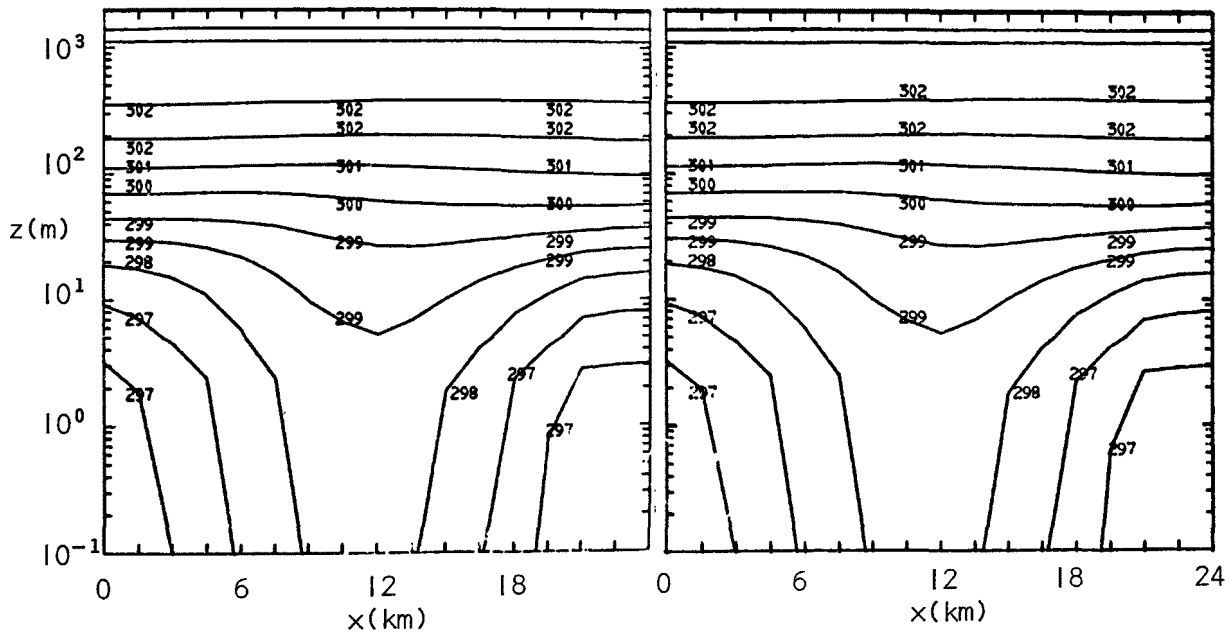


Figure 32. Potential Temperature Isopleths (in K) for Simulation 7



(a) Nonparticipating Simulation 3; $m_p = 2.5 \mu\text{g}/\text{m}^2\text{s}$

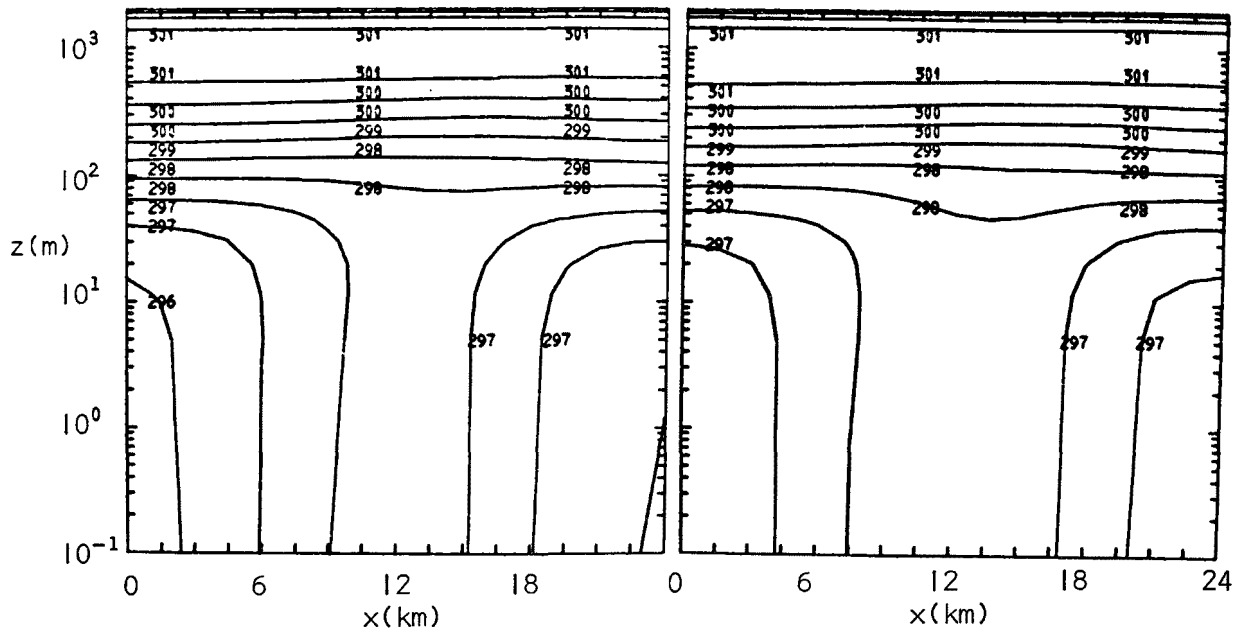
(b) Participating Simulation 4; SO_2 , $m_p = 2.5 \mu\text{g}/\text{m}^2\text{s}$



(c) Participating Simulation 5; C_2H_4 , $m_p = 2.5 \mu\text{g}/\text{m}^2\text{s}$

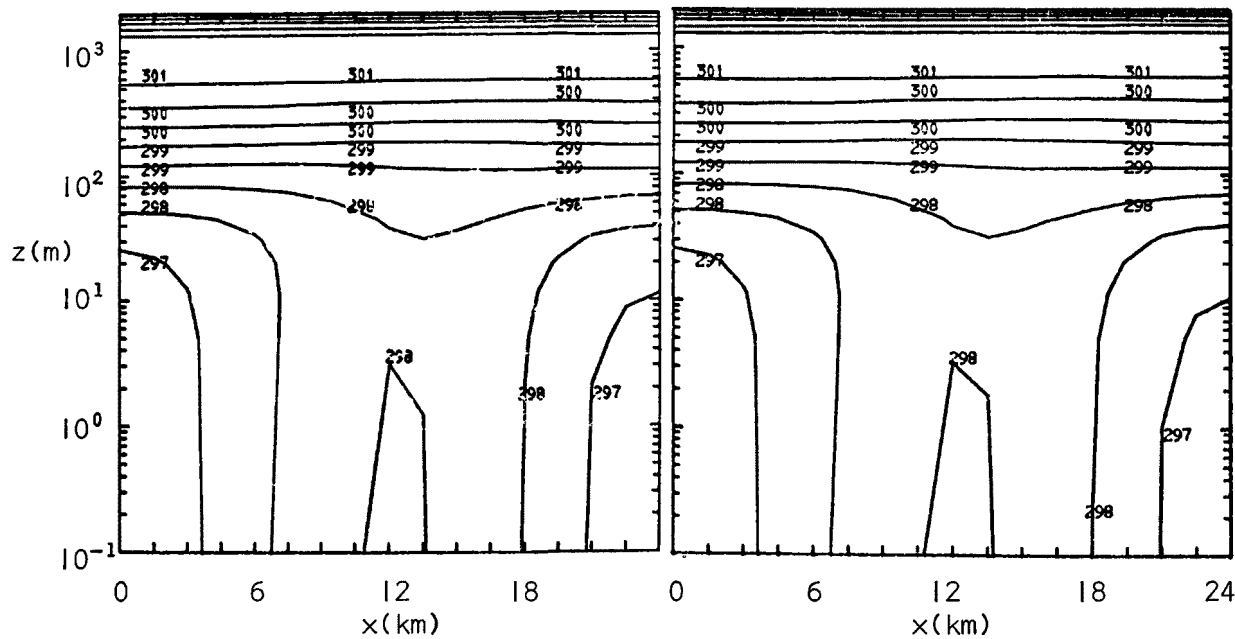
(d) Participating Simulation 6; C_2H_4 , $m_p = 5.0 \mu\text{g}/\text{m}^2\text{s}$

Figure 33. Comparison of Potential Temperature Isopleths (in K) between Simulations 3 (Part a), Simulation 4 (Part b), Simulation 5 (Part c), and Simulation 6 (Part d) at 24:00 of the First Day



(a) Nonparticipating Simulation 3; $m_p = 2.5 \mu\text{g}/\text{m}^2\text{s}$

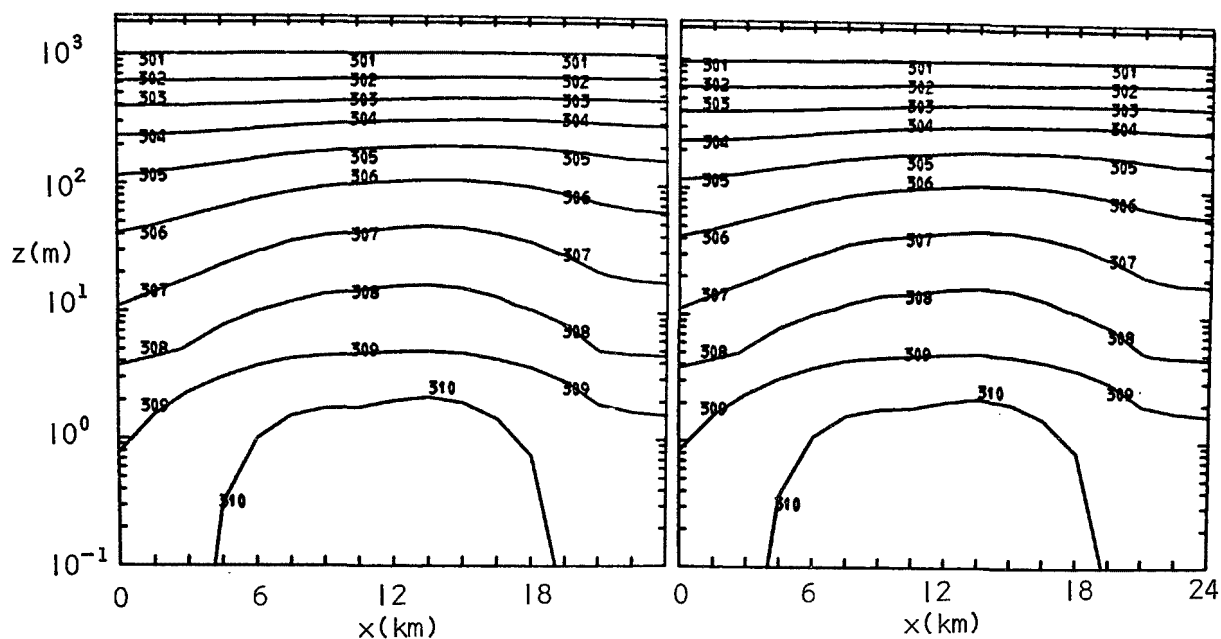
(b) Participating Simulation 4; SO_2 , $m_p = 2.5 \mu\text{g}/\text{m}^2\text{s}$



(c) Participating Simulation 5; C_2H_4 , $m_p = 2.5 \mu\text{g}/\text{m}^2\text{s}$

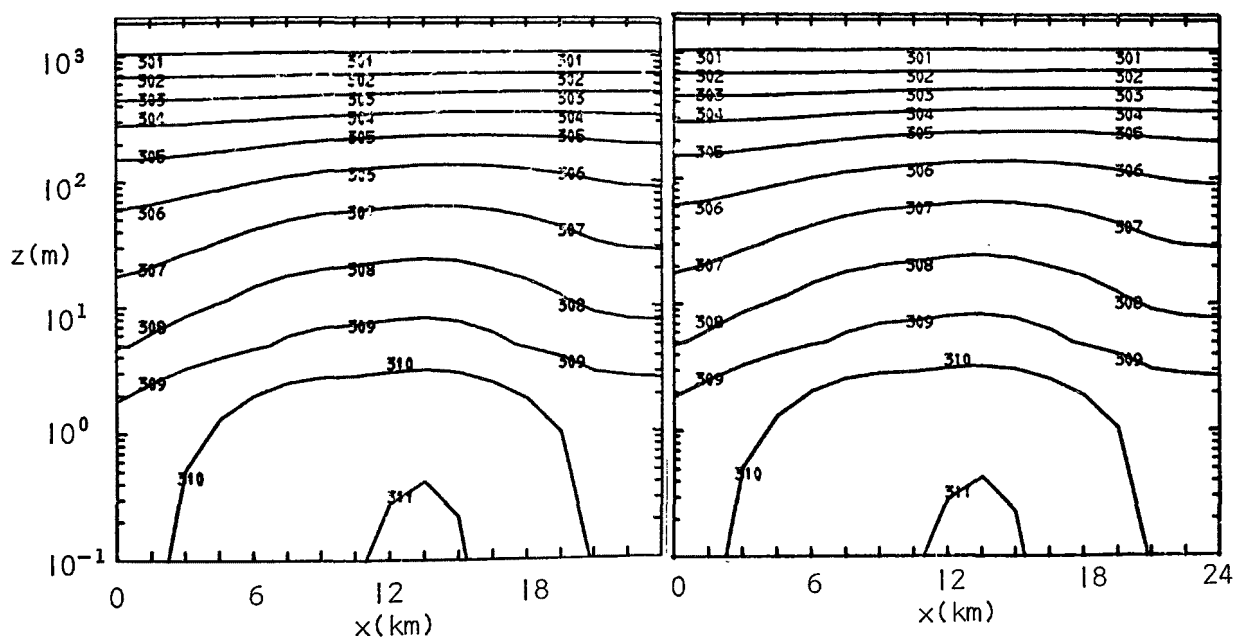
(d) Participating Simulation 6; C_2H_4 , $m_p = 5.0 \mu\text{g}/\text{m}^2\text{s}$

Figure 34. Comparison of Potential Temperature Isopleths (in K) between Simulations 3 (Part a), Simulation 4 (Part b), Simulation 5 (Part c), and Simulation 6 (Part d) at 12:00 of the Second Day



(a) Nonparticipating Simulation 3; $m_p = 2.5 \mu\text{g}/\text{m}^2\text{s}$

(b) Participating Simulation 4; SO_2 , $m_p = 2.5 \mu\text{g}/\text{m}^2\text{s}$



(c) Participating Simulation 5; C_2H_4 , $m_p = 2.5 \mu\text{g}/\text{m}^2\text{s}$

(d) Participating Simulation 6; C_2H_4 , $m_p = 5.0 \mu\text{g}/\text{m}^2\text{s}$

Figure 35. Comparison of Potential Temperature Isopleths (in K) between Simulation 3 (Part a), Simulation 4 (Part b), Simulation 5 (Part c), and Simulation 6 (Part d) at 12:00 of the Second Day

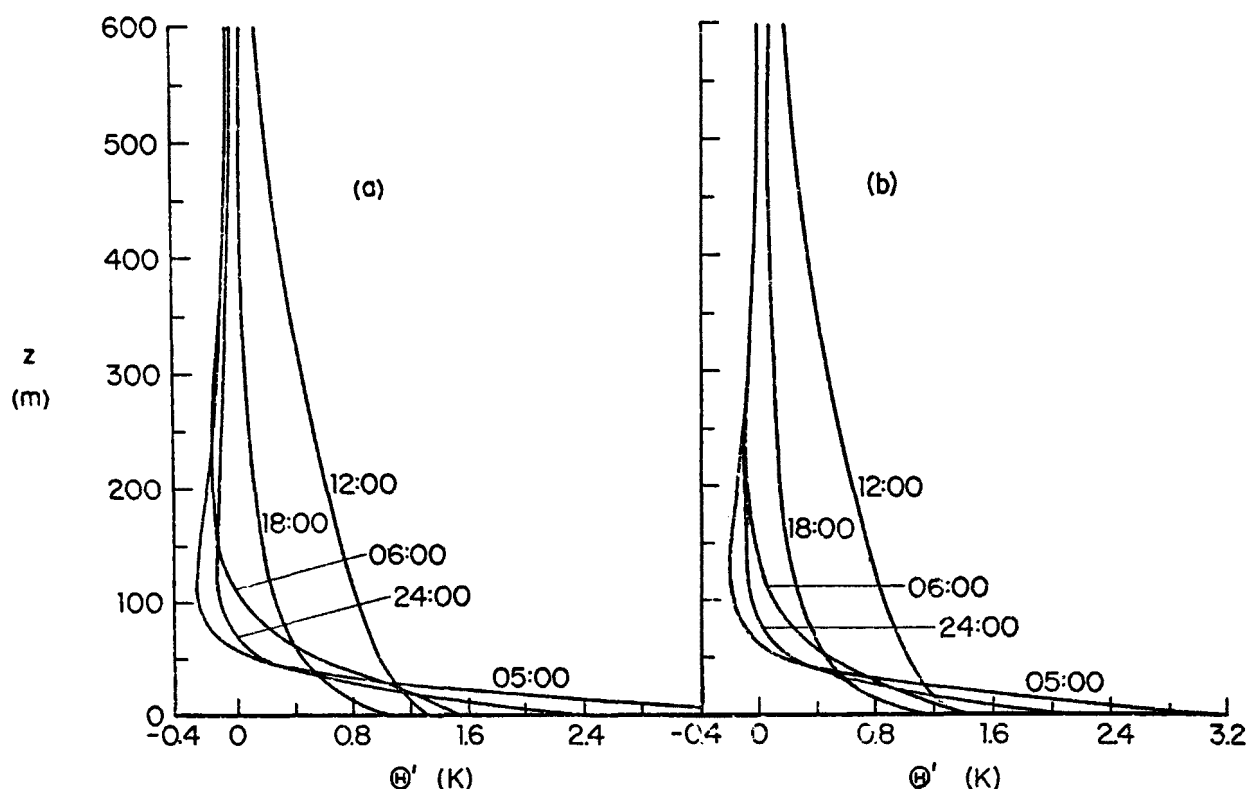


Figure 36. Perturbation of Potential Temperature (Temperature in the City Minus Temperature at the Upwind Rural Location) for Simulation 3

and noninteracting pollutants occurs at the surface. The results also show that the presence of radiatively participating pollutants in the urban atmosphere reduces the amplitude of the diurnal temperature variations. For example, in Simulation 3 the amplitude (maximum surface temperature minus minimum surface temperature) at the urban center is 15C while for Simulation 5 it is 14.2C.

The net effect of the city and the human activity on the temperature distribution can be examined by comparing the potential temperature perturbations at the urban center presented in Figures 36a and 36b for Simulations 3 and 5, respectively. The perturbation is defined as the temperature at the urban center minus the temperature at the upwind rural location. The perturbations are seen to be largest at the surface and are confined to about the lowest 600 meters of the planetary boundary layer. The maximum surface temperature perturbation (urban heat island intensity) for Simulation 3 with radiatively nonparticipating pollutants is 4.07C while for Simulation 5 with radiatively participating ones is 3.42C and occurs in the morning (05:00). The primary reason for the smaller urban center-rural temperature difference is the change in the upwind rural conditions between Simulations 3 and 5. For Simulation 5 the presence of background pollutants increased the downward thermal flux incident on the surface, and as a result, the rural temperature was somewhat higher than for Simulation 3.

When the pollutant gas is assumed to have the radiative properties sulfur dioxide (Simulation 4), the temperature distributions predicted are practically identical to those for the radiatively nonparticipating pollutant gas (Simulation 3). The reader should compare parts a and b of Figures 33, 34, and 35. This is due to the fact that SO_2 is a weakly absorbing gas. The results are consistent with those obtained using the one-dimensional model, Table 6.

When ethylene is considered to be the representative pollutant gas, considerably larger temperature differences are noted (see Table 12) between the simulations with radiatively interacting (parts c and d) and the simulations with radiatively noninteracting (part a) pollutant gas. The difference increases throughout the night, reaches a maximum of about 1.2°C before sunrise and becomes only about 0.4°C at noon. The reason the temperatures for Simulations 5 and 6 are higher than those for Simulation 3 is because ethylene is a much stronger absorber than sulfur dioxide. The temperatures downwind of the urban center are higher than those upwind due to the urban heat sources and other modifications of the environment. In Table 13 are listed the downward thermal fluxes at the surface as a function of the position along the city just before sunrise (05:00). It is interesting to note that the fluxes for the participating simulations show a pronounced increase in these surface values thus indicating that the presence of radiatively participating pollutant gases definitely modify the surface energy budget and contribute to the formation of thermal structure in the urban planetary boundary layer late at night and early in the morning up to sunrise. If the maximum values of the thermal fluxes for the simulations with radiatively participating pollutants are compared against the fluxes for the upwind rural nonparticipating Simulation 3, maximum increases in the downward thermal fluxes over the urban area of 2.3, 8.6, and 8.8 percent are noted for Simulations 4, 5, and 6, respectively. These computations agree well with the experimental observations made by Oke and Fuggle (1972) who measured an increase in the downward thermal flux of approximately 10 percent in Montreal, Canada.

In Table 14 are presented the ratios of the radiative flux divergence ($-\partial F_z / \partial z$) to the net transport by turbulent diffusion $[\partial / \partial z (K^0 \partial \theta / \partial z)]$ in the vertical direction for Simulation 3 with radiatively nonparticipating pollutants and for Simulation 5 with radiatively participating ones at several locations along the city. Inspection of the table indicates that the transport of energy by thermal radiation may be important in determining the thermal structure during the night. In the table, there is a large variation in the ratio of the divergence of the radiative flux to the divergence of sensible turbulent flux in the vertical direction with respect to both space and time. While the accuracy in determining this ratio from finite-difference approximations may not be satisfactory, the trends (and the table is intended only as an order of magnitude estimate) clearly show that thermal radiative transfer contributes significantly to the energy transport during the night. Likewise, turbulent diffusion dominates energy transport in the PBL during the day.

TABLE 13. COMPARISON OF DOWNWIND THERMAL FLUXES (IN W/m^2) AT THE SURFACE AS A FUNCTION OF THE HORIZONTAL LOCATION BEFORE SUNRISE (05:00)

Node Number	Horizontal Location (km)	Simulation			
		3	4	5	6
1	0	358.0	361.9	380.7	380.7
2	1.5	358.8	362.7	381.5	381.6
3	3.0	359.6	363.6	382.6	382.7
4	4.5	361.2	365.1	383.8	383.9
5	6.0	362.8	366.7	385.1	385.3
6	7.5	364.2	368.1	386.3	386.8
7	9.0	365.5	369.3	387.5	388.1
8	10.5	366.3	370.2	388.3	389.1
9	12.0	366.6	370.5	388.7	389.6
10	13.5	366.1	370.1	388.6	389.5
11	15.0	364.6	368.8	387.9	388.9
12	16.5	362.4	365.9	386.4	387.5
13	18.0	359.6	365.3	384.2	385.2
14	19.5	358.5	364.1	383.2	384.2
15	21.0	358.6	362.5	382.3	383.2
16	22.5	360.0	362.5	382.4	383.3
17	24.0	360.0	362.5	382.4	383.3

The simulated effects of pollutants on the temperature structure (temperature difference with and without radiatively participating pollutants) was always about 1.2°C higher (Simulation 6 minus Simulation 3) at the surface, see Figures 34d and 34a, respectively. This difference is, however, smaller than the 4.2°C change induced by urbanization before sunrise (05:00) for Simulation 3 with radiatively nonparticipating pollutants, see Figure 31. The results are consistent in trends with the simulations of Atwater (1972b, 1974) but are different in order of magnitude. The simulations show a thermal plume downwind of the urban center, but no elevated inversions were induced by the radiatively interacting pollutants possibly indicating limitations of the turbulence model.

Figures 37 and 38 illustrate the diurnal variation of the surface temperature for the first five simulations listed in Table 8 at the upstream rural location and the urban center, respectively. From the figures it is evident that the decrease in geostrophic wind speed causes an increase in the amplitude of the diurnal surface temperature variation while radiative participation by pollutants decreases it. During the day, the influence of radiatively participating pollutants is quite small (0.18°C difference between Simulations 5 and 3 at 12:00) while at night it is considerably larger (1.12°C difference between Simulations 5 and 3 at 05:00). For higher geostrophic wind speeds, the effect of radiatively participating pollutants on the surface temperature and the vertical thermal structure is even smaller.

TABLE 14. RATIO OF THE RADIATIVE FLUX DIVERGENCE ($-\partial F/\partial z$) TO THE TURBULENT DIFFUSION [$\partial/\partial z(k^0 \partial \theta/\partial z)$] IN THE VERTICAL DIRECTION BETWEEN SIMULATION 3 WITH RADIATIVELY NONPARTICIPATING POLLUTANTS (NP) AND SIMULATION 5 WITH RADIATIVELY PARTICIPATING POLLUTANTS (P)

<u>z(m)</u>	<u>Upwind Rural</u>		<u>Upwind Residential</u>		<u>Urban Center</u>		<u>Downwind Residential</u>	
	<u>NP</u>	<u>P</u>	<u>NP</u>	<u>P</u>	<u>NP</u>	<u>P</u>	<u>NP</u>	<u>P</u>
† = 18:00								
50	-0.597	-0.426	-0.517	-0.493	-0.388	-0.410	-0.434	-0.423
250	-1.025	-0.842	-0.928	-0.793	-1.52	-1.29	-1.31	-1.15
1000	-1.909	-1.76	-1.92	-1.62	-1.90	-1.60	-1.90	-1.58
† = 24:00								
50	-60.9	25.87	-0.502	-0.519	0.405	0.513	0.511	3.34
250	-0.583	0.531	-0.460	-0.428	-0.388	-0.377	-0.792	-0.994
1000	-2.02	7.16	-1.94	3.04	-1.83	7.78	-1.88	23.4
† = 05:00								
50	31.2	-9.67	-1.203	174	0.188	0.291	0.972	0.528
250	-1.16	-1.28	-0.868	-0.868	-0.485	-0.531	-2.38	-2.28
1000	-3.02	-2.80	-1.76	-2.55	-1.22	-2.32	-2.90	-2.20
† = 06:00								
50	0.0974	0.148	0.0395	0.0622	0.0253	0.0530	0.0115	0.0173
250	-0.368	-0.439	-0.303	-0.368	-0.336	-0.625	-0.177	-0.477
1000	-1.08	-1.23	-1.06	-1.18	-0.965	-1.091	-1.01	-1.13
† = 09:00								
50	-0.0470	-0.0708	-0.0662	-0.0776	-0.0782	-0.0824	-0.0812	-0.0869
250	-0.0302	-0.0367	-0.0273	-0.0292	-0.0221	-0.0194	-0.0232	-0.0191
1000	-0.313	-0.0921	-0.138	-0.103	-0.168	-0.165	-0.117	-0.120
† = 12:00								
50	-0.165	-0.258	-0.162	-0.200	-0.224	-0.263	-0.325	-0.463
250	-0.0436	-0.0748	-0.0291	-0.0442	-0.0275	-0.0471	-0.0371	-0.0486
1000	-0.128	-0.102	-0.101	-0.0916	-0.0821	-0.0715	-0.056	-0.0710

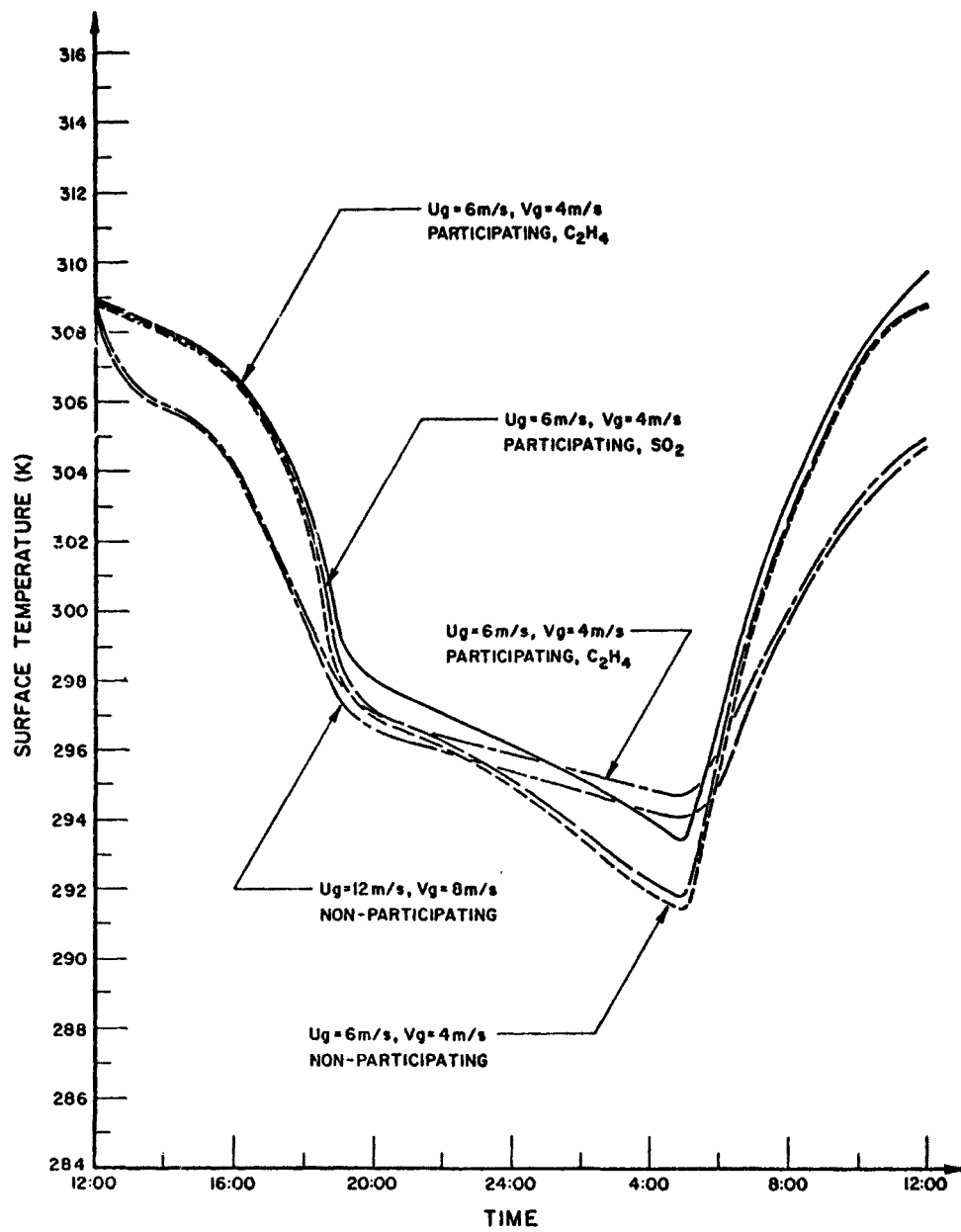


Figure 37. Comparison of Surface Temperatures at the Upwind Rural Location

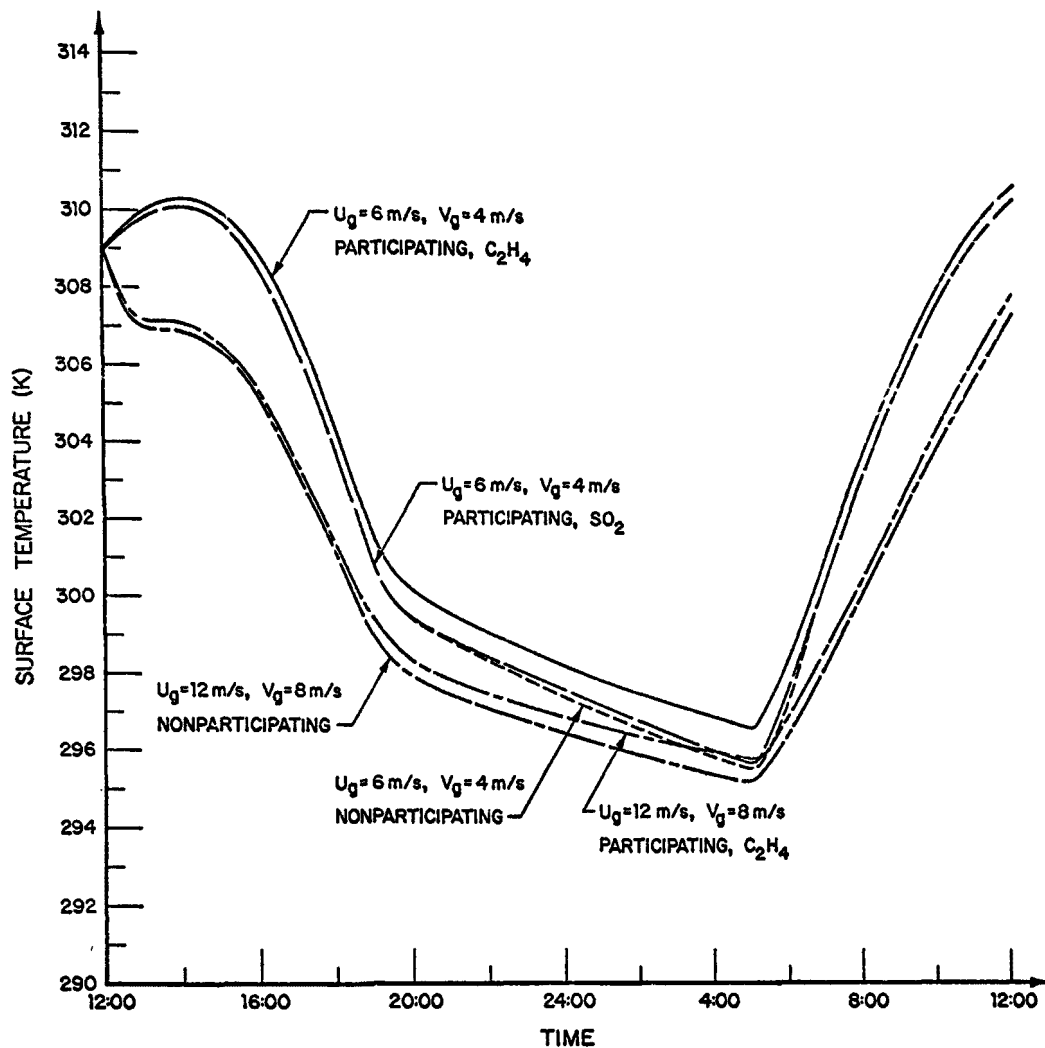


Figure 38. Comparison of Surface Temperatures at the Center of the City

However, in view of the results obtained with the one-dimensional model, it is expected that radiative participation by pollutants will have a marked effect on the thermal structure for more restrictive dispersion conditions and higher pollutant mass loadings.

Concentration Distribution

Radiatively Nonparticipating Pollutants

The concentration isopleths (in $\mu\text{g}/\text{m}^3$) over the urban area for the radiatively nonparticipating Simulation 3 with a Gaussian and for Simulation 7 with a rectangular distribution of pollutant emissions along the city are presented in Figures 39 and 40, respectively. Instead of illustrating concentrations at six-hour intervals as was done for the temperature, the isopleths are given for 24:00, 05:00, 06:00, and 12:00 because it was desirable to

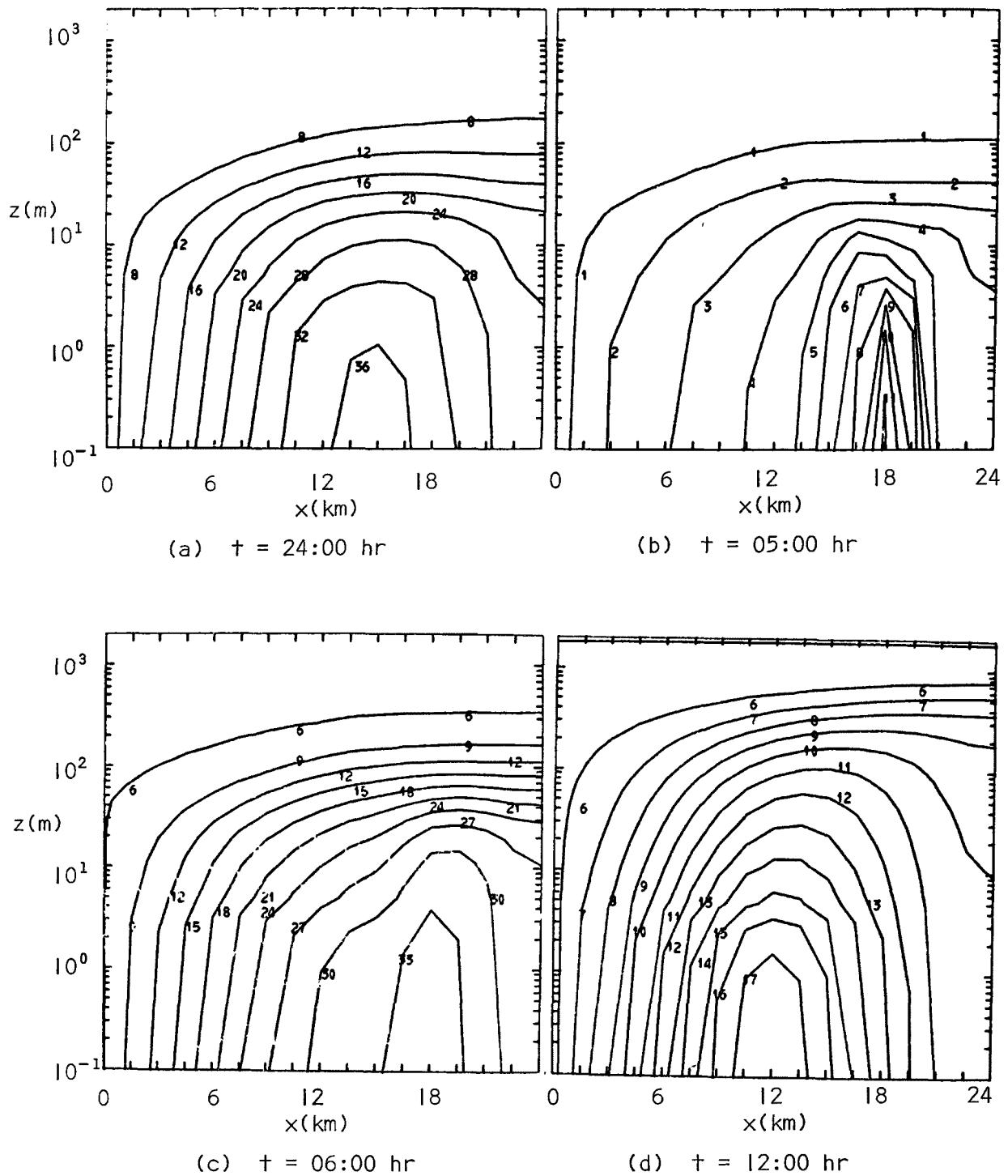


Figure 39. Gaseous Pollutant Concentration Isopleths for Simulation 3;
(Multiply Numbers in Parts a, c, and d by a Factor of 10 and
in Part b by a Factor of 10^2 to Obtain Concentrations in $\mu\text{g}/\text{m}^3$)

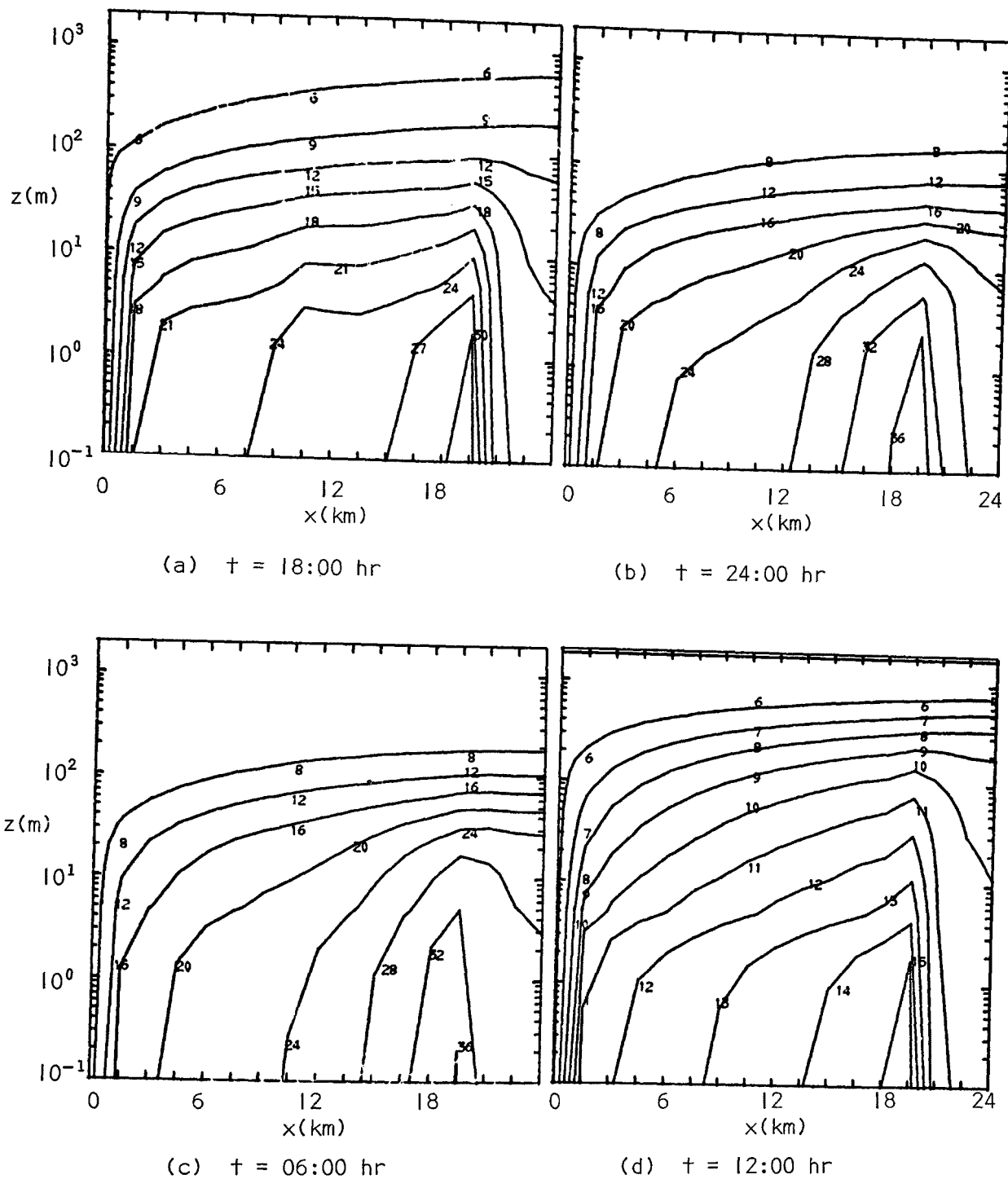


Figure 40. Gaseous Pollutant Concentration Isopleths for Simulation 7
(Multiply Numbers in the Figure by a Factor of 10 to Obtain
Concentrations in $\mu\text{g}/\text{m}^3$)

present the maximum pollutant concentrations which typically occurred just before sunrise (05:00). The total pollutant mass injected into the atmosphere is identical for both simulations, and since the aerosol emission flux at the surface was assumed to be identical to that of the pollutant gas, the aerosol concentrations are identical to those of the pollutant gas. The results show the buildup of pollutant concentration during the night. After sunrise, the atmosphere becomes unstable and the pollutant is dispersed rather effectively by vertical diffusion and horizontal advection. All of the isopleths show the formation of a pollutant plume downwind of the urban center. As expected from the pollutant surface emission distribution (see Figure 16), the pollutant concentrations over the urban center ($x = 10.5$ km) are higher for the Gaussian than for the rectangular distribution. For example, the surface emission at the center of the city for Simulation 3 is $4.344 \mu\text{g}/\text{m}^2\text{s}$ and for Simulation 7, it is $2.5 \mu\text{g}/\text{m}^2\text{s}$ while the corresponding ground pollutant concentrations are $404.4 \mu\text{g}/\text{m}^3$ and $336.4 \mu\text{g}/\text{m}^3$. The reason the surface concentrations have not changed proportionately with the emissions is because the temperatures are not the same. Since differences in stability between the two simulations change the turbulent diffusivities, the ground pollutant concentrations are also different.

Results presented in Figure 39b at 05:00 show unreasonably high pollutant concentrations downwind of the urban center ($x = 16.5, 18,$ and 19.5 km) in the vicinity of the surface. The surface concentration at $x = 18$ km exceeds $1100 \mu\text{g}/\text{m}^3$ which is unreasonably high. A careful examination of the figure reveals that most of the unrealistically high concentrations are confined to depths less than 10 meters. As already discussed, modeling of all pollutant emission as surface sources is not realistic. The surface concentrations are very sensitive to the turbulent diffusivities at the first few grid points above the ground. The diurnal trends in the surface pollutant concentrations can be explained on the basis of the diurnal variation of the turbulent diffusivity at the first vertical grid point. This is discussed in the next subsection.

Radiatively Participating Pollutants

The pollutant gas concentration isopleths (in $\mu\text{g}/\text{m}^3$) just before sunrise (05:00) for Simulations 3, 4, 5, and 6 are presented in Parts a, b, c, and d of Figure 41, respectively. At 05:00 the surface concentration builds up to a high value of about $1100 \mu\text{g}/\text{m}^3$ in Simulation 3 (Figure 41a) while the radiatively participating Simulation 5 illustrated in Figure 41c, the surface concentration increases to only $560 \mu\text{g}/\text{m}^3$. It is interesting to note that for Simulation 6 (Figure 41d), which is identical to Simulation 5 (Figure 41c) except that the pollutant emission flux has been doubled, predicts a buildup of $1200 \mu\text{g}/\text{m}^3$. This is almost the same for Simulation 3 (Figure 41a). The influence of thermal radiation transfer by pollutants is certainly evident in the peak concentrations that occur just before sunrise. After sunrise (06:00), the breakup of the stable layer near the surface is noted as shown in Figure 42. In a period of one hour (from 05:00 to 06:00) the ground pollutant concentrations at the urban center for Simulations 3, 4, 5, and 6 have decreased by 25, 26, 30, and 32 percent, respectively. The pollutants disperse most rapidly for Simulations 5 and 6 with the radiatively

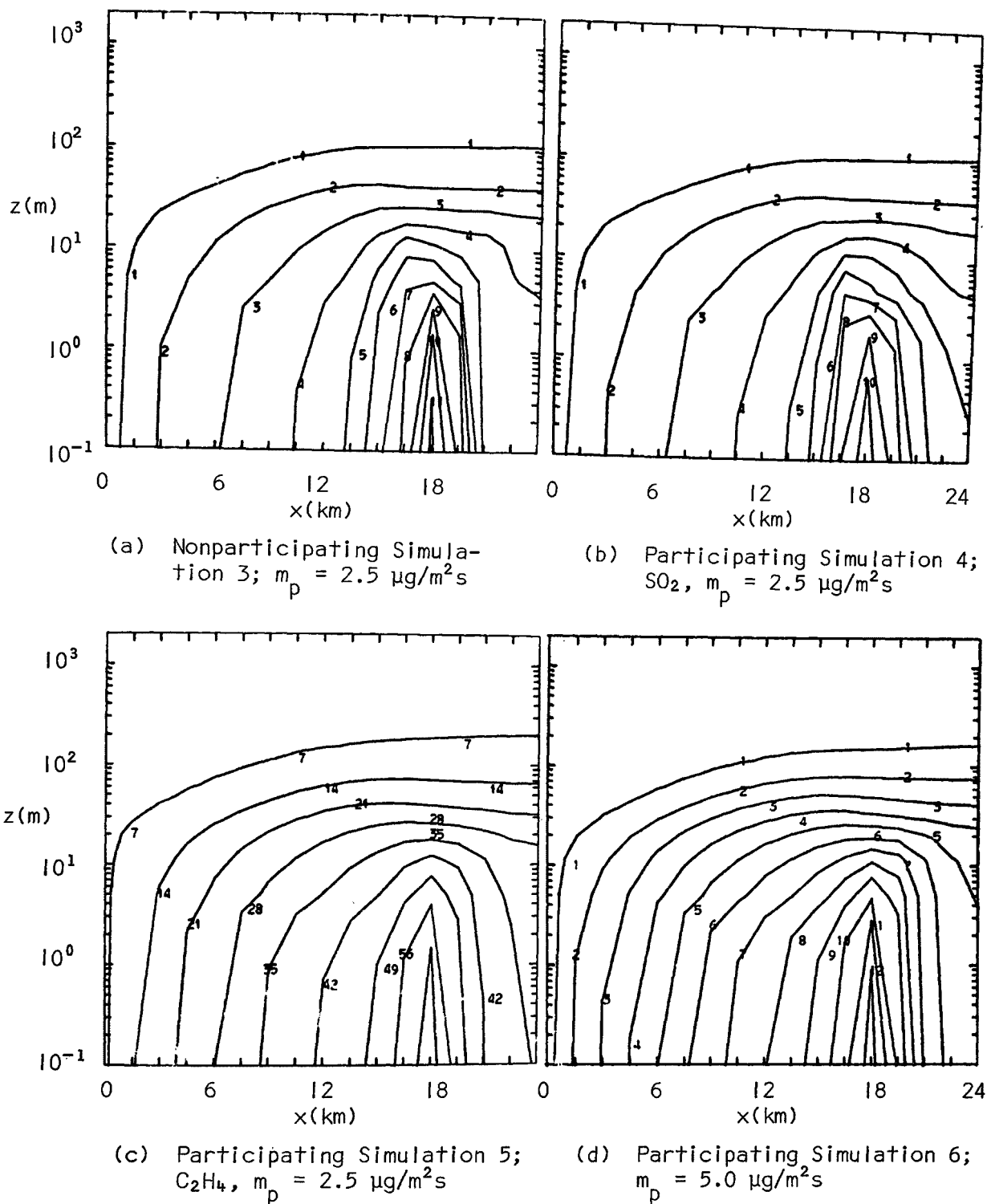


Figure 41. Comparison of Gaseous Pollutant Concentration Isopleths for Simulation 3 (Part a), Simulation 4 (Part b), Simulation 5 (Part c), and Simulation 6 (Part d) at 05:00 of the Second Day (Multiply the Numbers in Parts a, b, and d on the Figure by 10^2 and the Numbers in Part c by 10 to Obtain Concentrations in $\mu\text{g}/\text{m}^3$)

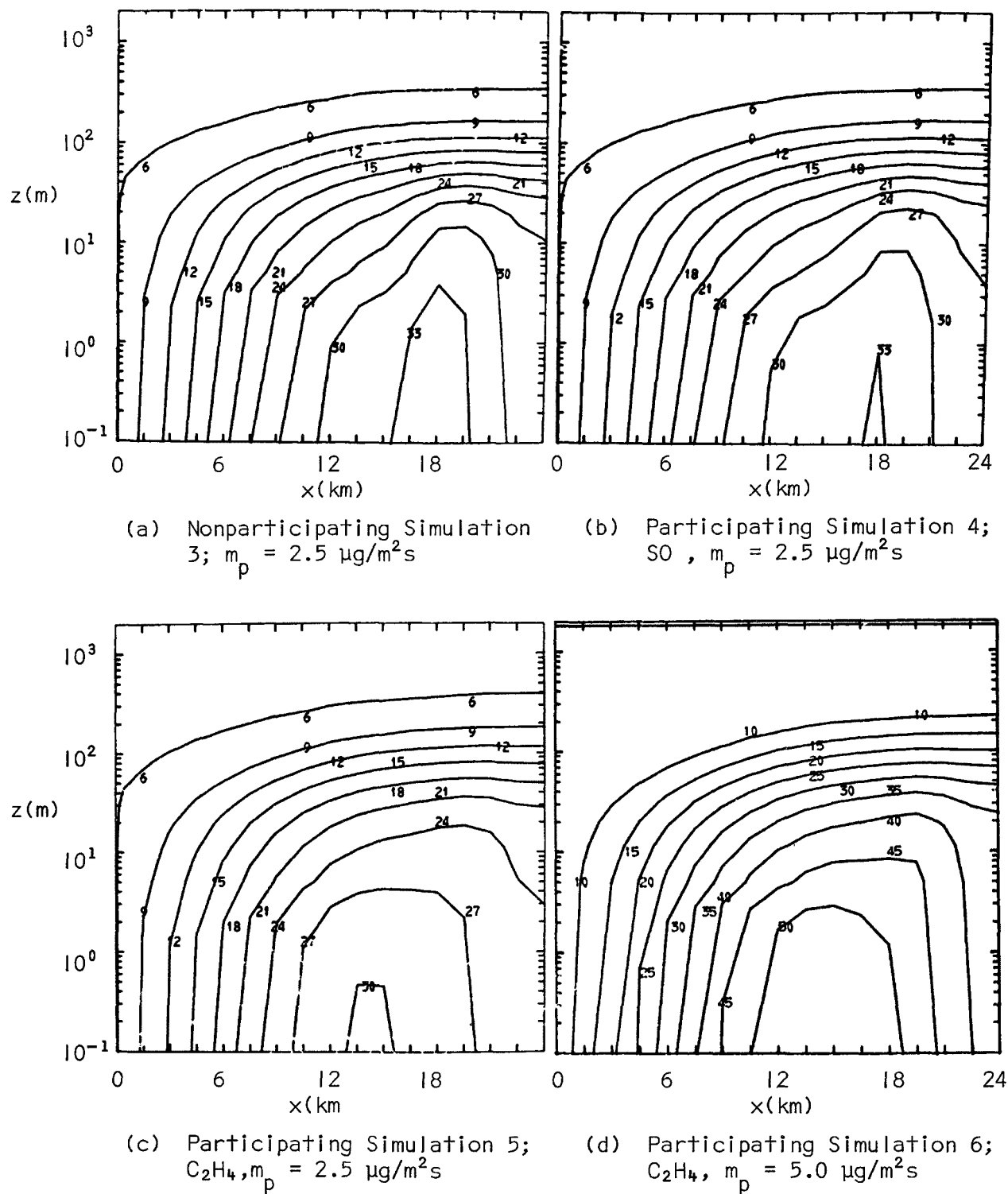


Figure 42. Comparison of Gaseous Pollutant Concentration Isopleths for Simulation 3 (Part a), Simulation 4 (Part b), Simulation 5 (Part c), and Simulation 6 (Part d) at 06:00 of the Second Day (Multiply the Numbers on the Figure by 10 to Obtain Concentrations in $\mu\text{g}/\text{m}^3$)

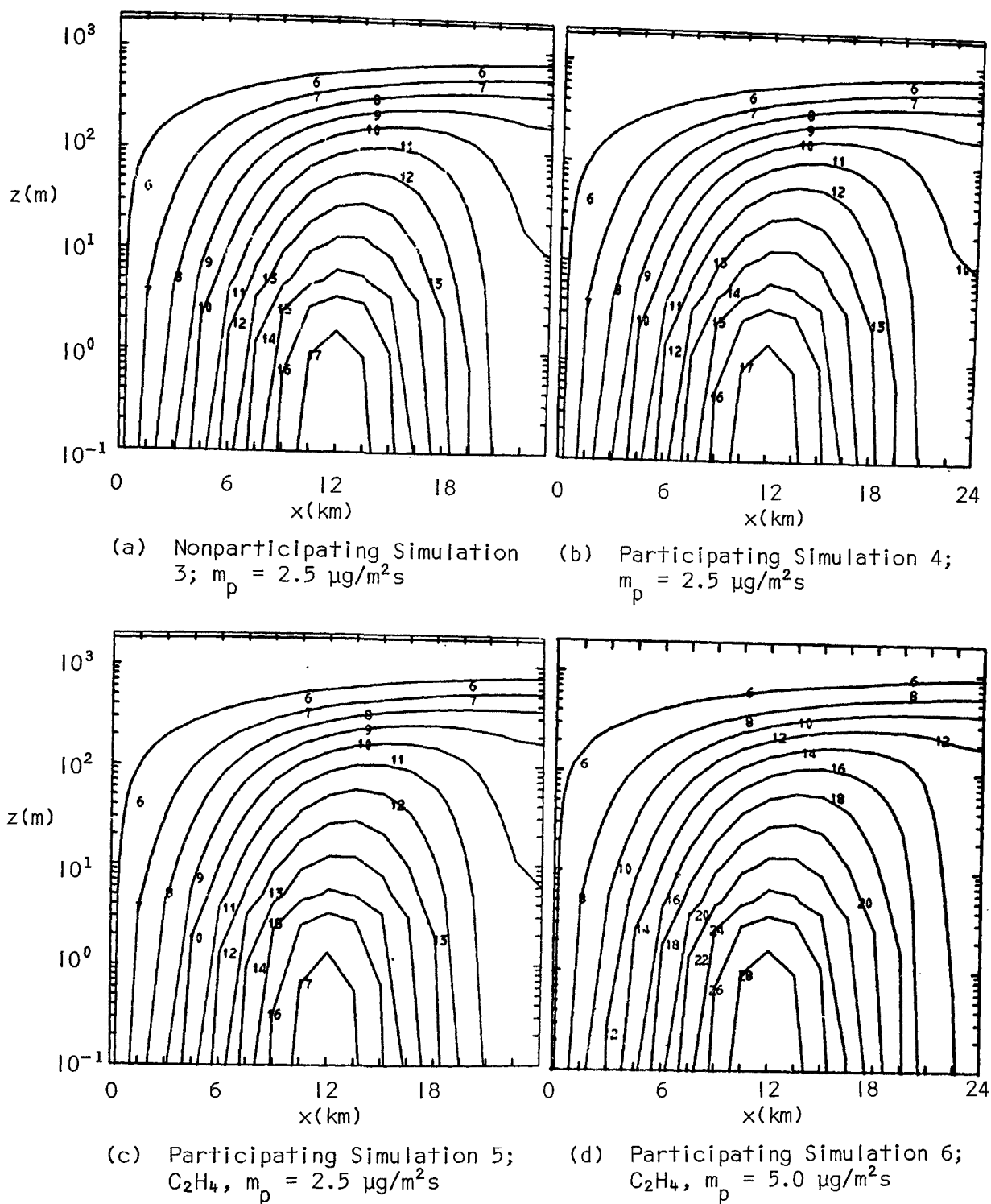


Figure 43. Comparison of Gaseous Pollutant Concentration Isopleths for Simulation 3 (Part a), Simulation 4 (Part b), Simulation 5 (Part c), and Simulation 6 (Part d) at 12:00 of the Second Day (Multiply the Numbers in the Figure by 10 to Obtain Concentrations in $\mu\text{g}/\text{m}^3$)

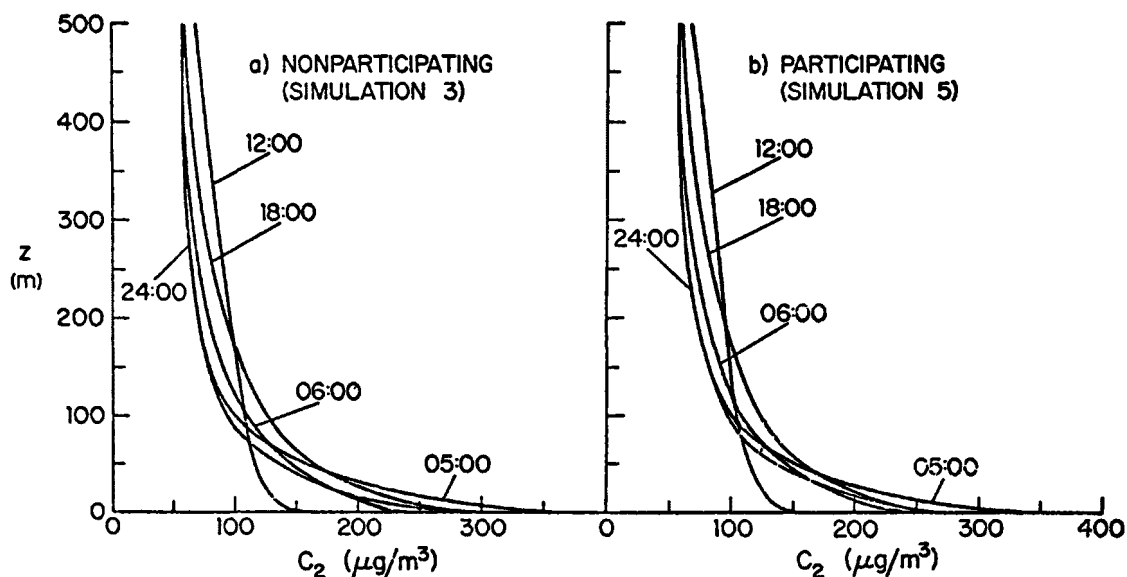


Figure 44. Comparison of Gaseous Pollutant Concentrations for Simulation 3 (Part a) and for Simulation 5 (Part b) at the Center of the City

participating pollutant gas having properties of ethylene. By noon (Figure 43) turbulent diffusion and advection dominate the transport, and the isopleths of pollutant gas concentrations are almost identical for all four simulations (3 through 6).

The gaseous pollutant concentration buildup at the urban center for Simulation 3 with radiatively noninteracting pollutants and for Simulation 5 with radiatively interacting pollutants are illustrated in Figure 44. Because the pollutant source is located at the surface, the increase in the concentrations is largest at that point. The pollutant dispersion and their concentrations near the ground (say, up to 10 m from the surface) are very sensitive to the turbulent diffusivities and their variation with time of the day during the diurnal cycle. In turn, the turbulent diffusivities are strongly influenced by the temperature and stability of the atmosphere. The diffusivities in the vicinity of the surface are relatively low (see Figure 45) particularly at night. As a result of the low diffusivities sharp concentration gradients are evident near the surface in Figure 44. Above 200 m the vertical dispersion is quite effective because of much higher diffusivities (Figure 46), and the concentration gradients are quite small. The pollutant concentrations above 500 m exceed only slightly the initial background value of 50 ppm.

Figures 45 and 46 show large variations of the diffusivities during the diurnal cycle and, what has already been indicated before, that the diffusivities are higher in the city than in the rural area because of increased roughness and higher temperatures. This difference in diffusivities between urban and rural locations is much larger near the surface (Figure 45) than at the height of, say, 200 m (Figure 46). At noon the

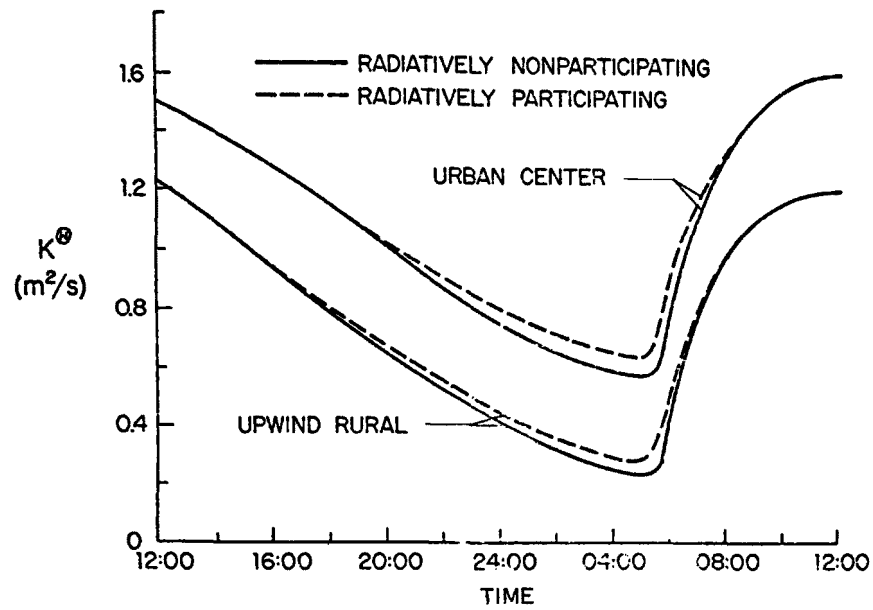


Figure 45. Comparison of the Turbulent Diffusivities of Heat for Simulations 3 and 5 at $z = 200$ m

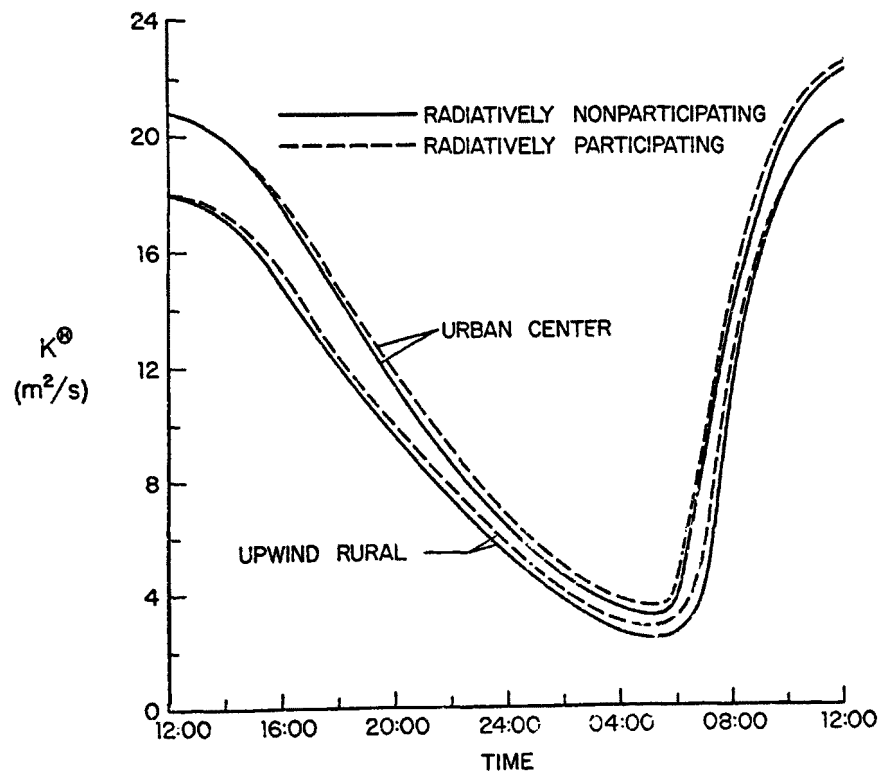


Figure 46. Comparison of the Turbulent Diffusivities of Heat for Simulations 3 and 5 at $z = 200$ m

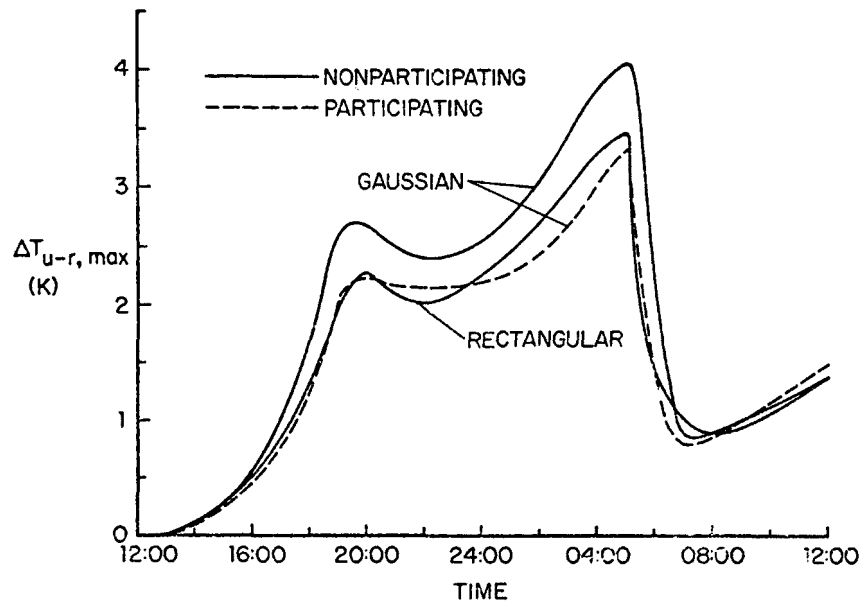


Figure 47. Comparison of Maximum Urban Minus Upwind Rural Surface Temperature Differences for Simulations 3, 5, and 7

diffusivities in the city are about 40% higher than in the rural area while before sunrise they are higher by about a factor of 2. The results also show that the diffusivities are larger for Simulation 5 with radiatively participating pollutants than for Simulation 3. This is due to decreased atmospheric stability for the simulation with interacting pollutants as a result of warmer nighttime temperatures. The radiatively participating pollutants are seen to affect the diffusivities much less than the urbanization (urban-rural parameter differences). This then explains why the difference between the pollutant concentration profiles presented in Figures 44a and 44b for the two simulations are relatively small.

The results presented show that the radiative participation by pollutants may have the potential of affecting their own dispersion, especially the peak concentrations before and after sunrise. The meteorological conditions considered in the numerical simulations were not critical for pollutant dispersion. Under more adverse dispersion conditions such as may arise for lower wind speeds and/or stable elevated layers, the coupling between the radiatively participating pollutants and their dispersion is expected to be stronger. Comparison of results presented in Figure 8 with those given in Figure 44 clearly show that an urban area cannot be realistically simulated using a one-dimensional model that neglects horizontal and vertical advection.

Urban Heat Island

The urban heat island is a well known and accepted physical phenomenon (Peterson, 1969; Oke, 1973b). In order to partially verify the predictions of the two-dimensional transport model, the urban heat island intensity

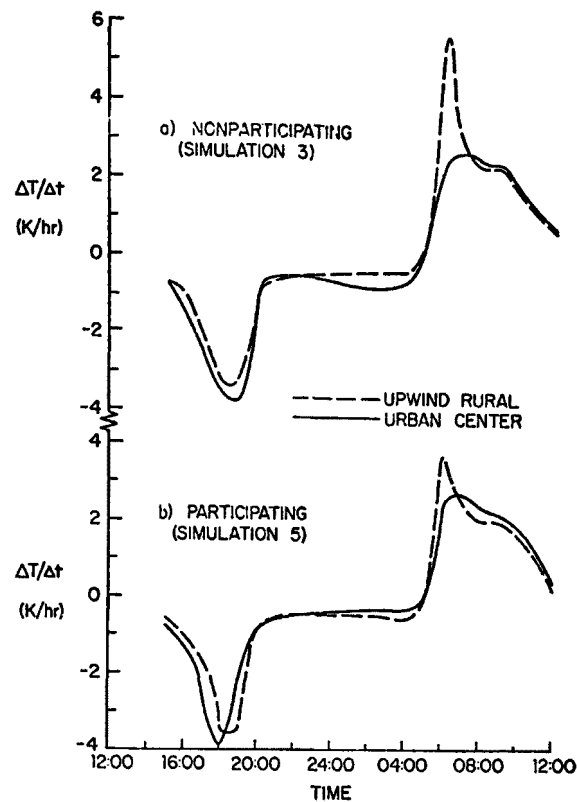


Figure 48. Variation of the Heating/Cooling Rates for Simulation 3 (Part a) and for Simulation 5 (Part b) during the Diurnal Cycle

(difference between upwind and rural and highest urban temperatures, $\Delta T_{u-r,max}$) was determined. The results for Simulations 3 and 5 without and with radiatively participating pollutants, respectively, having Gaussian distributions of anthropogenic heat and pollutant sources and for Simulation 7 without radiatively participating pollutants having a rectangular distribution of sources are shown in Figure 47. For the Gaussian distribution of urban heat sources, the maximum temperature during the night occurred at the urban center whereas for the rectangular distribution during the night it occurred from 1.5 to 6 km downwind of the center. The results presented in Figure 47 show that there is a double peak in $\Delta T_{u-r,max}$. The first smaller peak is noted in the evening at about 20:00. It arises due to the more rapid cooling at the upwind rural area than in the city. The second peak occurs before sunrise and increases to a value of about 4K for Simulation 3. The second peak is primarily due to the differences in the urban/rural parameters. This can be more readily seen by comparing Figures 38 and 39. For Simulations 1 and 2 with higher wind speeds ($u_g = 12$ m/s and $v_g = 8$ m/s) it was found that the maximum urban heat island intensity occurred in the evening at 19:00 and there was not second peak before sunrise.

The results of Figure 47 show that the maximum urban-rural surface temperature difference for the rectangular distribution of urban heat sources is approximately 0.6K lower than the corresponding results for the Gaussian distribution. This is indicative of the lower heat emissions employed a small distance downwind of the urban center (see Figure 16). For the population of the city and wind speeds considered in the simulations, the urban heat island intensity is in good agreement with the observations and empirical correlation of Oke (1973b). Urban-rural temperature differences of about 3K have been observed by Clarke and McElroy (1974) for the city of St. Louis, Missouri near sunrise on August 7, 12, 13, 21, and 22, 1973.

The heating/cooling rates ($\Delta T/\Delta t$) evaluated from the surface temperature versus time plots (see Figures 37 and 38) have been determined for Simulations 3 and 5 and are presented in Figure 48. The results are not given for the first few hours of the simulation because of the transient introduced by the choice of the assumed initial profiles. The slopes were evaluated graphically and are therefore subject to considerable inaccuracies; however, the trends indicated seem reasonable. The rural cooling/heating rates are expected to show larger changes because of the lower heat capacitance and considerably lower conductivity of the soil. The cooling rates of about 0.5K/hr predicted at night are in reasonably good agreement with the results reported by Oke and Maxwell (1975) for Montreal and Vancouver. The variations at sunset and sunrise are more extreme. The maximum cooling rate measured by Oke and Maxwell was about 3K/hr while the predicted values are about 4K/hr. The agreement is reasonable in view of the fact that the meteorological conditions in the simulations were different from those under which the field data were obtained ("summer nights with calm and clear conditions"). In addition, urban cooling rates depend on the man-made structures, shading, etc. which are not modeled in the numerical experiments.

SECTION VI

REFERENCES

- Ames, W. F., 1969: Numerical Methods for Partial Differential Equations, Barnes and Noble, Inc., New York, pp. 148-157.
- Atwater, M. A., 1970: Planetary Albedo Changes Due to Aerosols. *Science*, 170, 64-66.
- Atwater, M. A., 1970: Investigation of the Radiation Balance for Polluted Layers of the Urban Environment. Ph.D. Dissertation, New York University.
- Atwater, M. A., 1971: Radiative Effects of Pollutants in the Atmospheric Boundary Layer. *J. Atm. Sci.*, 28, 1367-1373.
- Atwater, M. A., 1972a: Thermal Effects of Urbanization and Industrialization in the Boundary Layer: A Numerical Study. *Boundary Layer Meteor.*, 3, 229-245.
- Atwater, M. A., 1972b: The Thermal Changes Induced by Urbanization and Pollutants. Conference on Urban Environment and Second Conference on Biometeorology. American Meteorological Society, Boston, pp. 153-158.
- Atwater, M. A., 1974: Thermal Changes Induced by Pollutants for Different Climatic Regions. Symposium on Atmospheric Diffusion and Air Pollution of the American Meteorological Society. American Meteorological Society, Boston, pp. 147-150.
- Bergstrom, R. W., Jr., 1972a: Predictions of the Spectral Absorption and Extinction Coefficients of an Urban Air Pollution Aerosol Model. *Atmos. Envir.*, 6, 247-258.
- Bergstrom, R. W., Jr., 1972b: Theoretical Study of the Thermal Structure and Dispersion in Polluted Urban Atmospheres. Ph.D. Thesis, Purdue University.
- Bergstrom, R. W., Jr., 1973: Comments on the Estimation of the Absorption Coefficients of Atmospheric Aerosols. *B. Phys. Atmos.*, 46, 198-201.
- Bergstrom, R. W., Jr., and R. Viskanta, 1973a: Modeling of the Effects of Gaseous and Particulate Pollutants in the Urban Atmosphere. Part I: Thermal Structure. *J. Appl. Meteor.*, 12, 911-912.

- Bergstrom, R. W., Jr., and R. Viskanta, 1973b: Modeling of the Effects of Gaseous and Particulate Pollutants in the Urban Atmosphere. Part II: Pollution Dispersion. J. Appl. Meteor., 12, 913-918.
- Bergstrom, R. W., Jr., and R. Viskanta, 1973c: Prediction of the Solar Radiant Flux and Heating Rates in a Polluted Atmosphere. Tellus, XXV, 486-498.
- Bergstrom, R. W., Jr., and R. Viskanta, 1974: Spherical Harmonics Approximation for Radiative Transfer in Polluted Atmospheres. Progress in Astronautics and Aeronautics. Volume 35, MIT Press, Cambridge, Mass., pp. 23-40.
- Blackadar, A. K., 1962: The Vertical Distribution of Wind and Turbulent Exchange in a Neutral Atmosphere. Geophys. Res., 67, 3095-3102.
- Boughner, R. E., 1972: Air Pollution Survey and Recommendations: Global Pollution and Upper Atmospheric Effect. NASA Langley Working Paper.
- Bornstein, R. D., 1972: Two Dimensional, Nonsteady Numerical Simulation of Nighttime Flow of a Stable Planetary Boundary Layer Over a Rough, Warm City. Conference on Urban Meteorology and Second Conference on Biometeorology. American Meteorological Society, Boston, pp. 89-94.
- Bornstein, R. D., 1973: Two-Dimensional, Nonsteady Numerical Simulations of Nighttime Flows of a Stable Planetary Boundary Layer Over a Rough, Warm City. Ph.D. Thesis, Department of Meteorology and Oceanography, New York University.
- Bornstein, R. D., and Y.-T. Tam, 1975: Anthropogenic Moisture Production and Its Effect on Boundary Layer Circulations Over New York City. Lawrence Livermore Laboratory Preprint UCRC-7722.
- Braslau, N., and J. V. Dave, 1973: Effect of Aerosols on the Transfer of Solar Energy Through Realistic Model Atmospheres. Parts I and II. J. Appl. Meteor., 12, 601-615, 616-619.
- Broderick, A. J., Editor, 1972: Proceedings of the Second Conference on the Climatic Impact.
- Carnahan, B., H. A. Luther, and J. O. Wilkes, 1969: Applied Numerical Methods. John Wiley and Sons, New York.
- Carson, D. J., and F. B. Smith, 1974: Thermodynamic Model for the Development of Convectively Unstable Boundary Layer. Advances in Geophysics. (F. N. Frankiel and R. E. Munn, Eds.) Volume 18a, Academic Press, New York, pp. 111-124.
- Chan, S. H., and C. L. Tien, 1971: Infrared Radiation Properties of Sulfur Dioxide. J. Heat Transfer, 93, 172-178.

- Chandrasekhar, S., 1960: Radiative Transfer. Dover Publications, New York.
- Clarke, J. F., and J. L. McElroy, 1974: Effects of Ambient Meteorology and Urban Meteorological Features on the Vertical Temperature Over Cities. Air Pollution Control Association. Annual Meeting, Paper No. 74-73, Denver, Colorado.
- Dabbert, W. F., and P. A. Davis, 1974: Determination of Energetic Characteristics of Urban-Rural Surfaces in the Greater St. Louis Area. U.S. Environmental Protection Agency, Office of Research and Development Report EPA-650/4-74-007, Washington, D. C.
- Deardorff, J. W., 1967: Empirical Dependence of the Eddy Diffusion Coefficient for Heat Upon Stability Above the Lowest 50 m. J. Appl. Meteor., 6, 631-643.
- Deardorff, J. W., 1973: Three Dimensional Numerical Model of the Planetary Boundary Layer. Workshop on Meteorology (D. A. Haugen, Ed.). American Meteorological Society, Boston, pp. 271-311.
- Deirmendjian, D., 1969: Electromagnetic Scattering of Spherical Polydispersions. Elsevier, New York, pp. 77-83.
- DeMarrais, G. A., 1975: Nocturnal Heat Island Intensities and Relevance to Forecasts of Mixing Heights. Mon. Wea. Rev., 104, 235-245.
- Donaldson, D. duP., 1973: Construction of a Dynamic Model of the Production of Atmospheric Turbulence and the Dispersal of Atmospheric Pollutants. Workshop in Micrometeorology (D. A. Haugen, Ed.). American Meteorological Society, Boston, pp. 313-390.
- Eagelson, P. S., 1970: Dynamic Hydrology. McGraw-Hill, New York.
- Elterman, L., 1970: Vertical Attenuation Model with Eight Surface Meteorological Ranges 2 to 13 Kilometers. Air Force Cambridge Research Laboratories Report AFCRL-70-0200, Bedford, Mass.
- Ensor, D. S., W. M. Porch, J. J. Pilat and R. J. Charlson, 1971: Influence of Atmospheric Aerosols on Albedo. J. Appl. Meteor., 10, 1303-1306.
- Eschelbach, G., 1972: Berechnungen des Strahlungsfeldes einer Dunsthabigen Atmosphäre in Solaren Spektralbereich. Doctoral Thesis, Johannes Gutenberg Universität, Mainz, FDR.
- Estoque, M. A., 1973: Numerical Modeling of the Planetary Boundary Layer. Workshop on Micrometeorology (D. A. Haugen, Ed.), American Meteorological Society, Boston, pp. 217-270.
- Estoque, M. A., 1973: A Numerical Model for the Atmospheric Boundary Layer. J. Geophys. Res., 68, 1103-1113.

- Frankiel, F. N., and R. E. Munn, Editors, 1974: Turbulent Diffusion in Environmental Pollution. Advances in Geophysics, Volumes 18a and 18b, Academic Press, New York.
- Friskien, W. R., 1972: The Atmospheric Environment of Cities. Report for Resources for the Future, Inc., Washington, D. C.
- Halstead, M. H., R. L. Richman, W. Covey, and J. D. Merryman, 1957: A Preliminary Report on the Design of a Computer for Micrometeorology. J. Meteor., 14, 308-325.
- Haltiner, G. J., and F. L. Martin, 1957: Dynamical and Physical Meteorology. McGraw-Hill, New York.
- Hänel, G., 1972: Computation of the Extinction of Visible Radiation by Atmospheric Particles as a Function of Relative Humidity, Based Upon Measured Properties. Aerosol Sci., 3, 377-386.
- Herman, B. M., and S. R. Browning, 1965: A Numerical Solution to the Equation of Radiative Transfer. J. Atm. Sci., 22, 559-566.
- Hoffert, M. I., 1972: Atmospehric Transport, Dispersion, and Chemical Reactions in Air Pollution. AIAA Journal, 10, 377-387.
- Johnson, R. O., 1975: The Development of an Unsteady Two-Dimensional Transport Model in a Polluted Urban Atmosphere. M.S. Thesis, Purdue University, West Lafayette, Indiana.
- Kondratyev, K. Ya., 1969: Radiation in the Atmosphere. Academic Press, New York.
- Kondratyev, K. Ya., 1972: Radiation Processes in the Atmosphere. World Meteorological Organization Publication No. 209, Geneva.
- Kondratyev, K. Ya., 1973: The Complete Atmospheric Energetics Experiment. Global Atmospheric Research Programme (GARP), GARP Publications Series No. 12, ICSU-WMO, Geneva.
- Korb, G., and W. Zdunkowski, 1970: Distribution of Radiative Energy in Ground Fog. Tellus, XX, 298-320.
- Kuhn, P. M., 1963: Radiometersonde Observations of Infrared Flux Emissivity of Water Vapor. J. Appl. Meteor., 2, 368-378.
- Landsberg, H. E., 1970: Man-Made Climatic Changes. Science, 170, 1265-1274.
- Landsberg, H. E., 1972: Inadvertent Atmospheric Modification Through Urbanization. Techn. Note No. BN 741, Institute of Fluid Dynamics and Applied Mathematics, University of Maryland.

- Lettau, H. H., and B. Davidson, 1957: Exploring the Atmosphere's First Mile, Volumes 1 and 2. New York, Pergamon Press.
- Lilly, D. K., 1968: Models of Cloud-topped Mixed Layers Under a Strong Inversion. *Quart. J. Roy. Meteor. Soc.*, 94, 292-309.
- Liu, C. Y., and W. R. Goodwin, 1975: A Two-dimensional Model for the Transport of Pollutants in an Urban Basin. AIChE Paper No. 47D Presented at the 79th National Meeting at AIChE, Houston, Texas, March 16-20, 1975.
- Ludwig, C. B., R. Bartle, and M. Giggs, 1969: Study of Air Pollution Detection by Remote Sensing. National Aeronautics and Space Administration Report NASA Cr-1380, Washington, D. C.
- McElroy, J. L., 1972: Effects of Alternate Land Use Strategies on the Structure of the Nocturnal Urban Boundary Layer. Conference on Urban Environment and Second Conference on Biometeorology, American Meteorological Society, Boston, pp. 185-190.
- McPherson, R. D., 1968: A Three-dimension Numerical Study of the Texas Coast Sea Breeze. Atmospheric Sciences Group, Report 15, University of Texas, Austin.
- Mellor, G. L., 1973: Analytical Prediction of the Properties of Stratified Planetary Surface Layers. *J. Atmos. Sci.*, 30, 1061-1069.
- Mitchell, J. M., 1971: The Effect of Atmospheric Aerosols on Climate with Special Reference to Temperature Near the Earth's Surface. *J. Appl. Meteor.*, 10, 703.
- Mudgett, P. S., and L. W. Richards, 1971: Multiple Scattering Calculations for Technology. *Appl. Opt.*, 10, 1485-1502.
- Oke, T. K., and R. F. Fluggie, 1972: Comparison of Urban/Rural Counter and Net Radiation at Night. *Boundary-Layer Meteor.*, 2, 290-308.
- Oke, T. K., 1973a: A Review of Urban Meteorology: 1968-1972. Department of Geography, The University of British Columbia, Vancouver.
- Oke, T. K., 1973b: City Size and Urban Heat Island. *Atmos. Envir.*, 7, 769-779.
- Oke, T. K., and G. B. Maxwell, 1975: Urban Heat Island Dynamics in Montreal and Vancouver. *Atmos. Envir.*, 9, 191-200.
- Olfe, D. B., and R. L. Lee, 1971: Linearized Calculations of Urban Heat Island Convection Effects. *J. Atmos. Sci.*, 28, 1374-1388.

- Pandolfo, J. P., M. A. Atwater, and G. E. Anderson, 1971: Prediction by Numerical Models of Transport and Diffusion in an Urban Boundary Layer. Final Report, Contract 4082, The Center for the Environment and Man, Inc., Hartford, Conn.
- Peterson, J. T., 1969: The Climate Over Cities: A Survey of Recent Literature. Air Pollution Control Administration, Publication No. AP-59, Washington, D. C.
- Peterson, J. T., 1970: Distribution of Sulfur Dioxide over Metropolitan St. Louis, as Described by Empirical Eigenvectors, and Its Distribution to Meteorological Parameters. *Atmos. Envir.*, 4, 501-518.
- Peterson, J. T., 1972: Sulfur Dioxide Concentrations over Metropolitan St. Louis. *Atmos. Envir.*, 6, 433-442.
- Plate, E. J., 1971: Aerodynamic Characteristics of Atmospheric Boundary Layers. U.S. Atomic Energy Commission, Division of Technical Information Extension, Oak Ridge, Tenn.
- Rasool, S. I., and S. H. Schneider, 1971: Atmospheric Carbon Dioxide and Aerosols: Effects of Increases on Global Climate. *Science*, 173, 138-141.
- Reagan, J. A., and B. M. Herman, 1971: Three Optical Methods for Remotely Measuring Aerosol Size Distribution. Proceedings of the Joint Conference on Sensing of Environmental Pollutants, American Institute of Aeronautics and Astronautics, New York, AIAA Paper No. 71-1057.
- Reck, R. A., 1974: Influence of Surface Albedo on the Changes in Atmospheric Radiation Balance Due to Aerosols. *Atmos. Envir.*, 8, 823-833.
- Roache, P. J., 1972: Computational Fluid Dynamics. Hermosa Publishers, Albuquerque, N. M.
- Robinson, G. D., 1970: Some Meteorological Aspects in Radiation Measurements. Advances in Geophysics (H. E. Landsberg and J. van Mieghen, Eds.), Volume 14, Academic Press, New York, pp. 285-306.
- Sasamori, T., 1970: A Numerical Study of Atmospheric and Soil Boundary Layers. *J. Atm. Sci.*, 27, 1122-1137.
- SCEP, 1970: Study of Critical Environmental Problems, MIT Press, Cambridge.
- Shir, C. C., 1972: A Numerical Computation of Air Flow Over a Sudden Change of Surface Roughness. *J. Atmos. Sci.*, 30, 1327-1339.
- SMIC, 1971: Study of Man's Impact on Climate. MIT Press, Cambridge.
- Smith, M., 1968: Recommended Guide for the Prediction of the Dispersion of Airborne Effluents. The American Society of Mechanical Engineers, New York.

- Stern, A. C., H. C. Wohlers, R. W. Boubel, and W. P. Lowry, 1972: Fundamentals of Air Pollution, Academic Press, New York.
- Taylor, P. A., and Y. Delage, 1971: A Note on Finite-difference Schemes for the Surface and Planetary Boundary Layers. Boundary Layer Meteor., 2, 108-121.
- Tennekes, H., 1974: The Atmospheric Boundary Layer. Physics Today, 27, 52-63.
- Terjung, W. H., 1973: Urban Climates. Progress in Biometeorology (S. W. Troup, Ed.), Swets and Zeitlinger, Amsterdam.
- Turner, D. B., 1968: The Diurnal and Day-to-day Variations of Fuel Usage for Space Heating in St. Louis, Missouri. Atmos. Envir., 2, 339-351.
- United Nations Conference on Human Environment, 1972: Recommendations 18, 25, 46, 57, 67, 73, 76, 77, 79, 80, 87, 90, 91, and 94. Stockholm, Sweden.
- U.S. Council for Environmental Quality, 1970: First Annual Report of the Council on Environmental Quality. U.S. Government Printing Office, Washington, D. C., pp. 93-104.
- Uthe, E. E., 1971: Lidar Observations of Particulate Distributions Over Extended Areas. Proceedings of the Joint Conference on Sensing of Environmental Pollutants, Paper No. 71-1055, American Institute of Aeronautics and Astronautics, New York.
- von Rosenberg, D. U., 1969: Methods for the Numerical Solution of Partial Differential Equations. American Elsevier Publishing Co., New York.
- Wagner, N. K., and T. Yu, 1972: Heat Island Formation: A Numerical Experiment. Conference on Urban Environment and Second Conference on Biometeorology, American Meteorological Society, Boston, pp. 83-88.
- Wang, W., and G. Domoto, 1974: The Radiative Effect of Aerosols in the Earth's Atmosphere. J. Appl. Meteor., 13, 521-534.
- Wu, S. S., 1965: A Study of Heat Transfer Coefficients in the Lowest 400 Meters of the Atmosphere. J. Geophys. Res., 70, 1801-1807.
- Wyngard, J. C., O. R. Cote, and K. S. Rao, 1974: Modeling the Atmospheric Boundary Layer. Advances in Geophysics (F. N. Frankiel and R. E. Munn, Eds.), Volume 18a, Academic Press, New York, pp. 193-211.
- Yamada, D. E., 1972: Urban Heat Island Effects on Air Pollution. Conference on Urban Environment and Second Conference on Biometeorology, American Meteorological Society, Boston, pp. 99-105.

Yamamoto, G., and M. Tanaka, 1972: Increase of Global Albedo Due to Air Pollution. J. Atm. Sci., 29, 1405-1412.

Yu, T., 1973: Two-dimensional Time-dependent Numerical Simulation of Atmospheric Flow Over an Urban Area. Atmospheric Sciences Group Report No. 32, The University of Texas, Austin.

Zdunkowski, W. G., and N. D. McQuague, 1972: Short-term Effects of Aerosols on the Layer Near the Ground in a Cloudless Atmosphere. Tellus, XXIV, 237-254.

APPENDIX
PUBLICATIONS

PAPERS

- R. W. Bergstrom, Jr., "Predictions of the Spectral Absorption and Extinction Coefficients of an Urban Aerosol Model," *Atmospheric Environment*, 6, 247-258, 1972.
- R. W. Bergstrom, Jr., and R. Viskanta, "Prediction of the Solar Radiant Flux and Heating Rates in a Polluted Atmosphere," *Tellus*, XXV, 486-498, 1973.
- R. W. Bergstrom, Jr., and R. Viskanta, "Modeling of the Effects of Gaseous and Particulate Pollutants in the Urban Atmosphere. Part I: Thermal Structure," *J. Appl. Meteor.*, 12, 901-912, 1973.
- R. W. Bergstrom, Jr., and R. Viskanta, "Modeling of the Effects of Gaseous and Particulate Pollutants in the Urban Atmosphere. Part II: Pollutant Dispersion," *J. Appl. Meteor.*, 12, 913-918.
- R. W. Bergstrom, Jr., and R. Viskanta, "Spherical Harmonics Approximation for Radiative Transfer in Polluted Atmospheres," *AIAA 8th Thermophysics Conference*, Palm Springs, California, July 16-18, 1973, AIAA Paper No. 73-749.
- R. W. Bergstrom, Jr., and R. Viskanta, "Modeling of Thermal Structure and Dispersion in Polluted Urban Atmospheres," *AIChE-ASME 14th National Heat Transfer Conference*, Atlanta, Georgia, August 5-8, 1973, ASME Paper No. 73-HT-8.
- R. W. Bergstrom, Jr., and R. Viskanta, "Spherical Harmonics Approximation for Radiative Transfer in Polluted Atmospheres," in *Progress in Astronautics and Aeronautics*, Volume 35, MIT Press, Cambridge, Mass., pp. 23-40.
- R. Viskanta, R. O. Johnson, and R. W. Bergstrom, Jr., "Effect of Urbanization on the Thermal Structure in the Atmosphere," *Conference on Metropolitan Physical Environment*, Syracuse, New York, August 25-29, 1975 (to be published in *Proceedings of the Conference*).

THESES

- R. W. Bergstrom, Jr., "Theoretical Study of the Thermal Structure and Dispersion in Polluted Urban Atmospheres," Ph.D. Thesis, Purdue University, August 1972.
- R. O. Johnson, "The Development of Two-dimensional Transport Model in a Polluted Urban Atmospheres," M.S. Thesis, Purdue University, August 1975.

TECHNICAL REPORT DATA <i>(Please read Instructions on the reverse before completing)</i>		
1. REPORT NO. EPA-600/4-76-002	2.	3. RECIPIENT'S ACCESSION NO.
4. TITLE AND SUBTITLE MODELING OF THE EFFECTS OF POLLUTANTS AND DISPERSION IN URBAN ATMOSPHERES	5. REPORT DATE February 1976 (Issuing Date)	6. PERFORMING ORGANIZATION CODE
	8. PERFORMING ORGANIZATION REPORT NO.	
7. AUTHOR(S) R. Viskanta, R. W. Bergstrom, Jr., and R. O. Johnson	10. PROGRAM ELEMENT NO. P.E. 1AA009 (ROAP 26AAS)	
9. PERFORMING ORGANIZATION NAME AND ADDRESS Purdue Research Foundation West Lafayette, IN 47907	11. CONTRACT GRANT NO. R801102	
	13. TYPE OF REPORT AND PERIOD COVERED Final 6/1/71 - 1/31/75	
12. SPONSORING AGENCY NAME AND ADDRESS Environmental Sciences Research Laboratory Office of Research and Development U.S. Environmental Protection Agency Research Triangle Park, NC 27711	14. SPONSORING AGENCY CODE EPA-ORD	
	15. SUPPLEMENTARY NOTES	
16. ABSTRACT <p>The short-term effects of radiatively participating pollutants upon the thermal structure and dispersion in an urban atmosphere were studied by constructing one- and two-dimensional transport models for the planetary boundary layer. Special attention was focused on the interaction of solar and thermal radiation with gaseous and particulate pollutants as well as natural atmospheric constituents.</p>		
17. KEY WORDS AND DOCUMENT ANALYSIS		
a. DESCRIPTORS	b. IDENTIFIERS/OPEN ENDED TERMS	c. COSATI Field/Group
Meteorology *Air pollution *Atmospheric diffusion *Mathematical models Boundary layer *Solar radiation *Thermal radiation		04B 13B 12A 20D 03B 20M
18. DISTRIBUTION STATEMENT RELEASE TO PUBLIC	19. SECURITY CLASS (This Report) UNCLASSIFIED	21. NO. OF PAGES 123
	20. SECURITY CLASS (This page) UNCLASSIFIED	22. PRICE